Design of a Quasi-Passive Parallel Leg Exoskeleton to Augment Load Carrying for Walking

by

Andrew Valiente

B.S., LeTourneau University (2003)

Submitted to the Department of Mechanical Engineering
in partial fulfillment of the requirements for the degree of

Master's of Science

at the

MASSACHUSETTS INSTITUTE OF TECHNOLOGY

August 2005

Author . . . . . .
Department of Mechanical Engineering
August 5 2005

Certified by. . . . . .
Hugh Herr
Assistant Professor of Media Arts and Sciences, MIT
Thesis Supervisor

Certified by. . . . . .
Ernesto Blanco
Professor of Mechanical Engineering
Thesis Supervisor

Accepted by . . . . . .
Professor Lallit Anand
Chairman, Departmental Committee on Graduate Students

Design of a Quasi-Passive Parallel Leg Exoskeleton to Augment Load Carrying for Walking

by
Andrew Valiente

Submitted to the Department of Mechanical Engineering
on August 5, 2005, in partial fulfillment of the
requirements for the degree of
Masters of Science

Abstract

Biomechanical experiments suggest that it may be possible to build a leg exoskeleton to reduce the metabolic cost of walking while carrying a load. A quasi-passive, leg exoskeleton is presented that is designed to assist the human in carrying a 75 lb payload. The exoskeleton structure runs parallel to the legs, transferring payload forces to the ground. In an attempt to make the exoskeleton more efficient, passive hip and ankle springs are employed to store and release energy throughout the gait cycle. To reduce knee muscular effort, a variable damper is implemented at the knee to support body weight throughout early stance. In this thesis, I hypothesize that a quasi-passive leg exoskeleton of this design will improve metabolic walking economy for carrying a 75lb backpack compared with a leg exoskeleton without any elastic energy storage or variable-damping capability. I further anticipate that the quasi-passive leg exoskeleton will improve walking economy for carrying a 75lb backpack compared with unassisted loaded walking. To test these hypotheses, the rate of oxygen consumption is measured on one human test participant walking on a level surface at a self-selected speed. Pilot experimental data show that the quasi-passive exoskeleton increases the metabolic cost of carrying a 75lb backpack by 39% compared to carrying 75 lbs without an exoskeleton. When the variable-damper knees are replaced by simple pin joints, the metabolic cost relative to unassisted load carrying decreases to 34%, suggesting that the dampening advantages of the damper knees did not compensate for their added mass. When the springs are removed from the aforementioned pin knee exoskeleton, the metabolic cost relative to unassisted load carrying increased to 83%. These results indicate that the implementation of springs is beneficial in exoskeleton design.

Thesis Supervisors: Hugh Herr and Ernesto Blanco
Title: Assistant Professor of Media Arts and Sciences, MIT
Title: Professor of Mechanical Engineering, MIT

Acknowledgments

I would like to first and foremost thank Jesus Christ my Lord and Savior for endowing me with a talent for engineering, and for the myriad of past blessings that he has given me.

I would like to thank my advisor Professor Hugh Herr for making the Biomechatronics group at the Media Lab an incredible place to work and for his insight in biomechanics. Thanks to my thesis reader, Ernesto Blanco, for his encouragement and insight in mechanics.

Thanks to my coworkers at Biomechatronics Group: Dan Paluska, Dr. Ken Pasch, Conor Walsh, William Grand, and Chi Won for their support and collaboration in building exoskeletons. I extend appreciation to Dan Paluska for his encouragement, for answering my endless questions and for taking time away from his thesis to help me with my research.

I would like to thank Spaulding Rehabilitation Hospital for lending us VO_2 equipment to conduct metabolic tests.

I would like to thank the Bill and Melinda Gates foundation for their fellowship that enabled me to study at MIT.

This research was done under Defense Advanced Research Projects Agency (DARPA) contract #NBCHC040122, 'Leg Orthoses for Locomotory Endurance Amplification'.

Table of Contents

Figures

Tables

Chapter 1 Introduction

1.1 Antigravity Experiments

Exoskeletons can enhance human locomotory performance and can augment human strength, endurance, and speed. Exoskeletons have application for military and service personnel, as well as for patients with muscular impairments. Exoskeletons have the ability to traverse non-paved terrain accessing locations where wheeled vehicles cannot. Exoskeletons promise to allow people to run farther, jump higher, and bear larger loads while expending less energy.

Recent physiological studies suggest that it may be possible to build an orthotic exoskeleton to dramatically increase the locomotory endurance of service personnel. Simulated reduced gravity experiments have demonstrated that the metabolic cost of walking and running can be reduced by 33% and 75% respectively, if gravity is reduced by 75% [Jiping et al. (1991); Farley & McMahon (1992)]. These experiments have shown that if gravity is decreased by at least 50%, then a person can run at a lower metabolic rate than he could have walked. Furthermore, studies by [Griffen et al, (2003)] have shown that a 10% and 30% increase in body mass (BM) will increase the required metabolic energy of walking by 15% and 47% respectively. Studies by Gottschall and Kram, 2003 have shown that a 10% bodyweight forward assist will cause a 47% reduction in metabolic energy, while a 10% drag force will cause a corresponding 150% increase in metabolic cost.

The reduced gravity experiments suggest that the metabolic energy expended by an average 200 lb person bearing a 75lb backpack (38% BM), will increase substantially. It can be reasoned that an exoskeleton placed in parallel to the human body can transmit the backpack forces to the ground relieving the human from supporting the load. Thus, it is reasoned that if an exoskeleton is designed correctly, a lower metabolic cost can be achieved for loaded walking. A summary of the metabolic studies is shown in Figure 1.

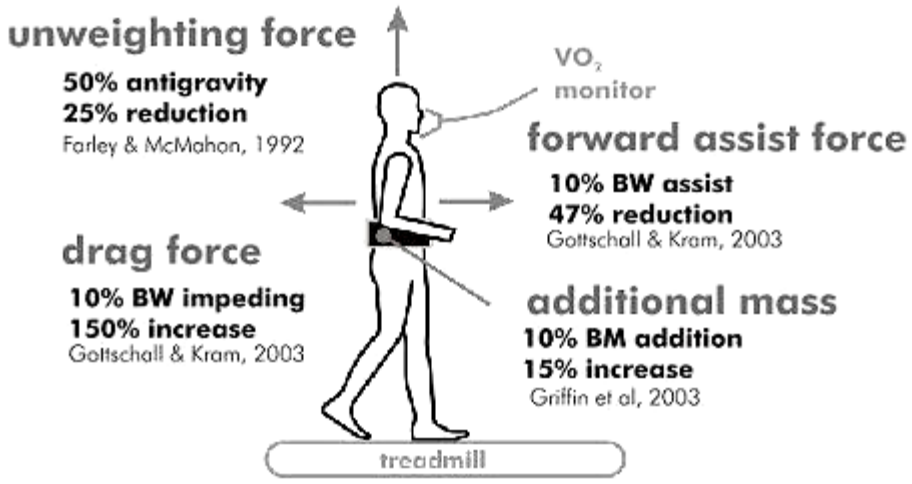

Figure 1 Summary of metabolic experiments.
Simulated antigravity experiments suggest that it may be possible to build an orthotic exoskeleton to augment human load carrying capabilities while reduce the metabolic cost of locomotion.

1.2 Past work

The idea of using exoskeletons to augment human locomotory performance dates back to 1890 when Nicholas Yagn conceptualized an apparatus for facilitating walking, running, and jumping [Yagn (1890)]. See Figure 2A. His device consisted of a large bow spring that was interconnected between a hip belt and a foot attachment. The bow spring stores energy developed by the weight of the body and by the act of walking, running, or jumping. Yagn's bow spring design lacked a degree of freedom at the knee. Therefore, to achieve steady state running the user would hop from one leg to the other. Bending of the knee for normal walking and running would require storing prohibitive amounts energy in the bow spring. Yagn's apparatus was completely passive and human powered.

In 1969, the 'kinematic walker' was developed [Vukobratović et al. (1990)]. See Figure 2B. Each leg of the 'kinematic walker' consisted of 2 degrees of freedom with an active joint at the hip and a passive joint at the ankle. The knee was locked straight and the hips were actuated via pneumatic pistons mounted on the waist. The resulting gait was of the 'sliding foot type'.

In 1970, the first active exoskeleton with 3 degrees of freedom per leg was developed [Vukobratović et al. (1990)]. See Figure 2C. This exoskeleton, know as the 'partial exoskeleton', introduced a degree of freedom at the knee. It employed 7 pneumatic

actuators and 14 electromagnetic solenoid valves. The exoskeleton enabled a paraplegic to walk, but was unable to provide dynamic stability. A rolling aid such as other people or crutches was needed to prevent the participant from falling sideways. The exoskeleton mated to the body by means of a phenolic resin corset lined with leather padding. Interfacing to the body proved challenging since prolonged usage of the exoskeleton led to the development of local wounds (decubitus) at various pressure points. Both the 'kinematic walker' and the 'partial exoskeleton' had an air compressor off board.

In 1978, the 'active suit' was developed [Vukobratović et al. (1990)]. See Figure 2D. The 'active suit' was a self-contained, microcomputer controlled active exoskeleton powered by servoelectric drives. A 100W servoelectric drive was employed for the hip joint, and a 50W servoelectric drive coupled to a worm-gear reducer was implemented for the knee joint. The system was controlled by a chest-mounted microprocessor control system and powered by nickel-cadmium batteries. The exoskeleton corset was manufactured using strong felt and light alloy stiffeners. The exoskeleton was tested by a patient with muscular dystrophy. The patient was able to adapt to the suit quickly and use it without difficulty.

In 1991, the 'Spring Walker' was developed as a passive exoskeleton for running [Dick et al. (1991); Dick et al. (2000)]. See Figure 2E. The 'Spring Walker' was a complex, human powered, kinematic exoskeleton. The exoskeleton consisted of a kinematic linkage whose joints incorporated springs. The legs of the 'Spring Walker' were in series to the human, such that the human feet do not touch the ground. Although very complex, the 'Spring Walker' allowed the human to achieve a moderate running pace.

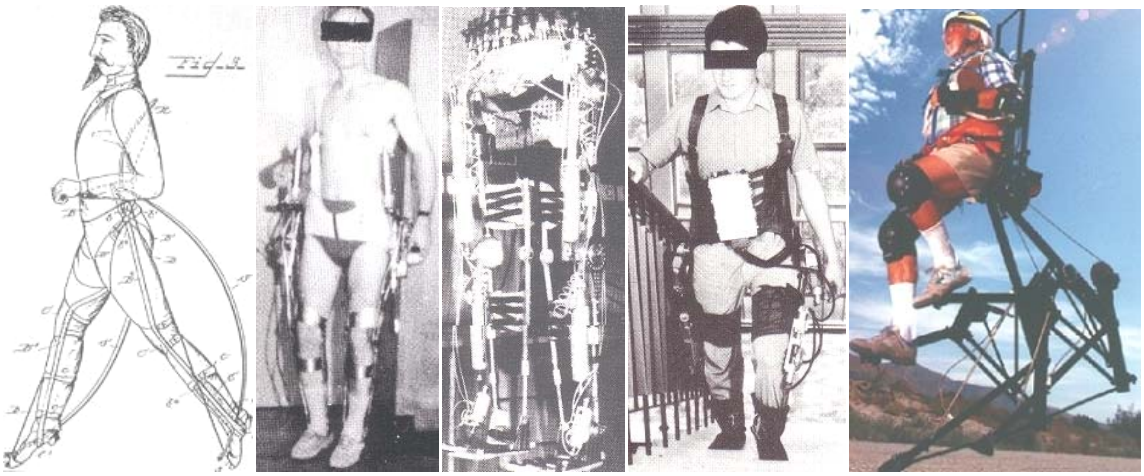

(A) (B) (C) (D) (E)

Figure 2 Historic exoskeletons.
(A) Yagn's apparatus to facilitate walking, running, & jumping [Yagn (1890)]. It implemented a bow spring interconnecting the hip and ankle which stored energy when compressed. It did not allow for the knee to bend. (B) The 'Kinematic Walker', circa 1969, was an exoskeleton with 2 degrees of freedom at the hip and ankle [Vukobratović et al. (1990)]. It was pneumatically actuated at the hip. The knee remained locked straight. (C) The 'Partial Exoskeleton,' circa 1970, was the first 3 degree of freedom exoskeleton with a degree of freedom for each the hip, knee, and ankle joints [Vukobratović et al. (1990)]. It had 7 pneumatic actuators and 14 valves. (D) The 'Active Suit,' circa 1978, was a self-contained, microcomputer controlled active exoskeleton powered by servoelectric drives [Vukobratović et al. (1990)]. It had a 100W servoelectric drive for the hip and a 50W servoelectric drive for the knee. (E) The 'Spring Walker', circa 1991, was a complex, human powered, kinematic exoskeleton [Dick et al. (1991)]. The passive spring legs were in series to the human legs. It allowed the human to achieve a moderate running pace.

In 2002, Tsukuba University in Japan developed an exoskeleton called the 'Hybrid Assistive Leg' (HAL-3) [Kawamoto et al. (2002)]. See Figure 3B. The exoskeleton employed harmonic drive motors at the hip, knee, and ankle joints. Power for the motors was supplied by a battery pack mounted on the backpack. The control strategy was to estimate the human's joint torques and use a feed forward algorithm to command torques to the motors. The human joint torques were estimated by measuring the foot's ground reaction force and activation level of the leg muscles. Muscle activation was achieved by measuring the myoelectricity (EMG) signals on the surface of the skin. The ground reaction force was measured using a load cell embedded beneath the exoskeleton foot. At publication, the EMG based control strategy was not fully solved, and the wearer experienced discomforts due to controller errors. The exoskeleton's mass was 17kg.

In 2004, the 'Berkeley Lower Extremity Exoskeleton' (BLEEX) used linear hydraulic actuators to power the hip, knee, and ankle in the sagital plane [Kazerooni et al. (2005)]. See Figure 3C. The exoskeleton is powered by an internal combustion engine which is

located in the backpack. The hybrid engine delivered hydraulic power for locomotion and electrical power for the electronics. The exoskeleton interfaced to the human by means of a vest, waist belt, and boots that clip into snowboard bindings. The control strategy allowed the human to provide the intelligent control while the actuators provided the necessary strength for locomotion. This control algorithm essentially minimized the interaction forces between the human and the exoskeleton. The complex control algorithm was implemented using only measurements from the exoskeleton and not from the human or the human-machine interface. The Berkeley exoskeleton was able to carry a 75lb load at a walking speed of 1.3m/s.

In 2004, Sarcos of Salt Lake City, Utah, created an exoskeleton similar to that of Berkeley [Huang (2004)]. See Figure 3D. Rotary hydraulic actuators were located at the hip and knee with a linear hydraulic actuator for the ankle. Sarcos' control algorithm is similar to that of Berkeley's where the exoskeleton senses what the user's intent is and assists in performing the task. Twenty sensors on each leg are processed by an onboard computer to deliver what Sarcos dubbed, 'Get out of the way control'. Sarcos also has a portable internal combustion engine to deliver the hydraulic power necessary for locomotion. The Sarcos exoskeleton is able to carry a 90kg payload. One drawback for both the Berkeley and Sarcos exoskeletons is that an internal combustion engine may be undesirable for military applications, since the noise from the engine may give away the position of soldiers in a covert operation. At the time of this thesis, none of these three present-day exoskeletons had published metabolic results.

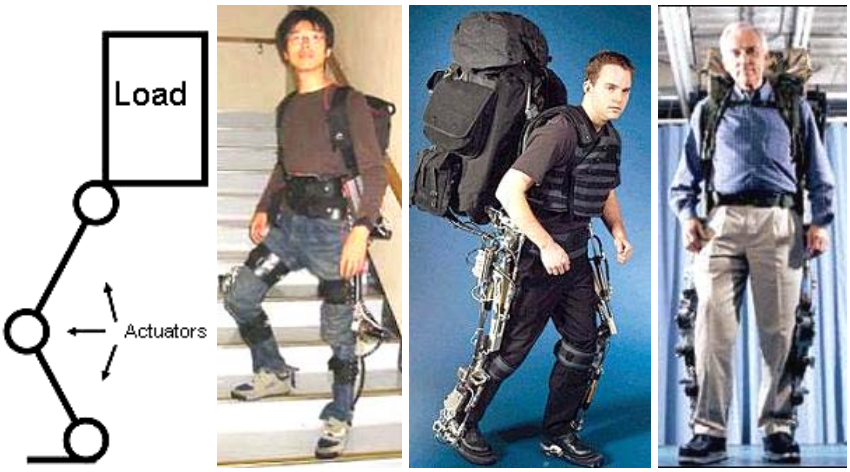

(A) (B) (C) (D)

Figure 3 Present day exoskeletons.
(A) Recent exoskeleton developments have implemented three actuators per leg. (B) Tsukuba University's Hybrid Assistive Leg (HAL-3) implements servoelectric drives at the the hip and knee which are powered by a battery pack [Kawamoto et al. (2002)]. Hal-3's controller is based on EMG feedback measured from the surface of the leg muscles. (C) The Berkeley Lower Extremity Exoskeleton (BLEEX) uses linear hydraulic actuators at all three joints [Kazerooni et al. (2005)]. An internal combustion engine provides the necessary electric and mechanical power for the exoskeleton. (D) The Sarcos exoskeleton implements rotary hydraulic actuators at the hip and knee and a linear hydraulic actuator for the ankle [Huang (2004)]. The Sarcos exoskeleton is also powered by a small internal combustion engine which can be mounted in the backpack. All three of these mentioned exoskeleton implement a variation of 'get out of the way' control in which the controller senses the intention from the human and amplifies the torques needed for locomotion.

Recent trends in exoskeleton development have placed emphasis on powered exoskeletons for load carrying, adding power to the hip and knee joints. Powered exoskeletons for military applications are estimated to require 600 W of steady state power at running speeds when carrying a maximum payload [Jansen et al. (2000)]. Supplying this amount of power cannot be achieved using current battery technology, but can be realized with a small internal combustion engine that can be mounted in the backpack [Kazerooni (1996)].

A powered exoskeleton may be more complex than necessary to achieve a metabolic reduction for load carrying for level ground walking. Is it possible to achieve this goal with a simpler architecture?

1.3 Biomechatronics Quasi-Passive Exoskeleton

The MIT Biomechatronics group approached the exoskeleton load carrying problem via a different paradigm. The exoskeleton described in this thesis is quasi-passive and

non-actuated. The fundamental exoskeleton architecture was inspired by biological design. Humans walk in an inverted pendulum fashion, in which they alternate pivoting over each of their legs as seen in Figure 4 [Farley et. al. (1998)]. Thus, when the human's foot is on the ground, the exoskeleton is designed to act as a rigid column and transfer the forces from the loaded backpack to the ground. When the human foot is off the ground, the exoskeleton is designed to track with the motion of the leg with minimal impedance. The exoskeleton is also designed with passive elements which help minimize the energy that the human would have to exert for walking. The exoskeleton is quasi-passive since a minimal amount of power (2W) is required for the electronic damper.

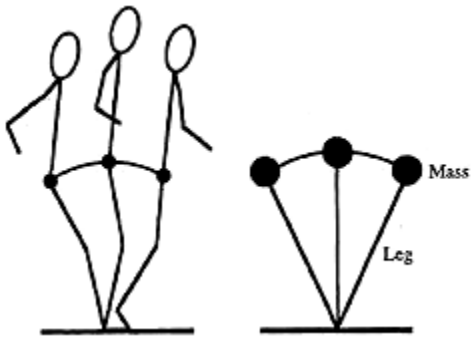

Figure 4 Inverted pendulum motion model for walking [Farley et. al. (1998)]
The exoskeleton is desired to mimic the functionality of the human leg. When the exoskeleton leg is on the ground, it acts as a rigid column allowing the backpack load to pivot over it. When the exoskeleton leg is off the ground, it does not hinder motion but rather tracks the motion of the leg.

Instead of actuators, the exoskeleton contains springs at the hip and ankle joints that store and release mechanical energy throughout the gait cycle. An electronic damper is implemented to dissipate negative power at the knee joint. The hip and ankle springs store energy during periods of negative joint power causing a torque about the joint. The torque assists locomotion during the subsequent period of positive joint power. The torque required by the human is thus reduced, which minimizes the mechanical power required by the human for locomotion. It is reasoned that the less power the human would have to exert, the lower the metabolic cost. However, the spring and damper elements may or may not lower the metabolic cost for walking. Each passive element added to the exoskeleton leg is an additional distal mass. Distal mass has been shown to increase the metabolic cost of walking [Royer et al. (2005)]. Would the energy advantages of the passive elements merit the additional distal mass on the leg?

The exoskeleton interfaces to the human via shoulder straps, a waist belt, thigh cuffs, and a shoe connection. The intimate fit between the exoskeleton and the human enables the exoskeleton to passively track the human's leg motion. The exoskeleton is implemented with three degrees of freedom at the hip, one for the knee, and one for the ankle. A cam mechanism is implemented at the hip joint to enable hip abduction/adduction. The exoskeleton is human controlled, except for the electronic knee damper which has a microprocessor to vary damping. Power for locomotion is supplied by the human and the regenerative energy elements located at the hip and ankle. A small battery powers the electronic knee damper which is sufficient energy for one day. The electronic damper consumes an average of 2W of power for normal walking.

1.4 Thesis Overview

This thesis postulates the following thesis statements and attempts to answer them.

- Hypothesis 1: I hypothesize that a quasi-passive leg exoskeleton implementing elastic storage elements at the hip and ankle and a dissipative variable damper at the knee will improve metabolic walking economy for carrying a 75lb load compared with unassisted loaded walking.
- Hypothesis 2: I hypothesize that a quasi-passive leg exoskeleton implementing elastic storage elements at the hip and a dissipative variable damper at the knee will improve metabolic walking economy for carrying a 75lb load compared with a leg exoskeleton without any elastic energy storage or variable-damping capability.

Table 1 Hypotheses stated

This road map of this thesis proceeds as follows:

Chapter 2 presents an analysis of biomechanics data to gain insight in how to implement energy passive elements to minimize the residual energy that the human would need to expend for loaded walking.

Chapter 3 presents the mechanical design of the exoskeleton. Kinematics theory was applied to co-locate the exoskeleton joints to the human joints as best as possible. Mechanical design was done to implement passive elements into the exoskeleton.

Chapter 4 covers the experimental methods and metrics used to measure the effectiveness of the exoskeleton. The metric for determining the exoskeleton benefit was to quantify metabolic cost, which measures the volume of oxygen consumption.

Chapter 5 presents the metabolic results in comparing walking with a 75 lb load with and without the exoskeleton.

Chapter 6 is a discussion on those results and possible explanations.

Chapter 7 presents the next steps and future work that arise from the discussion of the results.

Chapter 8 presents the final conclusions of this thesis.

1.5 Completed Exoskeleton

Figure 6 is a photograph of the completed exoskeleton with both legs fully abducted. The backpack carried a payload of 75lb. The exoskeleton weighed 34 lb and had a mass of 15kg. The mass distribution of the exoskeleton is shown in Figure 5.

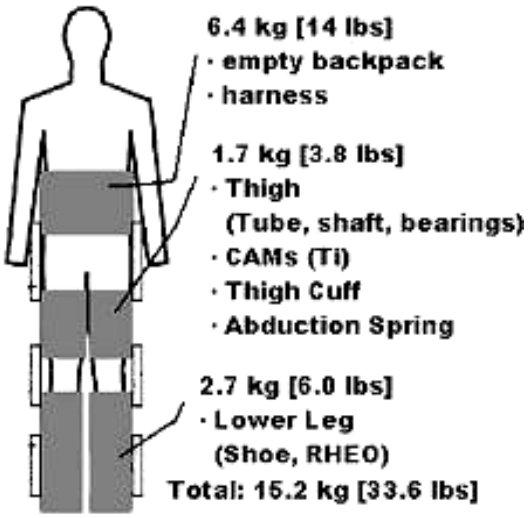

Figure 5 Distribution of exoskeleton mass

Figure 6 The author in all his glory - wearing the completed exoskeleton

The exoskeleton interfaced to the human by means of the backpack shoulder straps, a waist belt, thigh cuffs, and cycling shoes. The exoskeleton hip joint has 3 degrees of freedom to mimic the biological ball and socket joint. Hip extension/flexion is realized by a rotary Kaydon bearing, abduction/abduction is realized by the means of a cam mechanism, and the hip yaw is realized by means of a plain Igus bearing located above the knee. Since the exoskeleton hip joint is not co-located to the biological hip center, a discrepancy in leg length between the exoskeleton and biological legs occur when the hip is abducted. The cam mechanism corrects for this leg length discrepancy and projects the exoskeleton hip center near the biological hip center. Springs are implemented in the

design at the hip and ankle to reduce the residual energy that the human would have to expend for walking. The carbon fiber foot-ankle and variable-damping knee are both products manufactured by Össur of Reykjavik, Iceland.

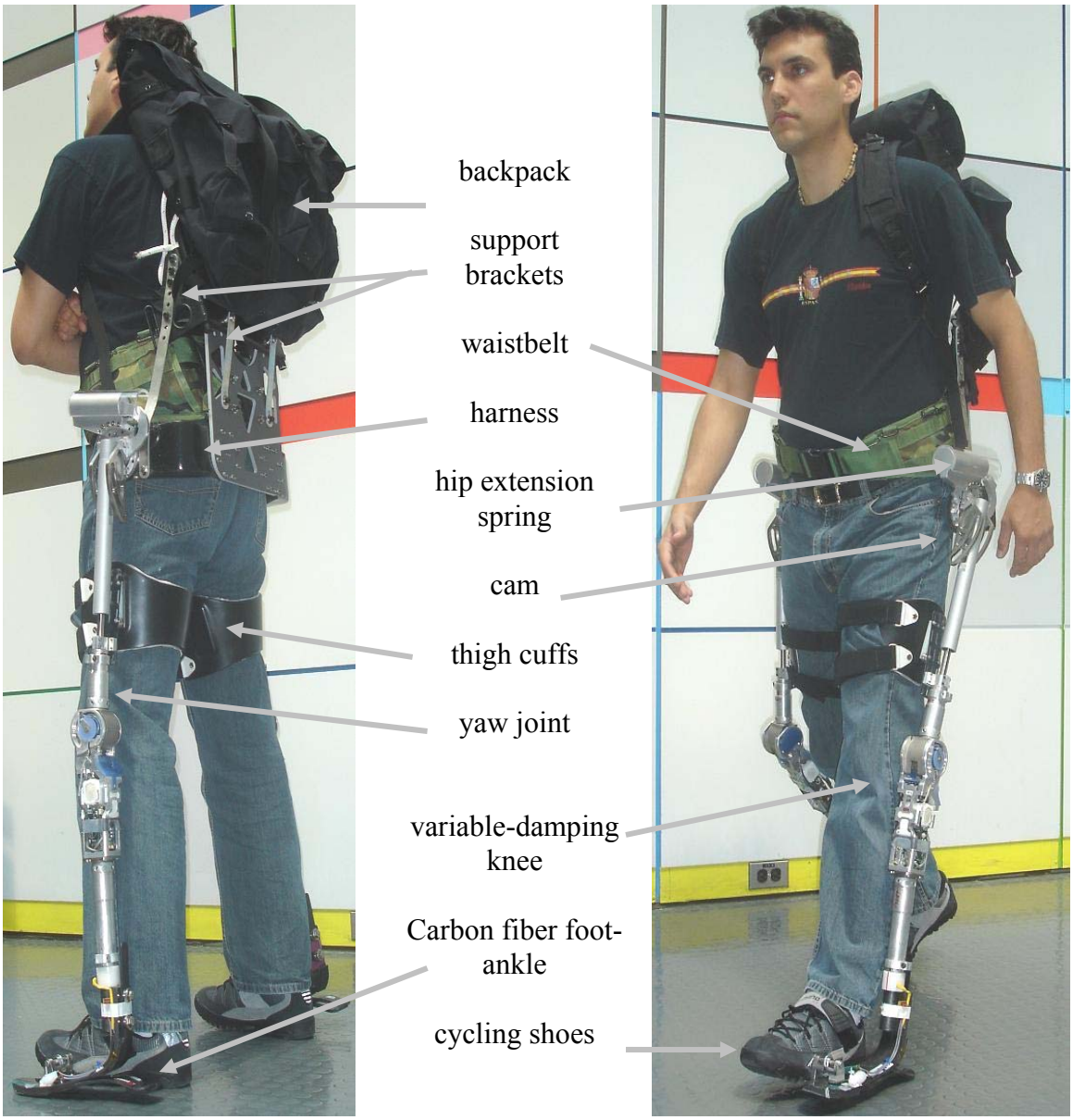

Figure 7 Exoskeleton architecture and major components
The exoskeleton was designed to track the human leg motion. Three degrees of freedom were implemented at the hip, one at the knee, and one at the ankle. The exoskeleton interfaces to the human through shoulder straps, a waist belt, thigh cuffs, and a shoe attachment.

1.6 Definitions

This thesis describes various parts of the body and their movements. Figure 8 outlines the definitions for describing the different planes and axis of the body.

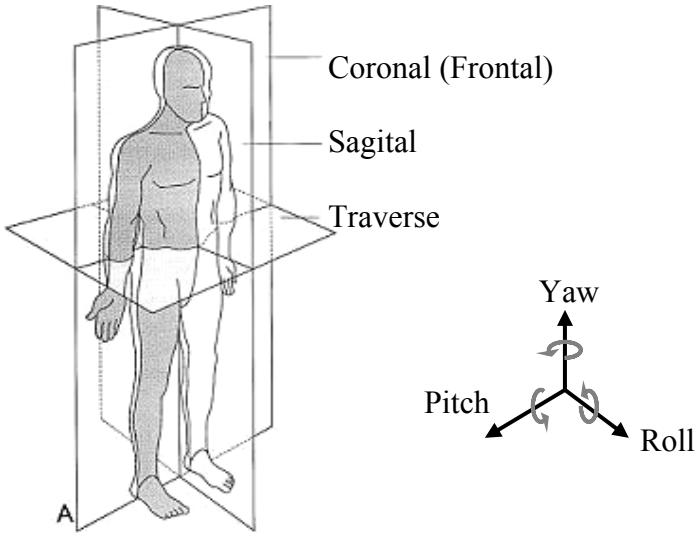

Figure 8 Body plane and axis definitions [Sutherland, et al. (1994)]

Chapter 2 Passive Element Optimization

2.1 Introduction

Passive elements were implemented in the exoskeleton to either store or dissipate energy with the objective of reducing the residual energy that the human would have to expend for locomotion. It was found that unidirectional springs should be implemented at the hip and ankle joints and a damper for the knee joint. Biomechanics data of the hip, knee, and ankle joints was analyzed to optimize the spring constants and damper values. The cost function was to minimize the residual power. Microsoft Excel's Solver was used as the optimizing method. The resulting spring constants and damper that were found are tabulated below in Table 2 along with the decrease in energy that they provided.

Torsional Hip Spring		
Spring Constant	1043	[lb-in/rad]
Spring Constant	118	[Nm/rad]
Engagement Angle	21.1	[deg]
Energy Decrease	**62**	[%]
Linear Hip Spring		
Spring Constant	111	[lb/in]
Spring Constant	19432	[N/m]
Hip Moment Arm	3	[in]
Engagement Angle	21.1	[deg]
Energy Decrease	**62**	[%]
Knee Damper		
Damping Constant	4.2	[Nm-s/rad]
Engagement Period	54 < %gc < 62	[%gait cycle]
Energy Decrease	**23**	[%]
Torsional Ankle Spring		
Spring Constant	7703	[lb-in/rad]
Spring Constant	870	[Nm/rad]
Engagement Angle	-0.5	[deg]
Energy Decrease	**50**	[%]
Total Energy Decrease	**46**	[%]

Table 2 Summary of results from the passive element optimization

Several key assumptions were made in conducting this analysis. The data set used for the kinematic analysis was not exoskeleton data, but rather kinematic data from Natick Army Labs based on a participant walking normally and carrying a 47kg backpack [Harman (2000)]. It was decided that this data set could be used to analyze the exoskeleton to a first order approximation. It was also assumed that the gait kinematics remained unchanged despite the addition passive elements. Although, the passive elements may alter the kinematics since the exoskeleton is a dynamic system, the results of the analysis were still implemented as a first order approximation. Chapter 7 suggests acquiring biomechanic data directly from the exoskeleton with the passive springs implemented. This new data set would enable a more accurate kinematic analysis leading to more accurate passive element values.

2.2 Motivation

The power characteristics of the leg throughout the walking cycle suggest that it may be possible to implement passive elements at the hip, knee, and ankle joints to either store or dissipate energy throughout the walking cycle thus reducing the metabolic load on the human. Springs as energy storage elements can be implemented at joints that have a period of negative power followed by a period of positive power. The spring could store energy during the negative power period and release it during the positive power period. I hypothesize that with the introduction of passive elements to the exoskeleton joints, the human muscles would absorb less negative power and produce less positive power, thus providing metabolic advantages. The metabolic cost of absorbing power is 0.3 to 0.5 times that of producing power [De Looze et al. (1994)]. Dampers can be implemented for joints that mainly dissipate energy. These dissipative joints have a negative average joint power. The hip and ankle both have periods of negative power followed by a period of positive power and are candidates for implementing a spring to store and release energy throughout the gait cycle. The knee joint has a negative net average power throughout the gait cycle and is a candidate for implementing a damper.

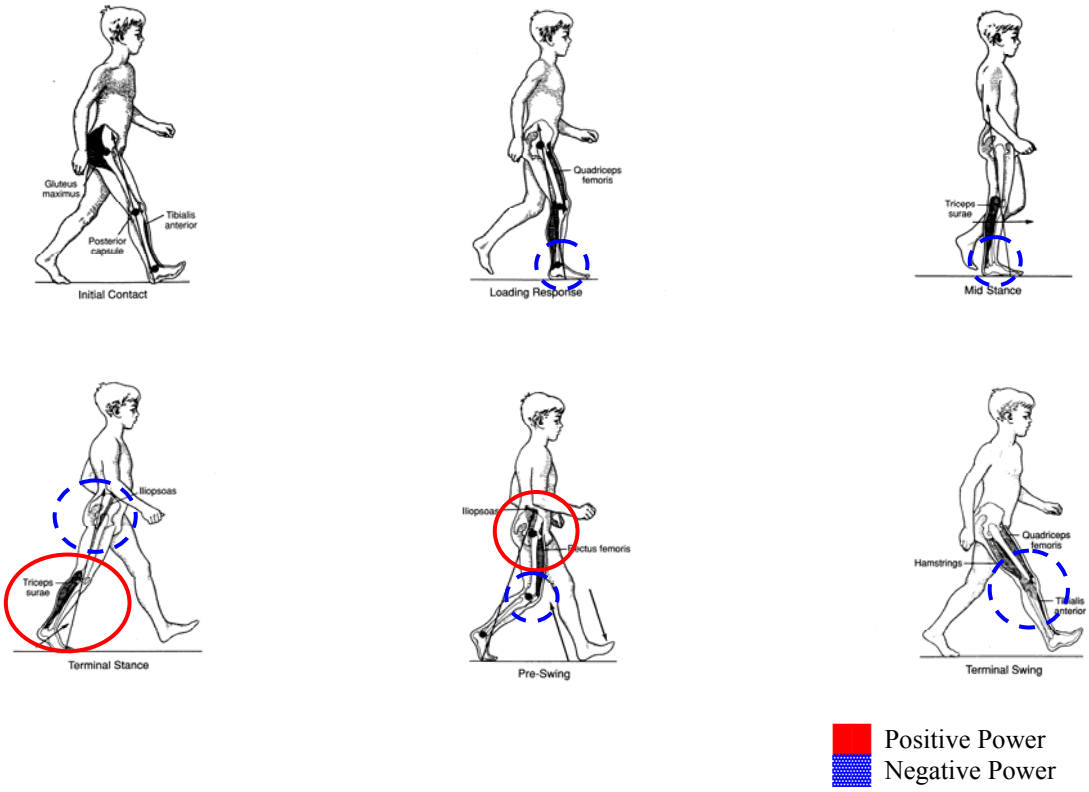

Figure 9 Negative and positive joint power during walking [Rab (1994)]
If a period of negative power precedes a period of positive power than it may be possible to capture the negative power in a spring and release it during the positive power period. This is such the case for the hip and ankle, where a spring may be implemented at these joints. The knee however, mostly dissipates energy throughout the walking cycle and is best suited with a damper located at this joint.

Biomechanics data was analyzed to find the desired spring and damper values. The springs created a torque about the joints reducing the torque required by the human. The spring and damper values were optimized such that the residual power that human needed to exert was minimized.

Adding passive elements to the legs for walking has been studied previously by Antonie Bogert in 2003 and Daniel Paluska and Hugh Herr in 2004. Antonie Bogert developed a simulation of an exoskeleton that comprises of co-located pulleys at the hip, knee, and ankle joints and a long elastic cord that would wrap around the pulleys [van der Bogert (2003)]. Bogert optimized the pulley diameters to minimize the residual power that the human would need to exert. One case consisted of two 'exotendons', one for each leg, that span across three pulleys across all three leg joints. Another case used two six-joint 'exotendons' and 12 pulleys, where each 'exotendon' went across both legs. Dan Paluska and Hugh Herr looked at energetics of the ankle. Paluska and Herr analyzed

the ankle using Bogert's data and found that during specific periods of the gait cycle, an ankle could be modeled as a spring. For normal unloaded walking, they calculated a torsional ankle stiffness for a 70 kg person. Motivated by the human body's gastroc and soleus muscles, Paluska modeled a bi-articular clutched tendon that would involve the ankle and knee joints [Paluska (2004)]. His two-clutch, single tendon model was able to produce an energy savings similar to that of Bogert's 12 pulley model. These results from these individuals are summarized in the table below.

	Leg Power Reduction [%]	Stiffness	
Bogert 3-joint exotendons, 6-pulleys, 2 tendons	47%		
Bogert 6-joint exotendons, 12-pulleys, 2 tendons	74%		
Paluska bi-articular clutched tendon , 4 tendons	75%		
Paluska normal ankle stiffness result		300	[Nm/rad]
		4.3	[Nm/rad-kg]

Table 3 Summary of results from Bogert and Paluska/Herr

The results from Bogert and Paluska reaffirm that it may be possible to implement springs in the exoskeleton to reduce the residual power required by the human for walking.

2.3 Biomechanics Data

2.3.1 Applying Backpack Data for Exoskeleton Analysis

After a careful literature search, loaded exoskeleton data was not available for analysis and design studies. Biomechanics data from Natick Army Labs [Harman et al. (2000)] comprising of ankle, knee, and hip torque as well as ankle and knee angle for walking carrying a 47 kg backpack was obtained. The Harman data is not exoskeleton data, but rather loaded walking data since the participant only walks with a loaded backpack. For the plots in this thesis, this data will be referred to as 'backpack'. An assumption is made that although walking with an exoskeleton may be significantly different than walking with a backpack, the kinematics and kinetics of the Natick backpack data can be applied to the exoskeleton for a first-order analysis. It was decided

to use the Natick data to analyze the biomechanics of the exoskeleton for optimizing the passive elements.

The Harman data set did not include hip angle data, but provided the maximum and minimum hip angles for walking with a 47 kg backpack. The hip angle from a normal walking data set [Bogert (2003)] was scaled to fit the maximum and minimum angle constraints specified by the Harman data set. The angle data for the knee and ankle for both the Bogert and Harman data sets are reasonably similar. Thus, scaling the Bogert hip data set is a reasonable first-order approximation to that of the actual hip angle for a participant carrying a 47 kg backpack.

The total mass of the exoskeleton is 15.5 kg and it carries a payload of 34kg (75lb). The exoskeleton is capable of carrying a larger payload, but 75 lb was chosen as a representative load that a soldier or service personal may carry.

Approximately 6.5 kg of the exoskeleton mass is located around the hips, which would increase the effective backpack load to 40.5kg. An assumption is made that the biomechanics of a 40.5kg effective payload and a 9 kg net exoskeleton mass can be approximated by Harman's biomechanics data of carrying a 47 kg backpack. Table 4 summarizes the participants involved in the MIT and Natick studies.

[n]	Participants	Age [yr]	Sex [M/F]	Payload [kg]	Mass [kg]	Leg Length [m]	Walking Speed [m/s]
1	Participant 1	25	M	34 load + 15.5exo	91	0.94	0.82 ± 0.11
16	Natick / Harman	30 ± 9	16M 0F	47	77 ± 9	0.96 ± .04	1.33 ± 0.18
several	Bogert			0	70	0.9	1.2

Table 4 Summary of data used for analysis

The leg length and body mass for the Harman participants were reasonably close to that of the MIT test participant. The walking speed for the Harman data is 1.33 m/s and the MIT participant's speed was 0.82 m/s. Participant 1's exoskeleton walking speed was self selected, while the Harman data's speed was matched to an average walking speed for humans carrying no load. The faster walking speed in the Harman data set would lead to higher torques and powers. Participant 1's slower walking speed may result in a higher metabolic cost since the springs and dampers were optimized to the Harman data set. Although the walking speed is different between the physical

exoskeleton and the Harman data, the Harman data can be used to give a first-order approximation calculates the passive elements for the exoskeleton. To achieve more accurate results, it would be necessary to have biomechanics data measured directly from the exoskeleton for analysis. Acquiring this data is suggested in Chapter 7.

This thesis contains many plots and the convention for the 'x'-axis for most of them will be '% gait cycle,' which is time normalized. The following figure is a pictorial illustration of the gait cycle. The gait cycle begins with the heel strike.

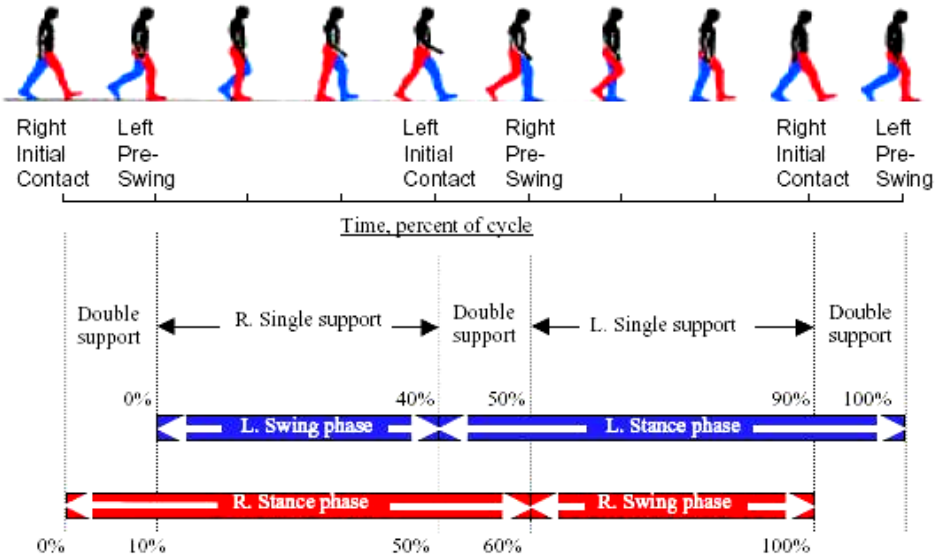

Figure 10 Gait cycle for normal walking [Inman (1981)]

2.3.2 Summary of Data

For the plots in this chapter, the data labeled 'Natural' (---) is the Bogert data set, and the data labeled '47 kg Backpack' (—) is the Harman data set from the Natick Army Labs. The Bogert data set is available online at [http://www.biomedical-engineering-online.com/content/2/1/17], and the Natick data is provided in the appendix of this thesis. Referring Figure 11 and Figure 12, it can be seen that the joint angle and velocity look similar to that of both the Bogert data and the Harman data. Based on qualitative experience looking at biomechanics data, the joint angle difference between the Bogert and Harman data sets are not significant. The joint velocities are slightly larger for the Harman data than that of the Bogert data, and this is because the Harman participants walk at a speed that is 11% greater than that of the Bogert participants. For walking, the

human legs act as an inverted pendulum and the body center of mass pivots over them [Farley et al. (1998)]. Intuitively, since the fundamental inverted pendulum walking motion should not change with the addition of a load, it is reasonable to expect that the joint kinematics are similar.

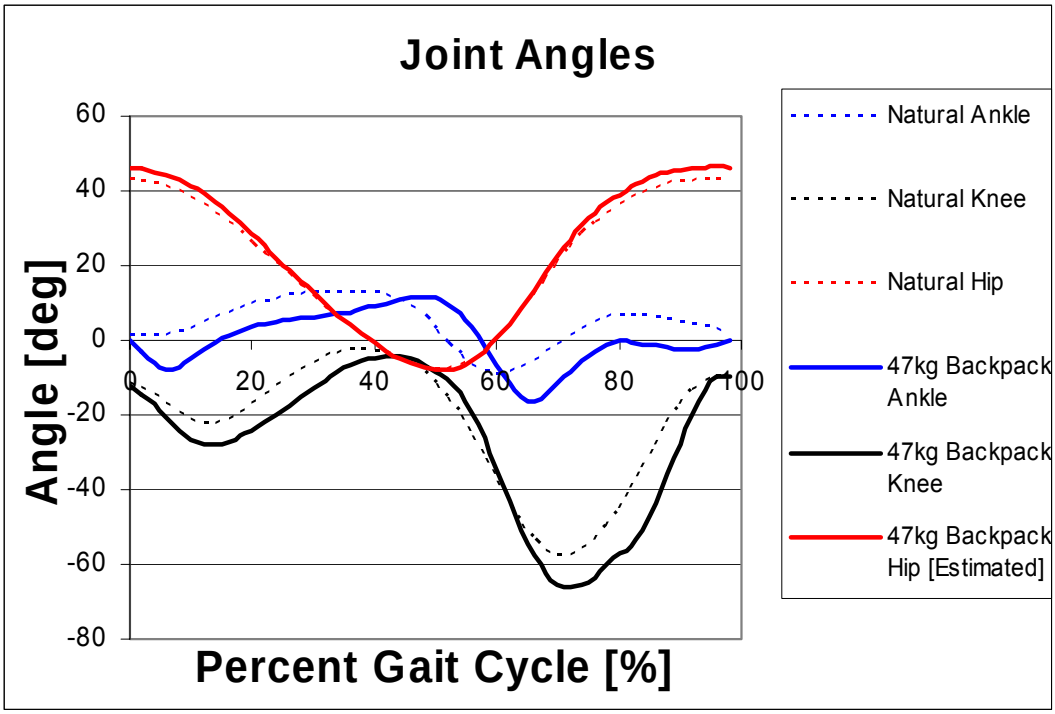

Figure 11 Joint angles, natural and 47 kg backpack

The joint angles for both normal and loaded walking are similar. The human kinematics are not substantially altered when walking with a loaded backpack.

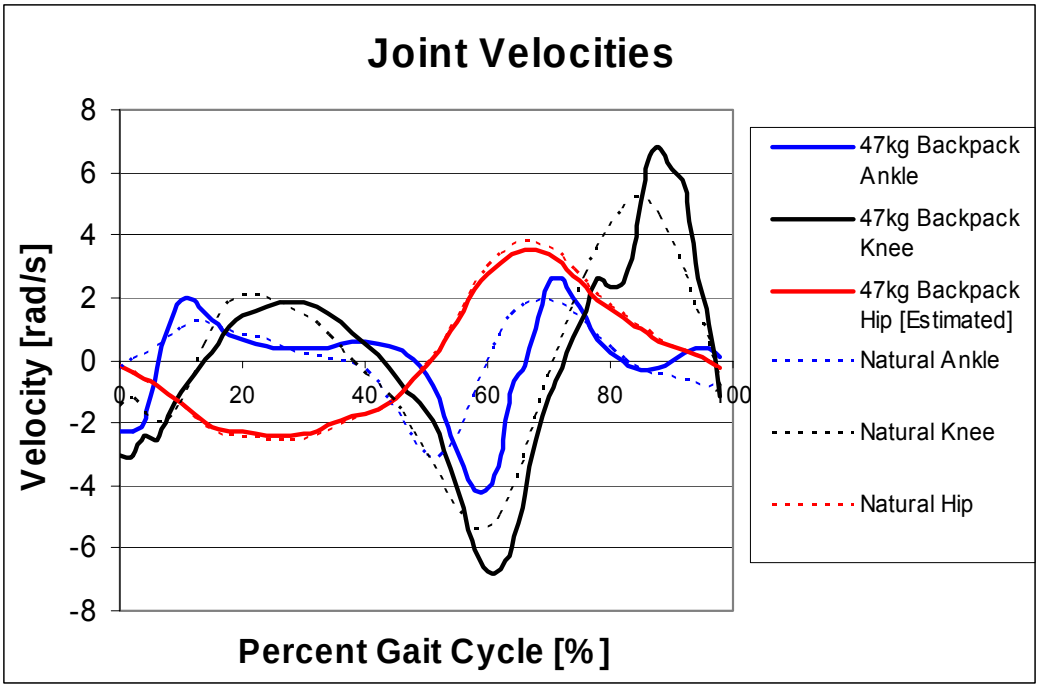

Figure 12 Joint velocities, natural and 47 kg backpack
The joint velocities for the Natick data are slightly larger than Bogert's since the participants for the Natick data walked 11% faster. The human kinematics are not substantially altered when walking with a loaded backpack.

The backpack load did however increase the joint torque and power as compared to the normal unloaded case. This is reasonable since the added load increases the downward force significantly and translates into larger moments. If the walking speed is maintained, then the joint power will also increase since:

$$P = T \cdot \dot{\theta} \tag{2.1}$$

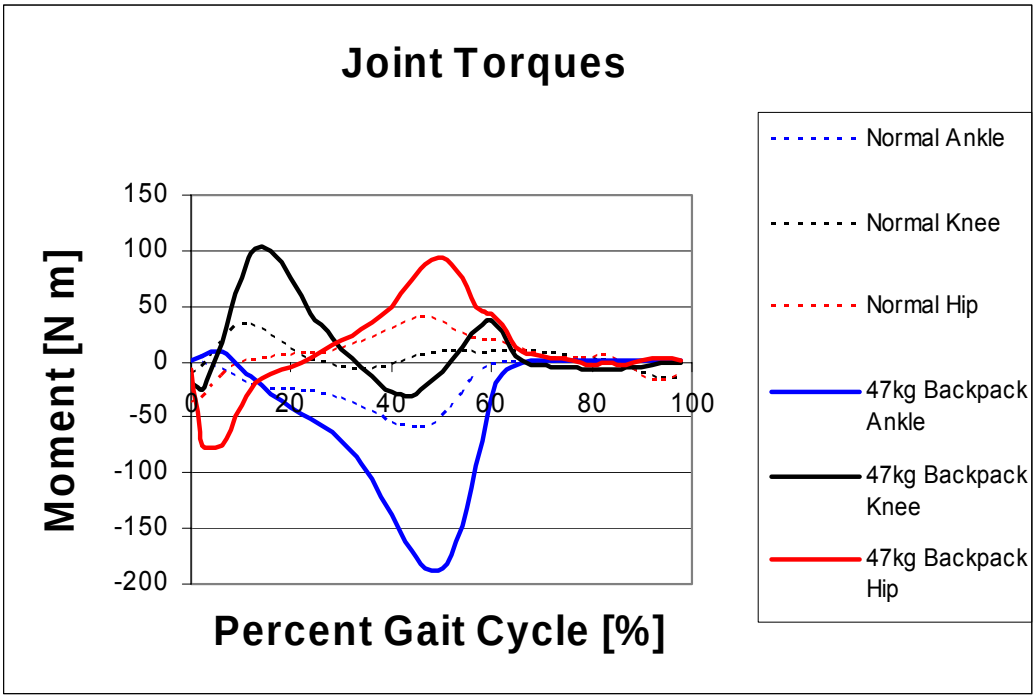

Figure 13 Joint torques, natural and 47 kg backpack
The joint torques were larger for the backpack case compared to normal walking. This is expected since the larger forces are present due to the additional mass on the back.

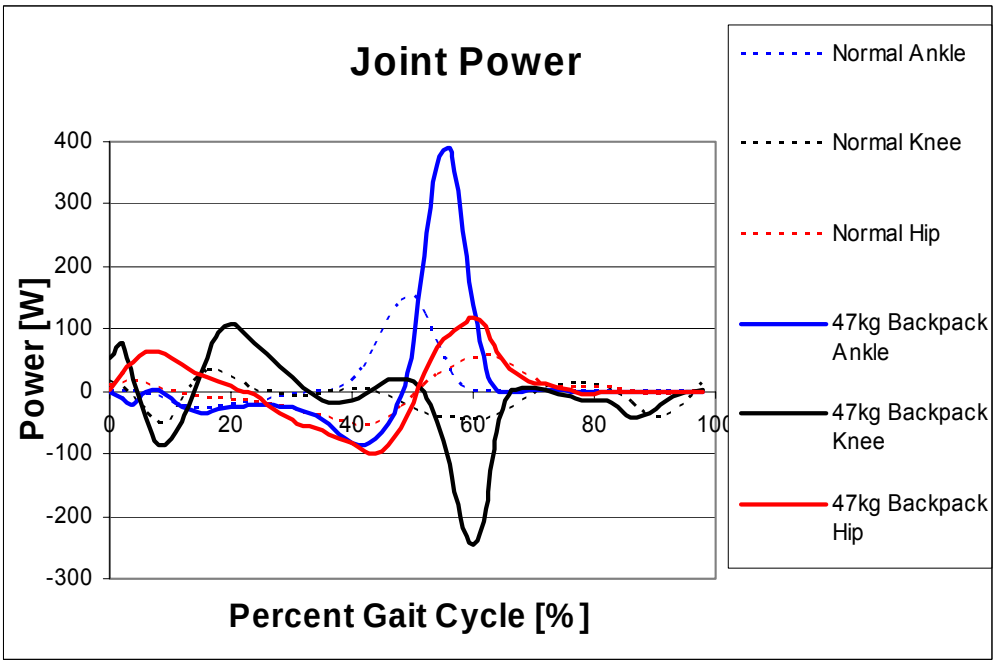

Figure 14 Joint power, natural and 47 kg backpack
The joint powers were larger for the backpack case compared to normal walking. This is also expected since larger forces are present due to additional mass on the back.

2.4 Analytical Methods

2.4.1 Optimizing the Hip and Ankle Springs

The backpack data from Harman was analyzed and optimized to determine how to implement a spring or damper to the exoskeleton to reduce the residual energy that the human would need to exert. Excel and Excel Solver were used to analyze and optimize the data. The optimization function is to minimize residual power that the human had to expend, which is the total joint power minus the passive element power. Optimizing residual power was chosen since the thesis goal is to reduce the human's metabolic cost of carrying a load. Joint torque, T, and joint angle, Θ, were given by the Harman data for an average participant carrying a 47 kg backpack. Angular velocity was calculated by taking the derivative of angular position with respect to time. The walking period was not given but inferred from a chart that tabulated walking cadence, step length, and body height [Skinner (1994)]. The gait period was found to be 1.07 seconds.

$$\dot{\theta} = \frac{d\theta}{dt} \tag{2.2}$$

Mechanical power is calculated by:

$$P = T \cdot \dot{\theta} \tag{2.3}$$

A unilateral spring is chosen to be implemented for the exoskeleton hip and ankle. The unilateral spring would store and release energy during compression, but would be disengaged during extension. This one sided spring mechanism can be implemented simply by fixing the spring to only one of the members. Since the spring is unilateral it will only compress when the joint angle exceeds a specific threshold and transmit a torque. If the joint angle is less than the specified threshold angle, then the spring will not compress and energy will not be stored. The force in the spring is given by the following formula where 'Θ' is the joint angle and 'k' is the spring constant.

$$\text{Spring Force} = \begin{cases} k \cdot (\theta - \theta threshold) & if \quad \theta > \theta threshold \\ 0 & if \quad \theta < \theta threshold \end{cases} \tag{2.4}$$

The spring force can be converted to a torque by multiplying by the moment arm between the location of the spring and the center of rotation of the joint, where 'r' is the

moment arm length. If the moment arm is not included, as in the case for the ankle, then the spring constant 'k' is calculated as a torsional spring rather than a linear spring.

$$\text{Spring Torque} = \begin{cases} r \cdot k \cdot (\theta - \theta threshold) & if \quad \theta > \theta threshold \\ 0 & if \quad \theta < \theta threshold \end{cases} \tag{2.5}$$

The spring would reduce the torque and power required for locomotion. The residual torque and residual power that would be required by the human are given by the following formula where 'T' is the total torque required by the human.

$$\text{Residual Torque} = \begin{cases} T - r \cdot k \cdot (\theta - \theta threshold) & if \quad \theta > \theta threshold \\ T & if \quad \theta < \theta threshold \end{cases} \tag{2.6}$$

$$\text{Residual Mechanical Power} = \begin{cases} \left[T - r \cdot k \cdot (\theta - \theta threshold)\right] \cdot \dot{\theta} & if \quad \theta > \theta threshold \\ T \cdot \dot{\theta} & if \quad \theta < \theta threshold \end{cases} \tag{2.7}$$

It is assumed that adding a spring at the hip and ankle will not alter the leg kinematics. This is a major assumption since the exoskeleton is a dynamic system, and adding spring elements will most certainly affect the leg kinematics. Since modeling how the kinematics change cannot be easily analyzed, it is assumed for a first-order approximation that the kinematics will be approximately the same. For future work, it would be recommended to measure the joint kinematics with the springs implemented using a Vicon camera system, which is available at Spaulding Rehabilitation Center in Boston, MA.

Since the goal is to reduce the metabolic cost of load carrying and increase the endurance of the exoskeleton wearer, the cost function to be minimized is the average residual power that the human would have to expend. It has been shown that the metabolic cost related to negative work is 0.3-0.5 times that of positive work [De Looze (1994)]. As a conservative estimate, 0.5 will be used as a weighting factor on the negative power. Considering this, the residual power cost function to be minimized is:

$$\text{MIN}\left[\frac{\sum \left|Positive\ \text{Re}\,sidual\right| + 0.5 \cdot \sum \left|Negative\ \text{Re}\,sidual\right|}{\sum \left|Total\ Positive\right| + 0.5 \cdot \sum \left|Total\ Negative\right|}\right] \tag{2.8}$$

And the percent savings is given by:

$$1 - \left[\frac{\sum \left| Positive\ \mathrm{Re}sidual \right| + 0.5 \cdot \sum \left| Negative\ \mathrm{Re}sidual \right|}{\sum \left| Total\ Positive \right| + 0.5 \cdot \sum \left| Total\ Negative \right|} \right] \tag{2.9}$$

The following variables in Table 5 are adjusted in Excel Solver to minimize the residual power that the human had to exert.

- k a linear spring constant in [N/m] with a moment arm specified
- k a torsional spring constant in [Nm/rad] with no moment arm
- $\Theta_{threshold}$ the spring engagement angle in [deg]

Table 5: Spring variables for residual energy minimization
Excel solver was used for the optimization and k and $\Theta_{threshold}$ were varied by Excel.

To implement a spring at a joint, it can be intuitively justified by looking at the power plots of the joints. These plots will be show later in this chapter. A spring can be implemented where there is a period of negative power followed by a period of positive power. This way, the spring can store energy during a period of negative power and release it during a period of positive power therefore reducing the power that the human leg would have to absorb or generate.

2.4.2 Optimization Algorithm for a Knee Damper

The exoskeleton knee joint mostly dissipates energy throughout the walking cycle. A damper in parallel with the human knee can dissipate the negative power and lessen the power that the human knee would have to absorb. Again, the optimization function is to minimize residual power that the human would have to expend. A rotary damper was chosen for the exoskeleton knee to provide a torque given by the following formula where 'B' is the dampening constant.

$$\text{Damper Torque} = \begin{cases} B \cdot \dot{\theta} & if \quad damper\ enabled \\ \sim 0 & if \quad damper\ disabled \end{cases} \tag{2.10}$$

It will be assumed that the damper can be enabled and disabled. The residual torque and residual power are therefore:

$$\text{Residual Torque} = \begin{cases} T - B \cdot \dot{\theta} & if \quad damper\ enabled \\ \sim T & if \quad damper\ disabled \end{cases} \tag{2.11}$$

$$\text{Residual Mechanical Power} = \begin{cases} \left[T - B\cdot\dot{\theta}\right]\cdot\dot{\theta} & \text{if damper enabled} \\ \sim T\cdot\dot{\theta} & \text{if damper disabled} \end{cases} \quad (2.12)$$

The cost function to minimize residual power for the damper case is equivalent to that of the spring case. The variables that can be adjusted to achieve the minimization are shown in Table 6. The gait cycle period was selected manually to match the large power spike in the swing-leg 'K4' region of Figure 16. Excel solver was used to vary the damping constant, 'B', to minimize the residual energy. Adding damping at the 'K1' region was not considered for reasons that will be discussed in section 2.4.4.

- B — the damping constant in [Nm-s/rad]
- $\%gs_{start}$, $\%gs_{end}$ — % gait cycle when damper is engaged and disengaged

Table 6: Damper variables for residual energy minimization
Excel solver was used for the optimization and B varied by Excel. $\%gs_{start}$, $\%gs_{end}$ were selected manually and set during the region of largest negative power.

2.4.3 Hip Power

Referring to the 'hip power' plot in Figure 15, a spring can be placed to store the negative energy produced by the region 'H2' and released afterwards during the period 'H3'. It can also be seen that an engagement angle around 20 degrees should be expected.

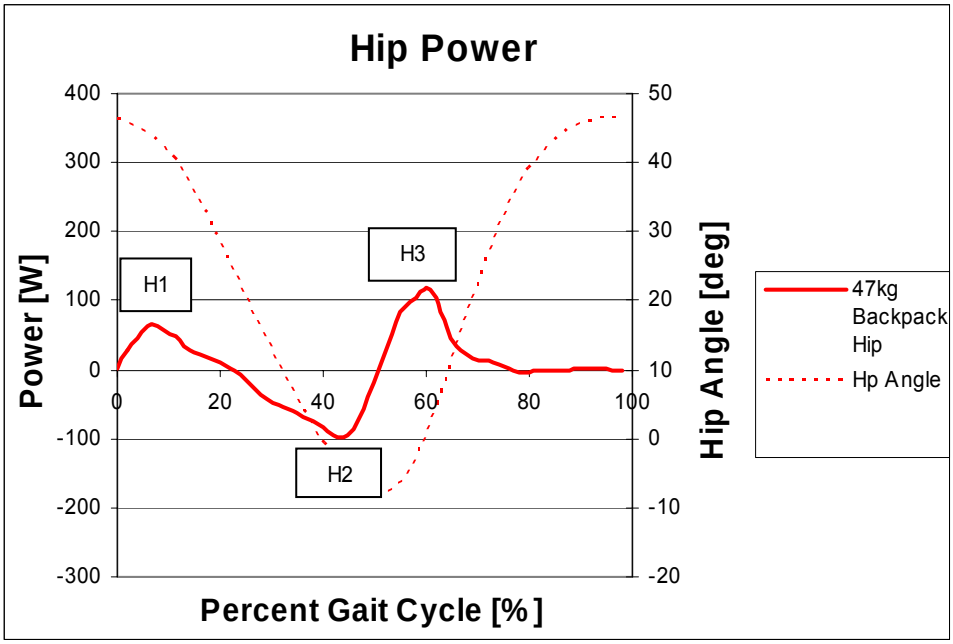

Figure 15 Hip power [Harman et al. (2000)]
Possible Explanations: (H1) Positive Power – Stabilization during heel strike. (H2) Negative Power – Body pendulums over the leg and stretches the quadriceps. (H3) Positive Power – Swinging the leg forward

2.4.4 Knee Power

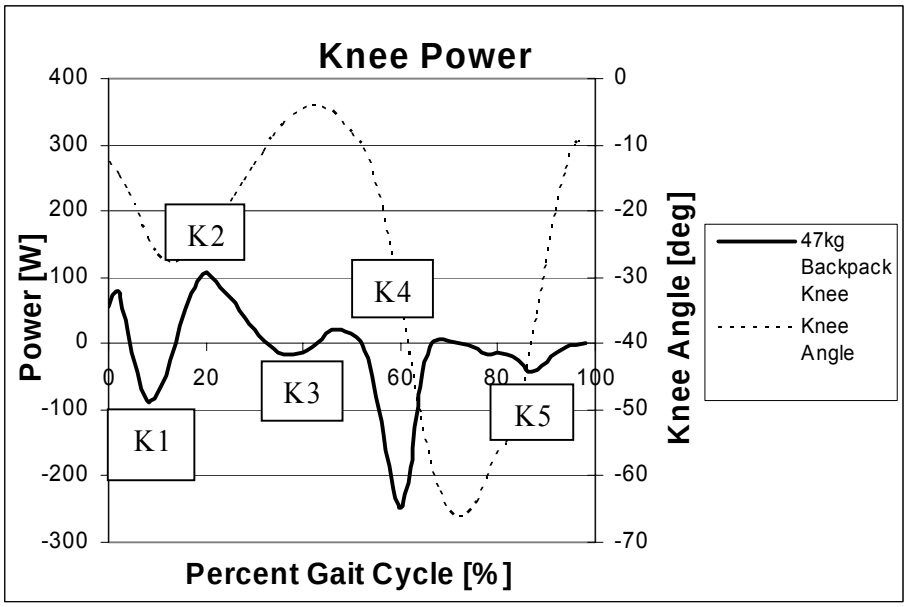

Figure 16 Knee power [Harman et al. (2000)]
Possible Explanations: (K1) Negative Power – Knee braking/bending after heel strike. (K2) Positive Power – Knee straightening. (K3) Negligible Power – Body's inverted pendulum motion over the leg. (K4) Negative Power – Knee bending during pre-swing and swing phase. (K5) Negative Power – Slowing of leg in terminal swing.

Referring to the 'knee power' plot in Figure 16, the only candidate period for a spring is in the 'K1-K2' region. This region is the period of walking that is shortly after heel strike when the knee quickly flexes and straightens during early stance. This quick flex and straightening motion is undesirable for the exoskeleton since it is preferred that the exoskeleton leg remain straight during this period. When the exoskeleton leg is completely straight, it acts as a column and all the downward vertical forces from the payload get transmitted through the exoskeleton leg. If the exoskeleton leg flexes after the heel strike impact, then the load bearing column effect is not supporting the load and the human leg has to bear the load. From wearing the exoskeleton, it is quite unpleasant when the exoskeleton is nicely carrying the payload and then for a split second the weight that the human has to support increases by 75 lbs. The 75lb force spike may have adverse effects on the human gait and it is expected to not be metabolically efficient.

Therefore, it is preferred that once the exoskeleton leg strikes the ground, it remains locked so that it can transfer the load to the ground while the body's center of mass pivots over the leg. If this walking cadence is executed correctly and the knee stays straight when the exoskeleton leg is on the ground then both the negative 'K1' region and the positive 'K2' region are quite flat and almost non-existent. This leaves regions 'K3', 'K4', and 'K5' to be considered. It can be seen in Figure 16 that an integration of power over these three regions is negative and that a dissipative element is more fitting for these regions than a spring. If a dissipative element such as a damper is tuned correctly to absorb all the energy in the 'K4' region a metabolic advantage could be attained since that is power that the human leg does not have to absorb. Another idea is to still use a spring and store the negative power in the 'K4' region, and then through some mechanism transfer that energy to another joint that could benefit from it. This is exactly what motivated Dan Paluska and Hugh Herr with the bi-articular clutched tendons, which was discussed in section 2.2. Their approach was to transfer the energy from the 'K4' region of the knee to the ankle by means of a spring and two clutches [Paluska (2004)]. Implementing a functioning dual clutch tendon mechanism is not trivial, it was decided that for this thesis to simply use a damper and dissipate the energy. The variable-damping knee that was chosen was developed by Hugh Herr and the MIT Leg Lab in the 1990's [Herr et al. (2003); Deffenbaugh et al. (2001)].

Integrating the knee power over the gait cycle shows that the overall knee power is largely negative. This observation is consistent for both the Harman and Bogert data sets.

47KG BACKPACK DATA (data from Harman)
Normalized Integrated Power

	positive energy	negative energy	total energy	% positive
hip	0.16	0.13	0.29	0.56
knee	0.12	0.22	0.34	0.36
ankle	0.24	0.13	0.37	0.65
totals	0.53	0.47	1.00	0.53

NORMAL DATA (data from Bogert)
Normalized Integrated Power

	positive energy	negative energy	total energy	% positive
hip	0.16	0.19	0.35	0.45

knee	0.07	0.25	0.32	0.22
ankle	0.26	0.07	0.34	0.78
totals	0.49	0.51	1.00	0.49

Table 7 Summary of positive/negative energy of joints
It can be seen that the knee mostly dominated by negative power. This motivates that a damper be implemented for the exoskeleton knee.

2.4.5 Ankle Power

The ankle has the largest peak power when compared to the other joints, so there is a definite advantage to minimizing residual power at this joint. Similar to the hip, it would be ideal if a spring element could capture the negative power of the 'A1' region and release it during the 'A2' peak. It is not intuitive as to what angle the ankle spring should engage at.

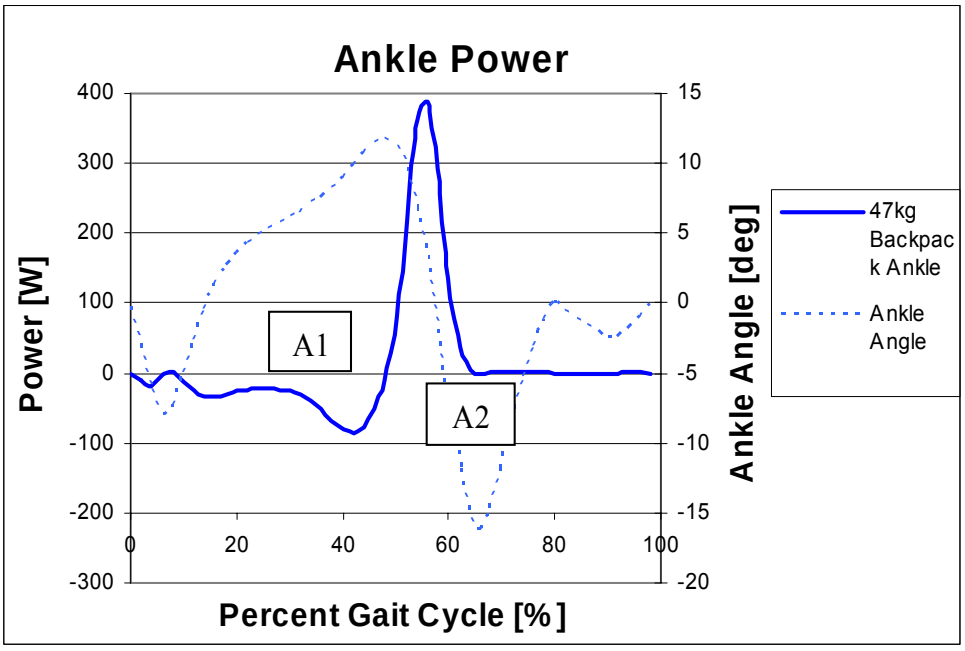

Figure 17 Ankle power [Harman et al. (2000)]
Possible Explanations: (A1) Negative Power – Extending ankle during heel strike. (A2) Positive Power – Propulsive plantar flexion to thrust body forward and pre-swing the leg

2.5 Analytical Results

2.5.1 Summary of Results

The results from the aforementioned outlined analysis are summarized below. The hip results is given by both a torsional spring constant as well as a linear spring constant with a given moment arm. The hip engagement angle, when the spring starts to be compressed, is defined in front of the body (flexion). The knee result is given by a dampening constant and by a period of gait cycle when the damper should be activated. The ankle result is given by a torsional spring constant with an engagement angle of -0.5 degrees, which for practical purposes is 0.0 degrees, or when the ankle is at a right angle.

Torsional Hip Spring		
Spring Constant	1043	[lb-in/rad]
Spring Constant	118	[Nm/rad]
Engagement Angle	21.1	[deg]
Linear Hip Spring		
Spring Constant	111	[lb/in]
Spring Constant	19432	[N/m]
Hip Moment Arm	3.07	[in]
Engagement Angle	21.1	[deg]
Knee Damper		
Damping Constant	4.2	[Nm-s/rad]
Engagement Period	$54 < \%gc < 62$	[%gait cycle]
Torsional Ankle Spring		
Spring Constant	7703	[lb-in/rad]
Spring Constant	870	[Nm/rad]
Engagement Angle	-0.5	[deg]

Table 8 Summary of passive elements implemented in the exoskeleton

Implementing the above values provided a decrease in the energy that the human would have to expend for walking with the exoskeleton. Two sets of results are presented. The first is a weighted case that penalizes negative power as 0.5 times as costly to that of positive power [De Looze (1994)]. The un-weighted results, which have an equal cost on positive and negative power, are also presented. The analytical results from this chapter are summarized in the table below. Since the integration to determine these results was done over percent gait cycle, rather than time, the units for this energy is defined as 'energies'.

The percent energy savings from adding the passive elements is given by the below equation. It calculates the percent energy benefit of adding the passive components. It also weights negative power to cost half as much as that of positive power.

$$1 - \left[\frac{\sum \left| Positive\ \mathrm{Re}\, sidual \right| + 0.5 \cdot \sum \left| Negative\ \mathrm{Re}\, sidual \right|}{\sum \left| Total\ Positive \right| + 0.5 \cdot \sum \left| Total\ Negative \right|} \right] \tag{2.13}$$

Weighted (cost of negative power = 0.5 cost of positive power)			
	Weighted Backpack [energies]	Weighted Residual [energies]	%Decrease [energies]
Hip	1456	548	**62%**
Knee	1482	1145	**23%**
Ankle	1930	957	**50%**
Total	4868	2651	**46%**
Un-weighted (cost of negative power = cost of positive power)			
	Backpack [energies]	Residual [energies]	%Decrease [energies]
Hip	1863	653	65%
Knee	2183	1509	31%
Ankle	2334	1012	57%
Total	6380	3174	50%

Table 9 Energy benefit due to passive elements
The theoretical benefit of the passive elements was computed two different ways. In the first case, negative power is weighted half as much as positive power [De Looze (1994)]. In the second case, positive power and negative power are equally weighted.

A summary of the joint residual power that the human has to expend for walking with the spring/damper optimized exoskeleton are summarized in Figure 18. The residual joint power is compared to the total joint power that would be needed for walking with the exoskeleton. The details of this plot will be explored further.

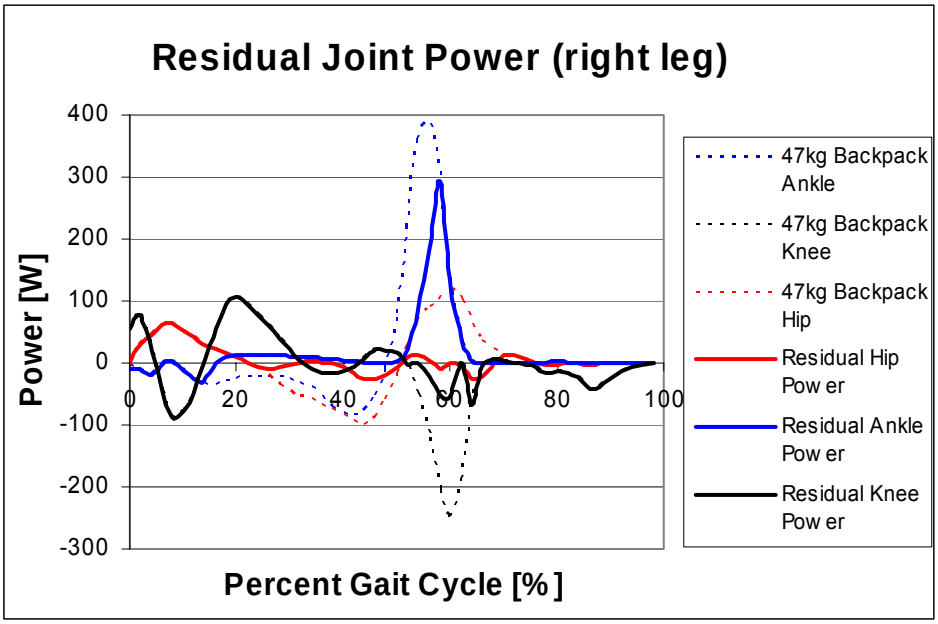

Figure 18 Residual joint powers
With the passive elements implemented on the exoskeleton, the human has to exert less power to complete the desired locomotion.

2.5.2 Hip Power

It can be seen that the power in the spring stores and releases energy nearly in sync with the hip negative and positive power regions.

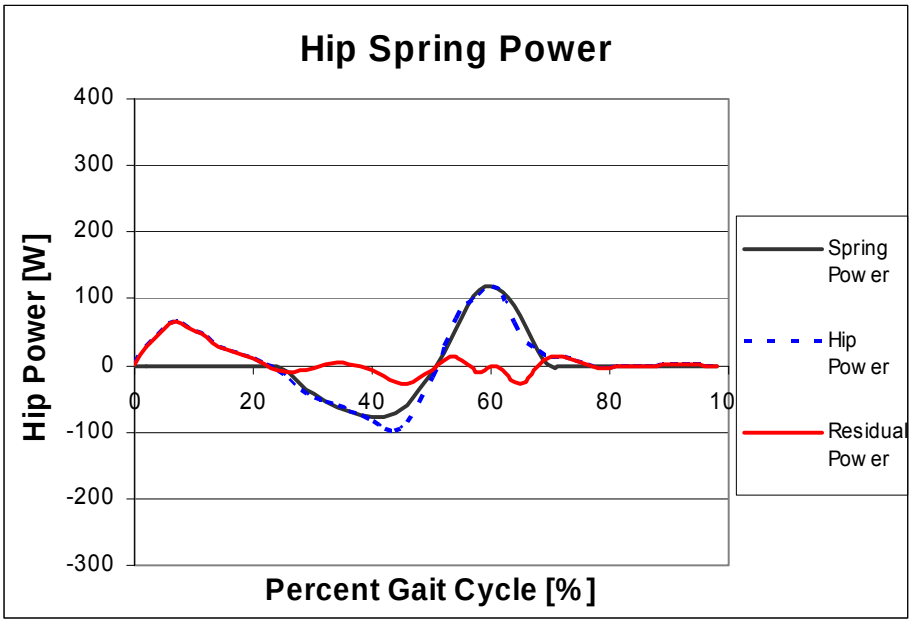

Figure 19 Residual hip power
The hip spring encapsulates much of the hip power from 30% - 70% gait cycle.

The residual hip torque is also minimized from the addition of the hip spring.

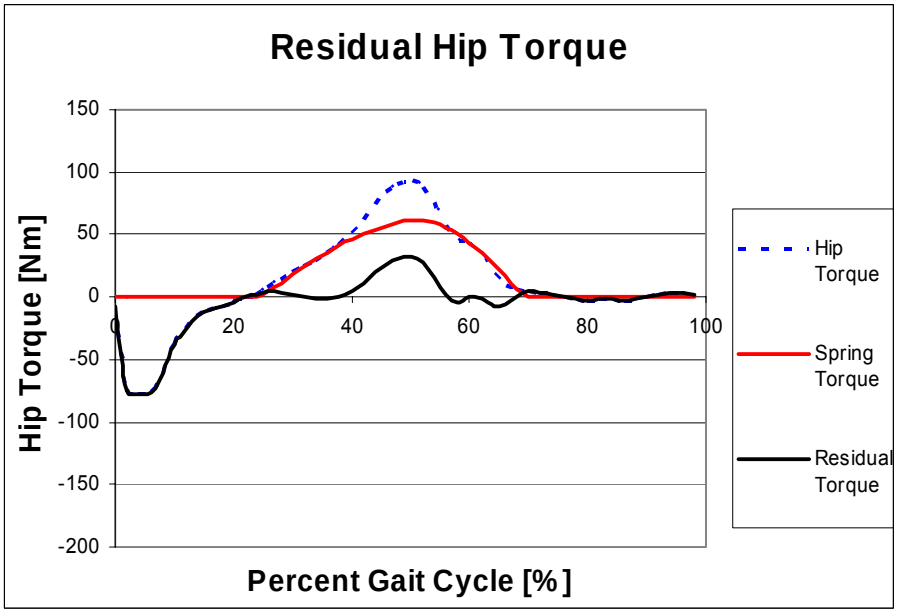

Figure 20 Residual hip torque
The human residual hip torque is minimized by the presence of the hip spring.

The hip spring stores about 15 Joules at its maximum compression.

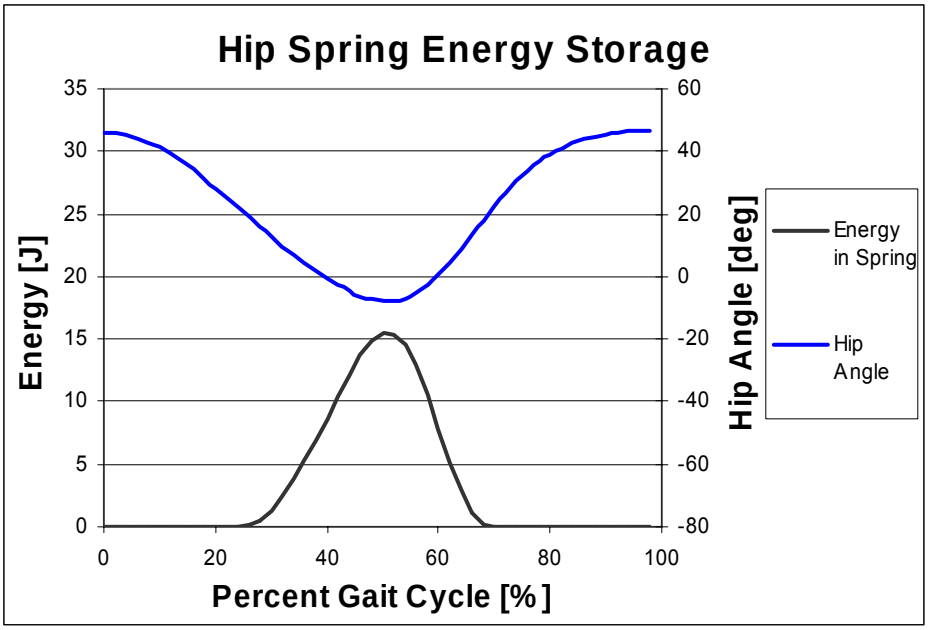

Figure 21 Hip spring energy
The hip spring stores about 15 Joules at its maximum compression.

Another way to visualize the hip spring is to look at the hip torque versus the hip angle. It can be seen that the spring closely follows the hip for a range of values.

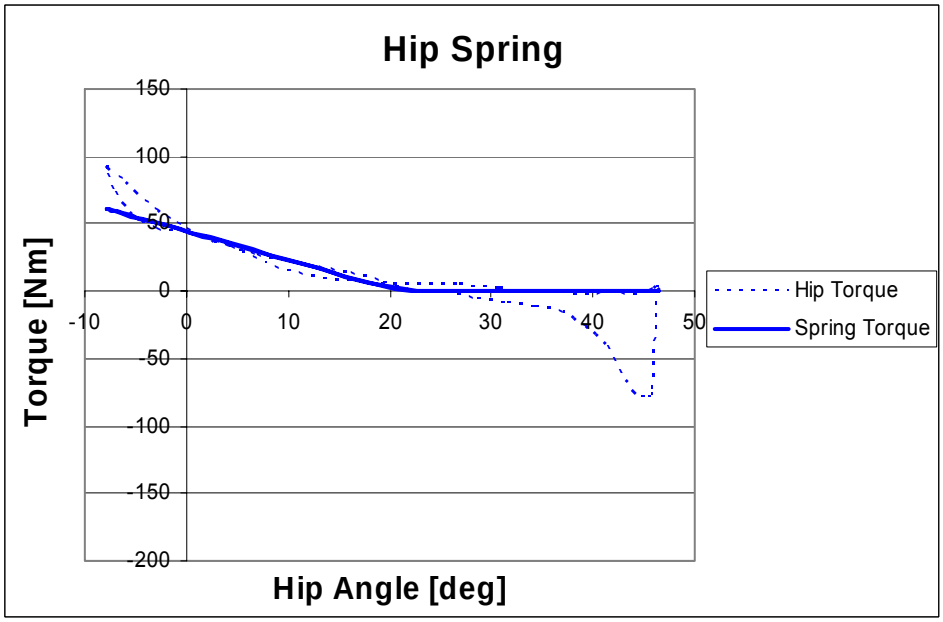

Figure 22 Hip spring
A torque vs angle representation of the hip spring illustrating the linear region in the hip torque which exhibits spring like characteristics.

2.5.3 Knee Power

It can be seen that the damper reduces the power for about an 8% period of the walking cycle, which corresponds to the braking of the knee during the pre-swing and swing phase of walking. Dampening for the first hump of negative power was not included since these powers are incorrect. This was explained earlier in this chapter in section 2.4.4.

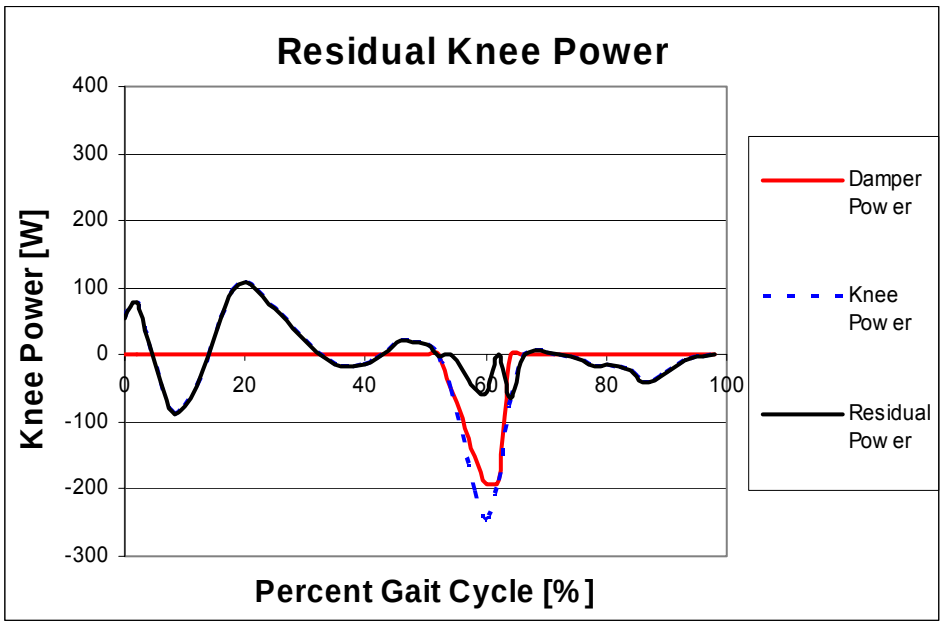

Figure 23 Residual knee power
The knee damper minimizes the power required by the human to brake the knee during the swing phase.

The knee torque is also significantly reduced during the pre-swing phase. Again, the initial hump in the knee torque might be lower since the exoskeleton leg would ideally be locked straight during this period.

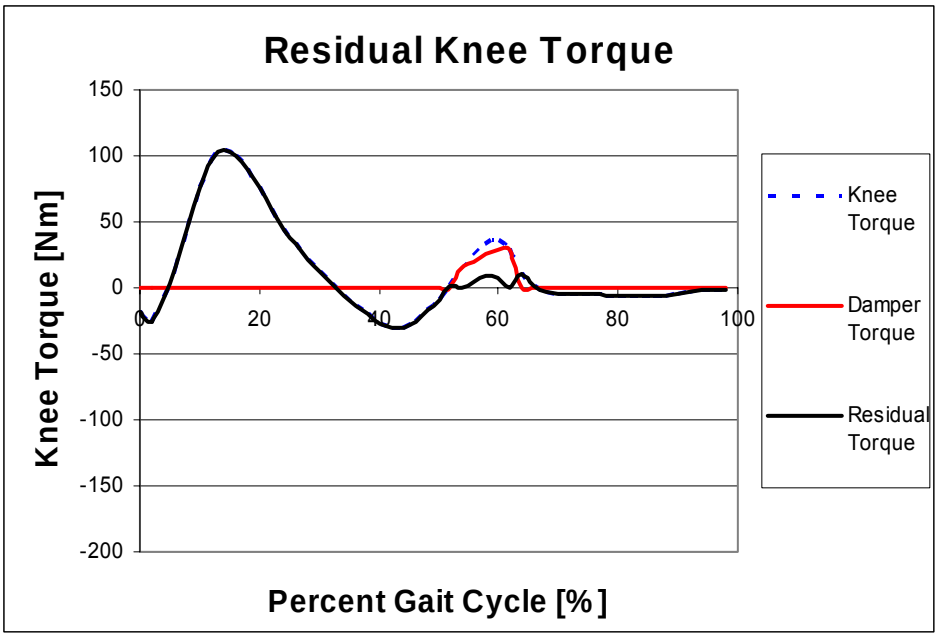

Figure 24 Residual knee torque
The knee torque during the swing phase is decreased after implementing the knee damper.

2.5.4 Ankle Power

The ankle spring stores almost all of the negative power during the first half of the gait cycle, and returns that energy during the positive power portion of the gait cycle. Energy in the spring must be conserved, such that the integral of the spring power must equal zero. It can be seen in Figure 25 that the area enclosed by the negative spring power is equal to that of the area enclosed by the positive spring power. The negative spring power closely encapsulates almost all of the negative ankle power. The difference in the total ankle power minus the spring power is the resultant residual power that the human would need to expend for locomotion. The residual ankle power can be seen in Figure 25.

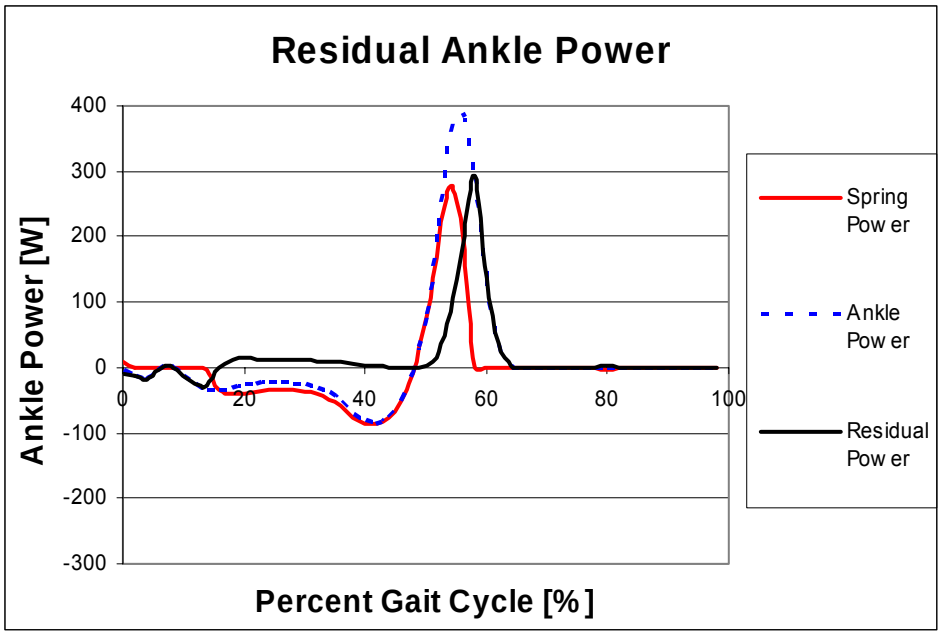

Figure 25 Residual ankle power
The ankle spring captures almost all of the negative power from 15% - 45% gait cycle. The energy in the spring is then released during power plantar flexion. The result is moderate residual power that the human would need to exert for power plantar flexion. Since the ankle spring is a passive element, the area bounded by the negative power curve is equivalent to the area bounded by the positive power curve.

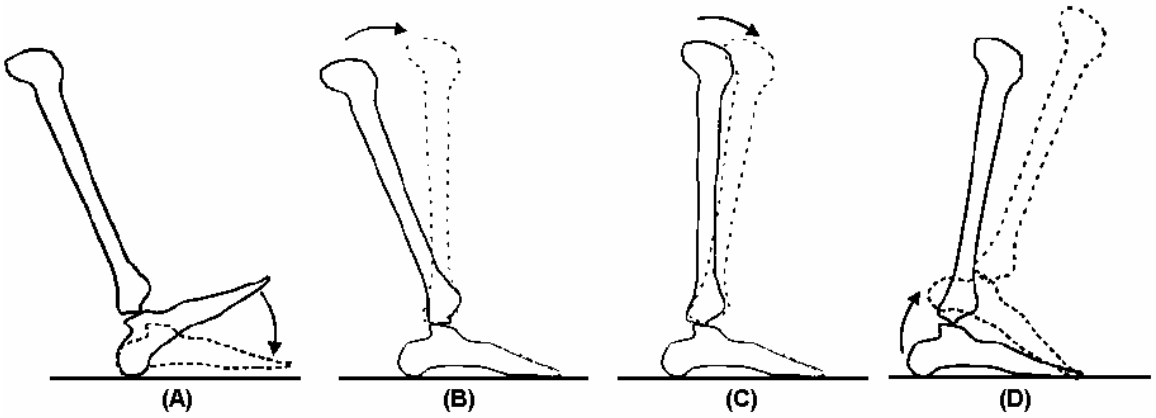

Figure 26 Graphical representation of ankle spring [Au (2005)].
(A) Heel strike and controlled dorsi flexion. (B) The shin rocks forward. (C) The ankle spring engages and begins to store energy. (D) The ankle spring releases energy during powered plantar flexion.

The residual ankle torque is also minimized. It can be observed that during the range of 20% to 40% gait cycle, the torque that the human would need to exert is in the opposite direction that they would normally do. This torque may be unintuitive and awkward for exoskeleton wearer. The human body is very adaptive and it may be the case that it is not a problem. This question may be answered later when the exoskeleton is built and tested.

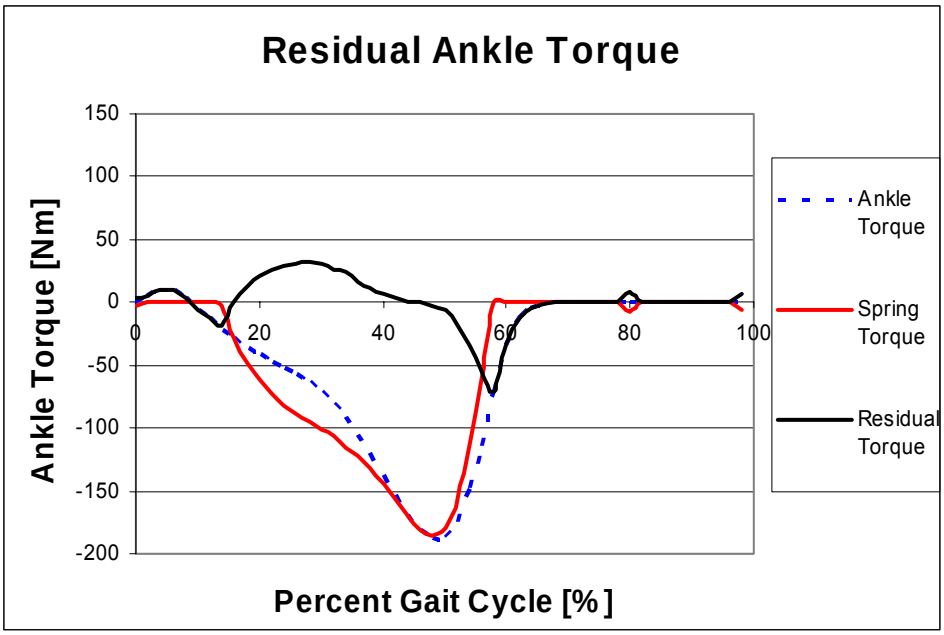

Figure 27 Residual ankle torque
The residual torque that the human would have to provide is greatly reduced. However, the torque that the human would have to exert from the 20% - 40% gait cycle is in the opposite direction that they would normally exert. This irregularity may cause discomfort.

The spring energy in the ankle spring peaks around 20 Joules.

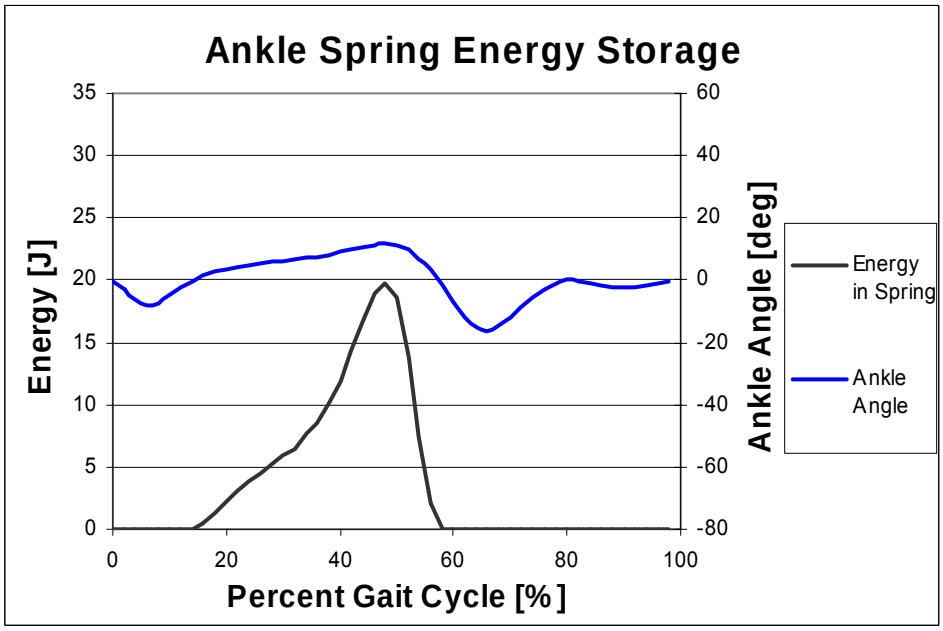

Figure 28 Ankle spring energy
The spring energy in the ankle spring peaks around 20 Joules.

The ankle spring does not track as well as the hip spring, and the reason is that the ankle spring does not eliminate all the positive power needed. There is still a significant residual power that the human has to expend.

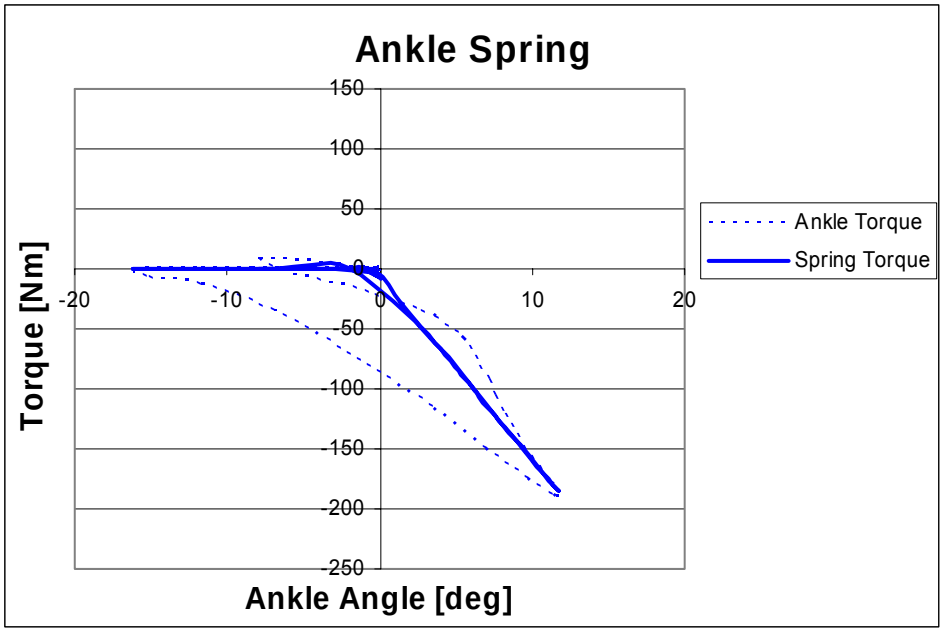

Figure 29 Ankle Spring
A torque vs angle representation of the ankle spring illustrating the pseudo linear region in the ankle torque which exhibits spring like characteristics.

2.6 Limitations and Future Work

It was assumed that the biomechanics data from Natick Army Labs was applicable for optimizing the passive elements implemented in the exoskeleton. The Natick data set was based on a participant carrying a 47kg backpack and walking normally [Harman (2000)].

A limiting assumption to the energy optimization analysis is that the gait kinematics remained unchanged despite the addition of springs and a damper. However, it is possible that the addition of these passive elements altered the gait kinematics. To determine if the gait kinematics was altered, it is necessary to obtain a new data set that is based on a loaded exoskeleton with the passive elements implemented. This newly acquired data set would enable another iteration of the analysis on the new kinematics to determine more accurate passive element values.

Chapter 3 Mechanical Design

3.1 Introduction

This chapter outlines the mechanical design of the exoskeleton, which was done by done by the author, Ken Pasch, Chi Wong, Dan Paluska, William Grand, and Conor Walsh. A rigid exoskeleton structure was implemented to transfer the backpack load forces to the ground. A parallel orthotic structure was implemented using prosthetic Aluminum tubing. The exoskeleton interfaces to the human by means of shoulder straps, a hip harness, thigh cuffs, and a shoe attachment. To preserve natural walking kinematics, the exoskeleton hip, knee, and ankle joints were co-located with their biological counterparts as best as possible. Various spring elements were implemented at the hip and ankle and a variable damper was implemented at the knee.

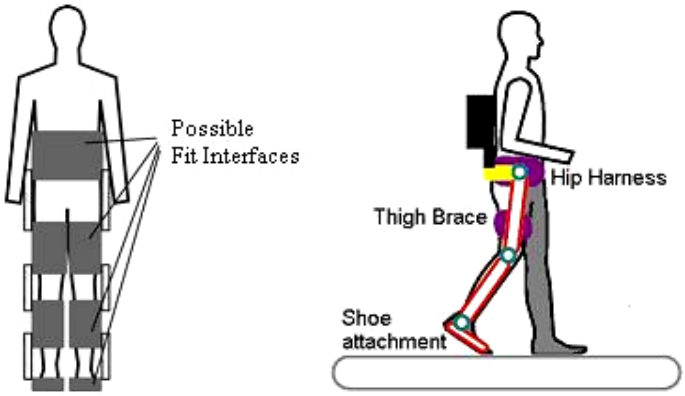

Figure 30 Human/exoskeleton interface
Left: Possible exoskeleton-human interfaces. Options are the hips, thighs, shins, and feet. Right: Actual exoskeleton-human interfaces. The hip harness and backpack shoulder straps ground the backpack to the human torso. A thigh cuff and a shoe attachment were implemented to help the exoskeleton track the leg motion. The thigh cuff was implemented using a semi-rigid brace and Velcro. A cycling shoe was modified and implemented as the foot attachment.

3.2 Force Transfer

A parallel orthotic structure was the basic framework to transfer the load from the backpack to the ground. The main structural elements consisted of standard prosthetic aluminum tubing which had a 30mm OD and a 26mm ID. This tubing was chosen since

it is lightweight, rated for human use, and interfaces with standard prosthetic connectors and components. A standard military issued backpack, Alice Pack, was selected to carry the load. A custom molded carbon fiber rigid hip harness was built to interface the backpack's aluminum frame to the exoskeleton legs. The backpack frame was fastened to an intermediary aluminum plate which had carbon fiber 'L' brackets extending from it. The exoskeleton legs would mount onto these 'L' brackets. Stiffeners were added to the hip harness to add rigidity to the structure. A compliant belt interfaced the lower torso to the backpack frame and the backpack's shoulder straps interfaced the upper torso.

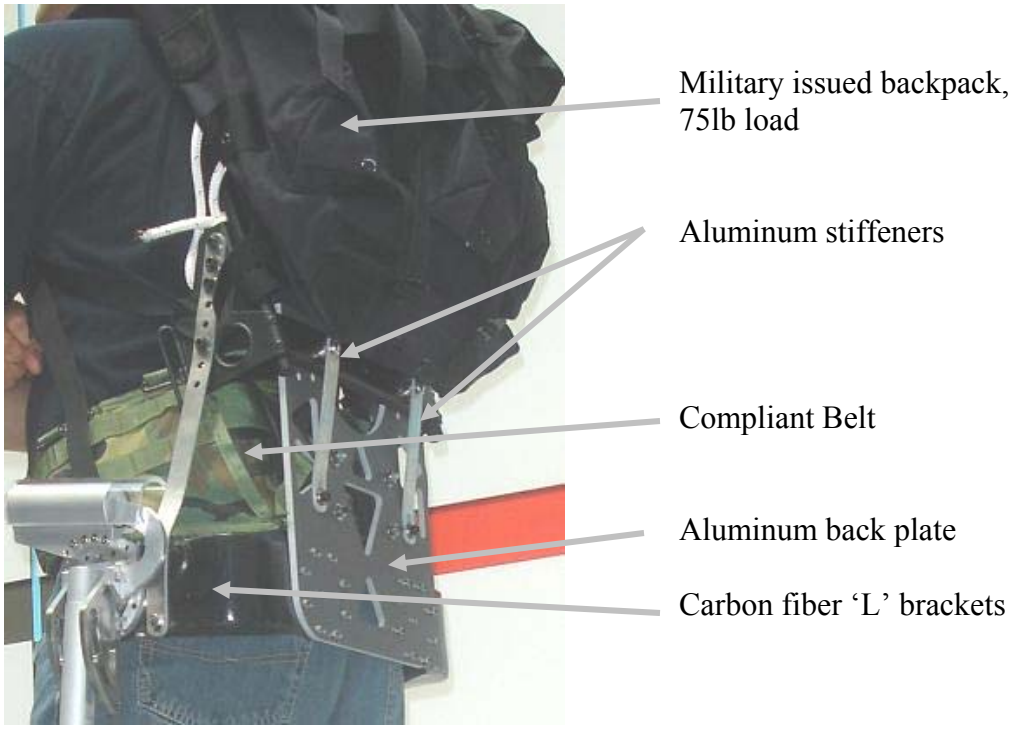

Figure 31 Backpack and hip harness
A military issued backpack was used to carry the 75 lb load. It interfaced to the human via shoulder straps and is grounded to the human by a compliant waist belt. An aluminium plate interconnected the rigid backpack frame, compliant belt, and carbon fiber 'L' brackets. The carbon fiber 'L' brackets extended along the side of the participant where the exoskeleton legs are mounted. Stiffeners were added to increase the rigidity of the overall structure.

3.3 Hip

3.3.1 Hip Kinematics

The exoskeleton hip joint can accommodate the hip's three degrees of freedom which are (1) flexion/extension, (2) abduction/adduction, and (3) medial/lateral rotation.

Medial/lateral rotation was realized by means of a ½" I.D. Igus GFI-080906 plain bearing located above the exoskeleton knee. Flexion/extension was realized by means of a 2" I.D. Kaydon JA020XP0 reali-slim ball bearing. Both the medial/lateral rotation and the flexion/extension degrees of freedom were designed and implemented without much difficulty.

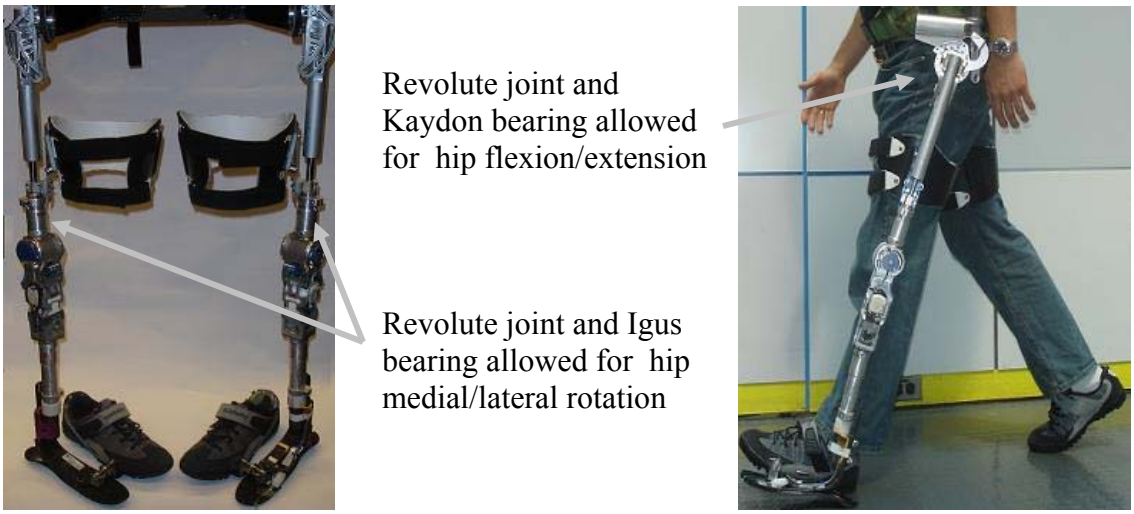

Figure 32 Hip medial/lateral rotation and flexion/extension
Left: A passive yaw joint was implemented above the knee to provide the hip medial/lateral rotation. The yaw joint was implemented by means of a ½" I.D. Igus GFI-080906 plain bearing. Right: A revolute joint for the hip allowed for hip flexion and extension and was implemented by means of a 2" I.D. Kaydon JA020XP0 reali-slim ball bearing.

The hip abduction/adduction degree of freedom was more complicated to implement. During abduction in the coronal plane there is a length change between the biological leg and the exoskeleton leg as seen in the Figure 33. The length change is created by the dissimilar centers of rotation between the biological leg and the exoskeleton leg. This effect can impede normal walking motion and cause discomfort. A mechanism was designed to automatically adjust the exoskeleton leg length and project the center of rotation of the exoskeleton leg to be near the biological hip center of rotation. The connection between exoskeleton and the human are modeled as perpendicular links motivated by biomimetic design.

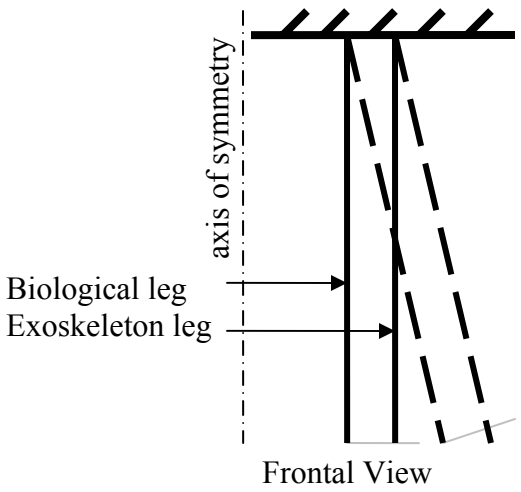

Figure 33 Change in leg length during hip abduction
The centers of rotation for the biological leg and the exoskeleton leg are offset. Thus, during hip abduction, a change in leg length occurs between the exoskeleton and human leg. This change in leg length can cause discomfort and impede normal walking.

3.3.2 Cam Design

A cam-roller mechanism was designed to mitigate the change in leg length during abduction and still transmit the payload forces to the ground. The exoskeleton leg would couple to the harness by the means of a slotted cam located on the side of the hip. As the biological leg abducted, a roller which was grounded to the exoskeleton leg would follow the contour of the cam and the exoskeleton leg would shorten and track the cam profile. The higher the roller went up the slotted cam, the more the exoskeleton leg would shorten. The mechanism had one degree of freedom, so that for a given leg abduction angle there was a unique leg length. The profile of the cam was designed by modeling the exoskeleton leg kinematics as a four bar linkage. Dr. Ken Pasch, was primarily responsible for the design of the cam mechanism and the author's contribution was the analysis.

The four bar linkage model can be seen in Figure 34. The human pelvis and biological leg were each modeled as an individual link and the exoskeleton leg was modeled as two collinear and telescoping links. Revolute joints are located at the biological hip center 'A', the exoskeleton leg center 'B', and the foot attachment joint 'D'. A telescoping joint is located at point 'C' of the exoskeleton leg. The cam-roller mechanism was designed to reproduce this telescoping joint. The biological leg

measurements were taken from *Human Factors Design* for a 50th percentile man [Tilley 1993]. Links 'r3' and 'r4' were modeled as a revolute joint between the exoskeleton and the shoe worn by the human. The change in angle at the exoskeleton-shoe joint is negligible. As the biological leg abduction angle, 'Θ', changes, the vector 'r6' changes in magnitude and direction. The cam mechanism was designed to reproduce the motion of vector 'r6' by means of a cam slot whose contour is equivalent to that of the trajectory traced out by vector 'r6'.

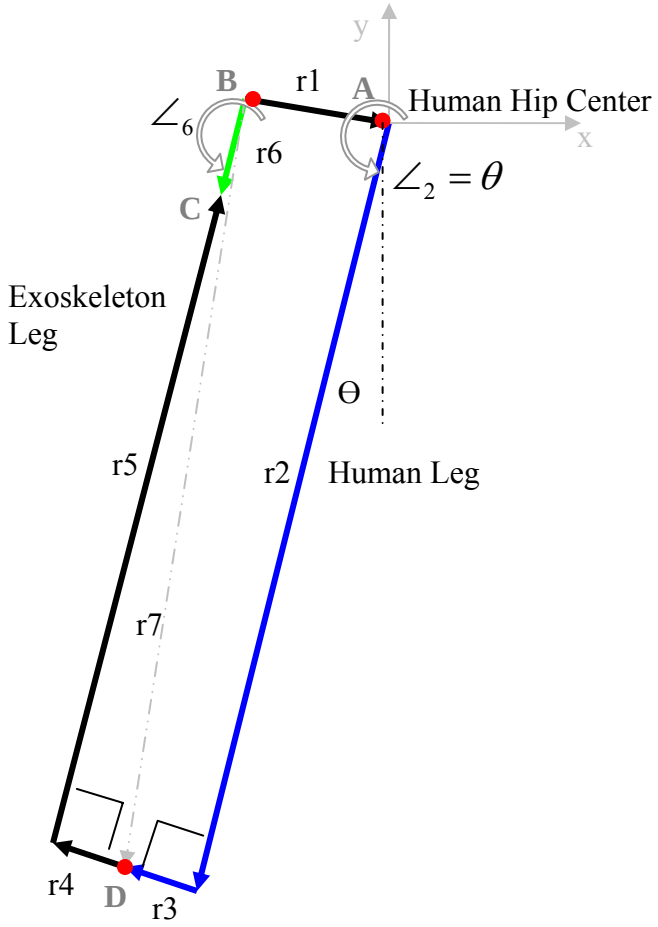

Figure 34 Vector representation of exoskeleton and human leg kinematics
A four bar linkage model represents the interaction kinematics between the exoskeleton leg and the human leg. The fixed link in this analysis is 'r1', which connects the exoskeleton hip joint and the biological hip joint. The joints of the four bar linkage are: (A) Biological hip joint: revolute joint (B) Exoskeleton hip joint: revolute joint (C) Exoskeleton leg: telescoping joint (D) Shoe connection: modeled as a revolute joint. Link 'r5' is perpendicular to link 'r4' and link 'r2' is perpendicular to link 'r3'. Link 'r5' is collinear to link 'r6'.

Where the dimensions in Figure 34 are:

r_1	= 5" $\vec{x}$ - 0.45" $\vec{y}$	$\|r_4\|$ =	2.5"
$\|r_2\|$ =	36.9"	$\|r_5\|$ =	33.9"
$\|r_3\|$ =	2.5"	$\|r_6\|$ =	Adjustable length

Table 10: Dimensions for the four bar linkage in Figure 34
The leg length dimensions are for a 50 percentile man [Tilley 1993].

The trajectory of vector 'r6' can be determined as a function of the hip abduction angle, 'Θ'. The magnitude, 'L_6', and direction, '$\angle_6$' of vector 'r6' are given by the below equations.

$$r_7 = r_1 + r_2 + r_3 \tag{3.1}$$

$$(L_5 + L_6)^2 + L_4{}^2 = L_7{}^2 \Rightarrow L_6 = \sqrt{L_7{}^2 - L_4{}^2} - L_5 \tag{3.2}$$

$$\angle_6 = \angle_7 - \sin^{-1}\left(\frac{L_4}{L_7}\right) \tag{3.3}$$

where $L_i = |r_i|$ *and* $\angle_i = \angle r_i$ *and* $r_2 \perp r_3$ *and* $r_4 \perp r_5$ *and* $r_5 \| r_6$ *and* r_1 *is fixed and* $\theta \in 250°$ *to* $280°$ ($-10°$ *inward adduction to* $20°$ *outward abduction*)

The trajectory that vector 'r6' traced out was used as the basis for designing the cam profile. The figures below show the magnitude and trajectory of vector 'r6' as the biological hip angle changes. The -10˚ angle refers to the maximum hip adduction angle and the 20˚ angle refers to the maximum hip abduction angle.

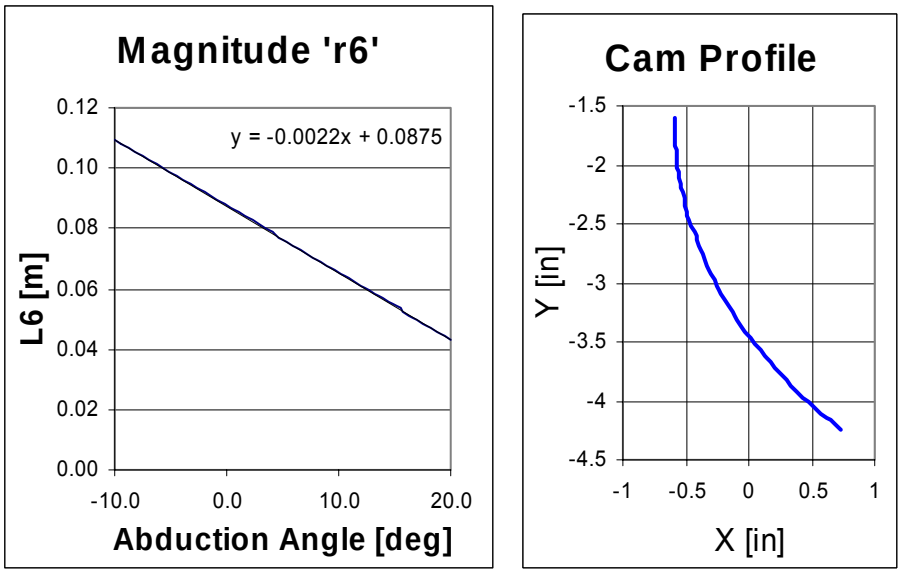

Figure 35 Cam profile described by 'r6' in Figure 34
Left: The magnitude of 'r6' decreases as the abduction angle increases. Right: The cam profile traced out by the 'r6' trajectory. The upper section corresponds to when the leg is fully abducted outward and the lower section corresponds to when the leg is fully adducted.

The cam was built out of titanium and installed on the exoskeleton. Titanium was chosen because its high hardness lessened the rolling friction of the steel rollers while being lighter than hardened steel. The cam mechanism performed the desired kinematics and shortened the exoskeleton leg appropriately.

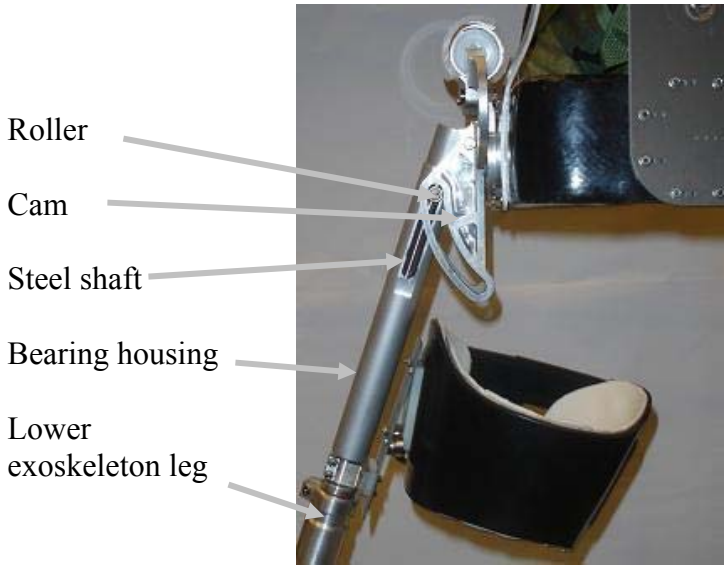

Figure 36 Cam mechanism
The cam mechanism was built out of Titanium to provide a hard, low friction surface for the roller to roll along. The roller is grounded to a ½" steel shaft. When the leg abducts, the roller rides up the cam and steel shaft slides up the bearing housing. The steel shaft is connected to the lower part of the exoskeleton leg. Thus, as the leg is abducted, the exoskeleton leg shortens.

By geometry, the cam mechanism effectively projects the center of rotation of the exoskeleton leg to hip center of the biological leg. This virtual center of rotation was found by determining the locus of instant center points of the 'r5' vector of Figure 34 as it was rotated. The 'r5' vector represents the lower portion of the exoskeleton leg. To find this locus of points, another vector was created that was fixed relative to the 'r5' vector as shown in Figure 37. As the 'r5' vector rotated, the trajectories of the 'r5' vector and the new vector were traced out. These two trajectories were then used to determine the instant center of rotation. Referring to Figure 37, point 'A' and 'B' translated a small distance as the vector 'r5' rotated. The path between these points was bisected and the intersection of these bisecting lines was solved to determine the center of rotation.

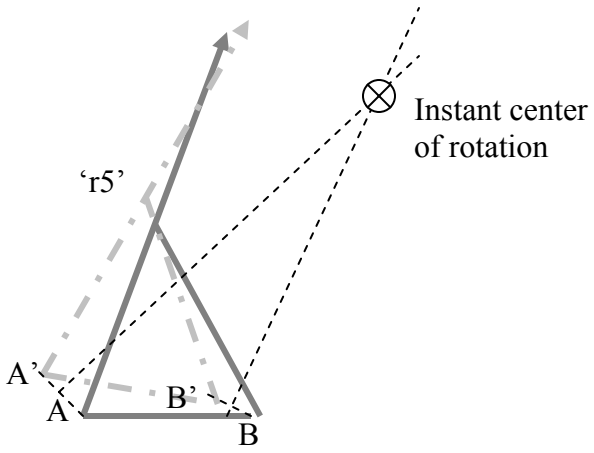

Figure 37 Instant center of rotation for the exoskeleton leg
The instant center of rotation of the exoskeleton is equivalent to the center of rotation for 'r5' in Figure 34. An arbitrary vector was chosen which is fixed to 'r5'. The trajectory of the end of the 'r5' vector (point 'A') and the end of the arbitrary vector (point 'B') were tracked through the hip abduction range of motion. The trajectory was split into discrete intervals and each interval was bisected and the intersection of these lines gave the instantaneous center of rotation of 'r5'. This procedure provided a locus of points that described the projected center of rotation of the exoskeleton leg due to the addition of the cam mechanism. The center of rotation of the exoskeleton leg is not fixed, but rather a locus of points and is centered about the biological hip center. When the exoskeleton leg is abducted outward, the center of rotation is below the biological hip center and conversely, when the leg is adducted inward, the center of rotation is above the biological hip center. This is illustrated in Figure 38.

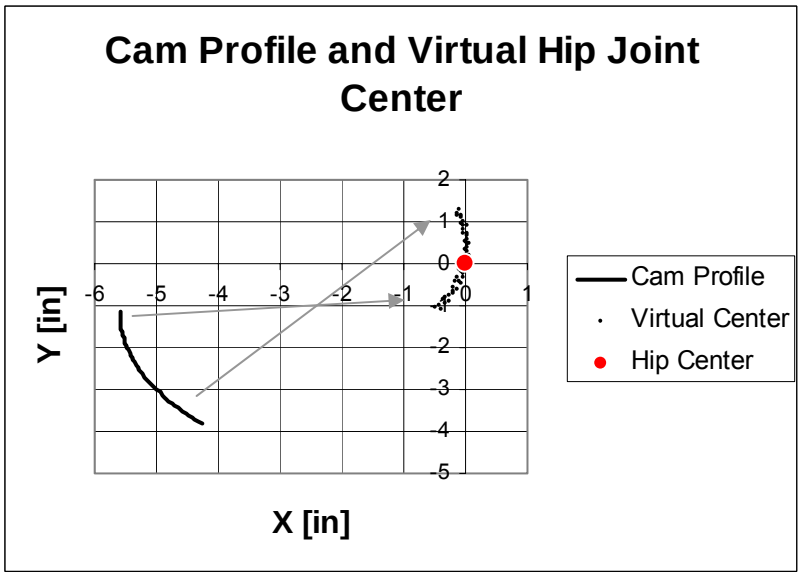

Figure 38 Virtual center of exoskeleton leg and the cam profile

The center of rotation of the exoskeleton leg is a locus of points that are centered around the biological hip center. When the leg is fully abducted, the roller is up high in the cam and the corresponding center of rotation of the exoskeleton leg is below the biological hip center. When the leg is fully adducted, the roller is low in the cam and the corresponding center of rotation of the exoskeleton leg is above the biological hip center.

The following figure further illustrates the center of rotation of the exoskeleton leg in reference to the human's biological hip center.

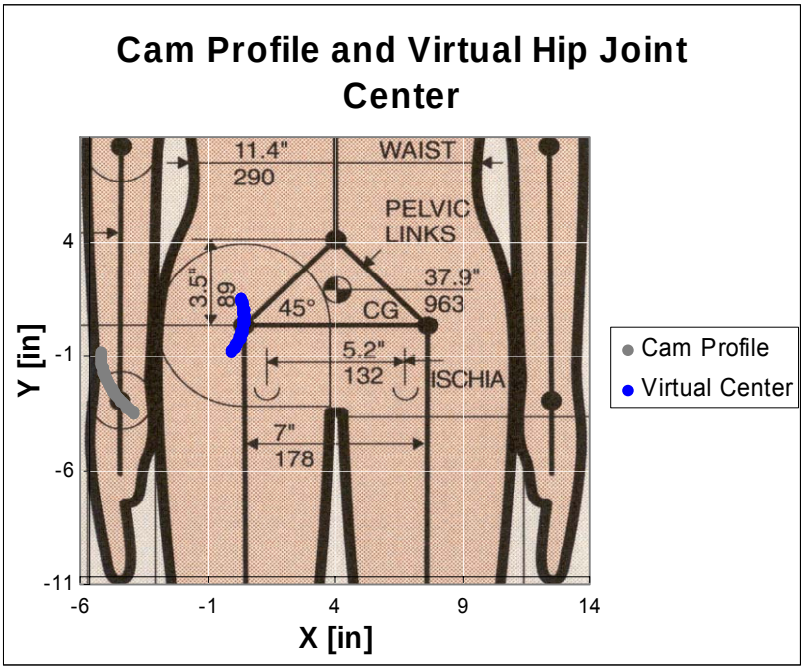

Figure 39 Virtual exoskeleton hip joint center superimposed on biological hip center of a 50 percentile man [Tilley 1993]

3.3.3 Leg Extension Bearing Analysis

The cam mechanism properly adjusted the exoskeleton leg length throughout the hip abduction range. However, when the exoskeleton was loaded with the desired 75lb load, the cam mechanism would stick and bind. The cause of the binding was excessive friction by the plain linear bearing in the telescoping joint of the exoskeleton leg. The 75 lb vertical load from the backpack caused a magnified side load on the plain bearing as noted in Figure 47. The plain Iglide-J Igus bearings initially used had a friction coefficient of $\mu_k = 0.2$ and an effective bearing contact area of $A_{contact} = 0.75$ in^2. The Igus bearing created a frictional force of more than 30 lb and rendered the cam mechanism ineffective. Other bearing materials and various lubricants were considered, but they all had coefficients of friction that were too high. Linear recirculating ball bearings from Thomson Industries were selected and they eliminated the friction problem.

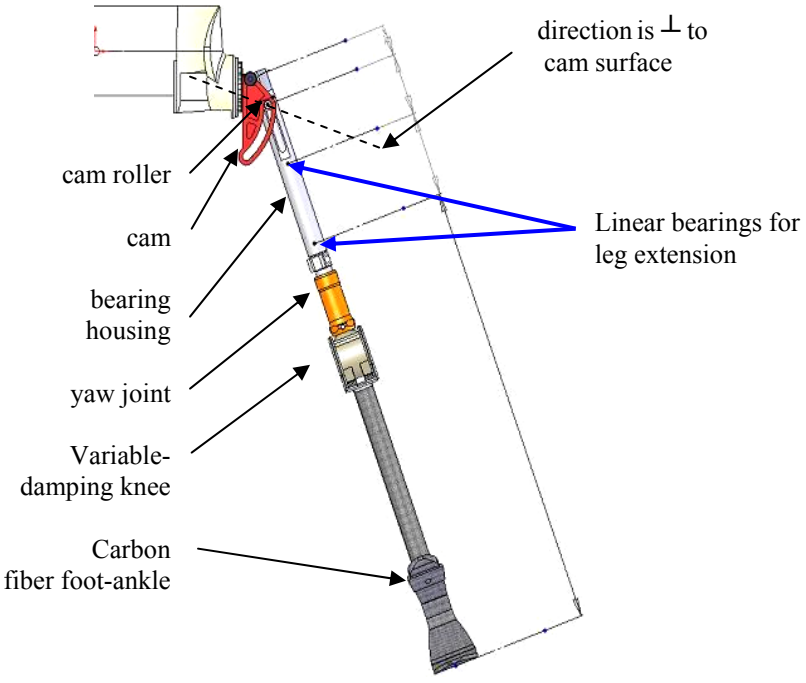

Figure 40 Exoskeleton leg diagram
The cam roller tracks the cam profile and is grounded to a steel shaft that slides along two linear bearings. The other end of the steel shaft is grounded to the yaw joint. As the hip abducts, the roller causes the steel shaft to slide along the linear bearings thus extending the exoskeleton leg.

To select the ball bearing, the mechanics of the cam mechanism was fully analyzed. The side load force on the bearing was amplified because of the geometry of the cam mechanism. To understand how the bearing force amplification occurred, multiple free body diagrams are studied to fully understand the mechanical system. For this analysis, the mechanism will be analyzed as a quasi-static machine, that meaning static analysis will be performed over a range of positions. For simplification of the analysis, friction is ignored.

The first free body diagram considers the forces on the cam roller. When the human stands on one leg, a component of the applied 75lb force is transmitted along the exoskeleton leg and is transmitted to the roller along the line of action parallel to the leg axis. A reaction force is generated normal to the cam surface and another is generated normal to the linear bearing. The direction of the linear bearing reaction force is normal to the exoskeleton leg axis. The applied forces on the roller must statically balance, over the range of hip abduction angles. The free body diagram of the cam roller is shown in Figure 41.

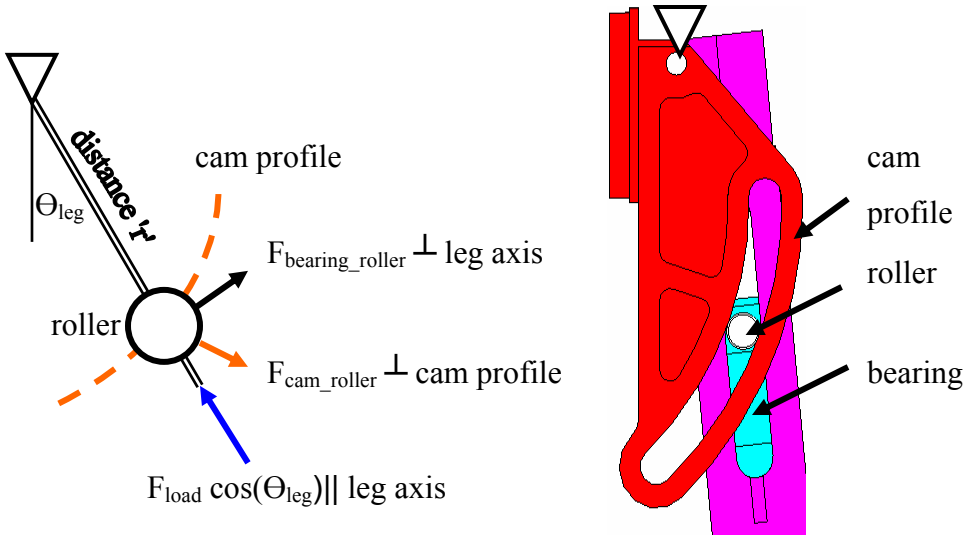

Figure 41 Free body diagram of the cam roller
Left: The loads on the roller are caused by the applied 75 lb load, F_{load} and two reaction forces. One reaction force is from the cam profile, F_{cam_roller} and its direction is normal to the cam surface. The second reaction force, $F_{bearing\_roller}$ is normal to the leg axis. Right: A diagram of the cam mechanism and the location of the cam roller.

The forces from the free body diagram in Figure 41 statically balance and form a force triangle shown in Figure 42.

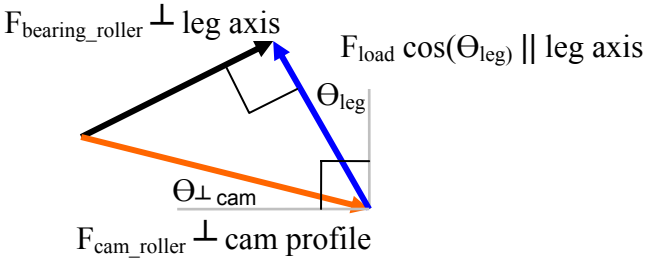

Figure 42 Force balance of the cam roller
The forces from Figure 41 create a force triangle which must be statically balanced. These forces can be solved by the law of sines since one side and the angles are known.

Since the directions of all the force vectors are known, the law of sines can be used to solve for the F_{roller} and the F_{cam} reaction forces. The equations yielding the unknown are given by the equations below.

$$\frac{F_{cam\_roller}}{\sin(\frac{\pi}{2})} = \frac{F_{bearing\_roller}}{\sin(\frac{\pi}{2} - \theta_{\perp cam} - \theta_{leg})} = \frac{F_{load}\cos(\theta_{leg})}{\sin(\theta_{\perp cam} + \theta_{leg})} \tag{3.4}$$

$$\Rightarrow \frac{F_{cam\_roller}}{F_{load}} = \frac{\sin(\frac{\pi}{2})\cos(\theta_{leg})}{\sin(\theta_{\perp cam} + \theta_{leg})} \tag{3.5}$$

$$\Rightarrow \frac{F_{bearing\_roller}}{F_{load}} = \frac{\sin(\frac{\pi}{2} - \theta_{\perp cam} - \theta_{leg})\cos(\theta_{leg})}{\sin(\theta_{\perp cam} + \theta_{leg})} \tag{3.6}$$

The results of the above calculations are displayed below in Figure 43 and are normalized to the 75lb applied force. A force amplification for both the $F_{bearing\_roller}$ and F_{cam_roller} can be noted Figure 43.

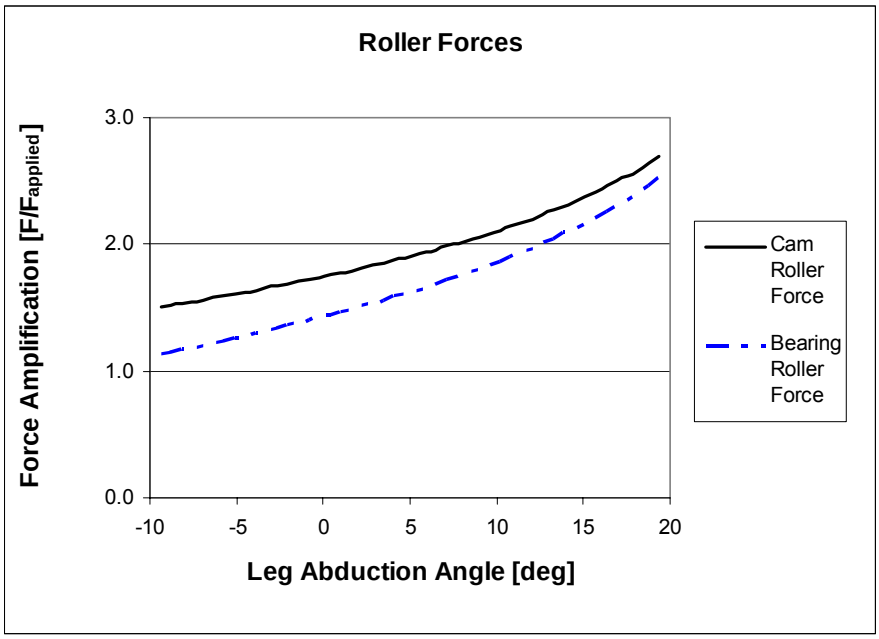

Figure 43 Force amplification on the roller.

The geometry of the cam mechanism in Figure 41 caused a force amplification on the roller. Both the F_{cam_roller} and $F_{bearing\_roller}$ forces increased as the abduction angle increased.

The next free body diagram to be considered is one of the entire leg exoskeleton which is shown in Figure 44. The F_{cam_roller} force is known from Figure 43, and the F_{load} force is 75lb. The unknown forces are F_{slip}, and the reaction forces at point 1, R_{1x} and R_{1y}.

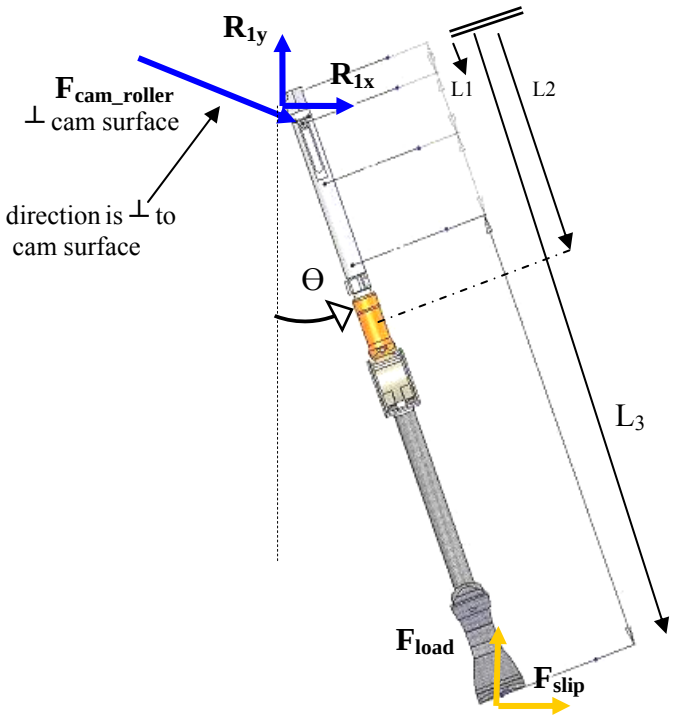

Figure 44 Free body diagram of the full exoskeleton leg.
The F_{cam_roller} force is oriented in a direction that is perpendicular to the cam surface. The lengths, L_1, L_2, and L_3 are variables and are dependent on the leg abduction angle. Known variables are F_{load} and F_{cam_roller}, where F_{load} is 75 lb and F_{cam_roller} was calculated previously and shown in Figure 43.

The equations resulting from the free body diagram in Figure 44 are listed in Table 11. The unknown variables R_{1x}, R_{1y}, and F_{slip} can be solved by the equations listed in Table 11.

$$F_x=0: \; R_{1x}+F_{slip}+F_{camx} = 0 \qquad (3.7)$$

$$F_y=0: \; R_{1y}+F_{load}-F_{camy} = 0 \qquad (3.8)$$

$$M_1=0: \; F_{camx} L_1 \cos(\Theta)-F_{camy} L_1 \sin(\Theta)+F_{slip} L_3 \cos(\Theta)+F_{load} L_3 \sin(\Theta) = 0 \qquad (3.9)$$

Table 11 Equations from the full exoskeleton leg free body diagram in Figure 44

The next free body diagram considered is a subset of the previous one to determine the internal forces. The right hand side free body diagram of Figure 45 shows interaction forces at the end of the steel shaft. The shaft slides inside of the bearing housing and provides for the exoskeleton leg extension.

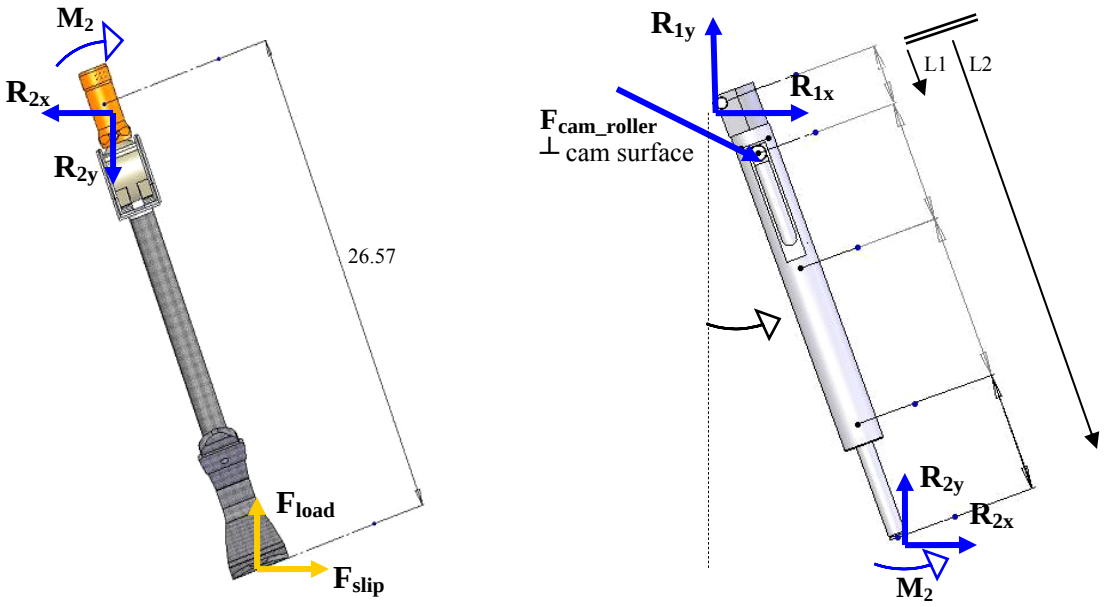

Figure 45 Free body diagram of the upper and lower parts of the exoskeleton leg
Left: Free body diagram of the lower exoskeleton leg. Right: Free body diagram of the upper exoskeleton leg. The F_{cam_roller} force is oriented in a direction that is perpendicular to the cam surface. Known variables are F_{cam_roller}, from Figure 43 and R_{1y} and R_{1x} which were calculated in Table 11.

The equations resulting from the free body diagram in Figure 45 are listed in Table 12. The known variables are R_{1x}, R_{1y}, and F_{cam_roller}. R_{1x} and R_{1y} are the solution from solving the equations solved in Table 11, and F_{cam_roller} is shown in Figure 43. The equations in Table 12 are used to solve for the unknown variables: R_{2x}, R_{2y}, and M_2.

$$F_x=0: \quad R_{1x}+R_{2x}+F_{camx} = 0 \qquad (3.10)$$

$$F_y=0: \quad R_{1y}+R_{2y}-F_{camy} = 0 \qquad (3.11)$$

$$M_1=0: \quad F_{camx}\, L_1 \cos(\Theta)-F_{camy}\, L_1 \sin(\Theta)+R_{2x}\, L_2 \cos(\Theta)+R_{2y}\, L_2 \sin(\Theta) +M_2 = 0 \qquad (3.12)$$

Table 12 Equations from upper exoskeleton leg free body diagram in Figure 45

The next free body diagram, shown in Figure 46, to be considered is of the steel shaft which slides in the bearings inside of the bearing housing which is illustrated in Figure 44.

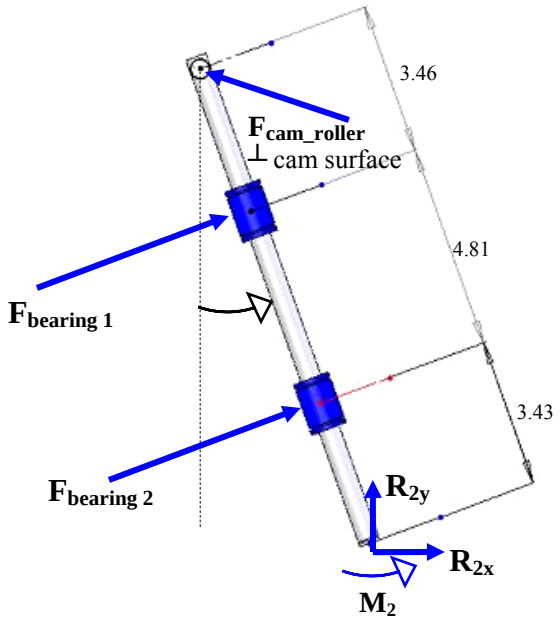

Figure 46 Free body diagram of the shaft and bearings

The F_{cam_roller} force is an equal and opposite reaction force to the F_{cam_roller} in Figure 45. The known variables are F_{cam_roller} from Figure 43 and R_{2y} and R_{2x} which were calculated in Table 12. The two unknown variables are the bearing forces, $F_{bearing1}$ and $F_{bearing2}$.

The unknown variables are $F_{bearing1}$ and $F_{bearing2}$. The equations resulting from the free body diagram in Figure 46 are listed in Table 13. From these equations, the forces on the bearings can be determined.

$$F_x=0: \ -F_{camx}+F_{b1}\cos(\Theta)+F_{b2}\cos(\Theta)+R_{2x} = 0 \qquad (3.13)$$

$$M_2=0: \ F_{camx}\,11.7\,\mathrm{Cos}(\Theta)+-F_{camy}\,11.7\,\mathrm{Sin}(\Theta)-F_{b1}\,8.24 - F_{b2}\,3.43 +M_2 = 0 \qquad (3.14)$$

Table 13 Equations from shaft and bearings free body diagram in Figure 46

The results of the analysis are shown in Figure 47. The bearing rating for the Thomson linear ball bearings that was selected is also shown. The loads on the bearing are below the bearing rating, assuring a safety factor greater than unity.

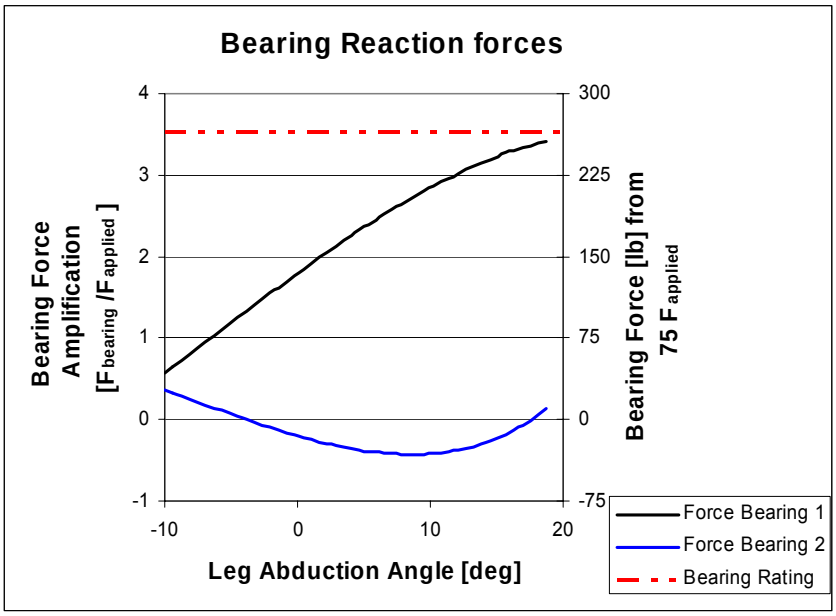

Figure 47 Bearing reaction forces

The bearing reaction forces of Figure 46 increase in magnitude as the leg is abducted. This can be expected since higher moment forces are created by F_{cam_roller} and the ground reaction forces. The forces on both bearings lie beneath the maximum bearing rating which is 265 lb specified by the Thomson catalog [*Linear Ball Bushing Bearings and Components* (2003)].

Below, Figure 48 shows how the exoskeleton leg lengths (L_1, L_2, and L_3) shorten as a function of the hip abduction. These leg lengths are pertinent to the free body diagrams in Figure 44 and Figure 45.

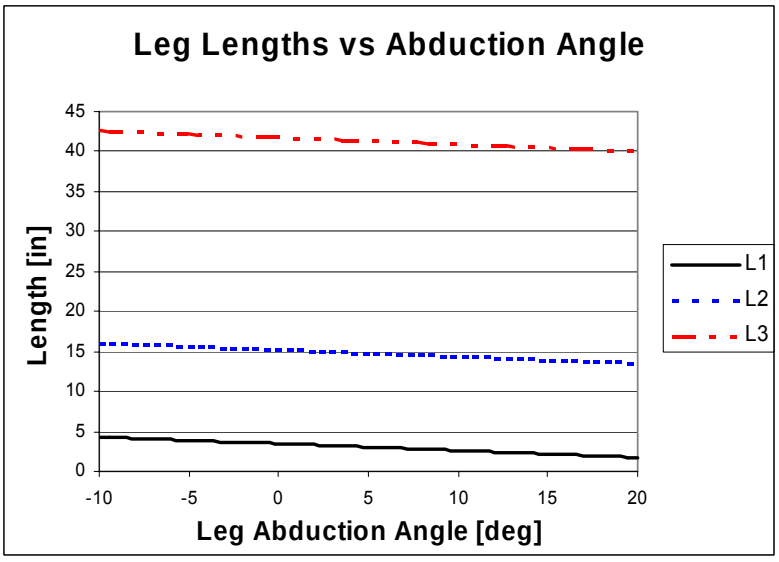

Figure 48 Leg length vs hip abduction angle

As the hip abducts, the leg length get shorter. L_1, L_2, and L_3 are defined in Figure 44.

3.3.4 Abduction Bearing Implementation

Linear recirculating ball bearings were chosen to replace the high friction plain Igus bearings discussed in section 3.3.3. The Thomson smart ball bearings were chosen since they offer a coefficient of friction on the order of 0.003 and can self correct for slight shaft misalignments. A Thomson 60 case hardened, chrome-plated linear race was chosen since it offered a hard surface for the ball bearings.

Half inch ID linear bearings were chosen since they fit inside the aluminum housing tube that mates to the Titanium cams. A larger ID bearing would add a greater load capacity, but the overall size of the bearing would necessitate that the Titanium cam to be remanufactured. It was deemed to costly time and money wise to remake the Titanium cams. The following parts were chosen to fit with the already existing cam.

Parts:

- ½" OD, 12" length Thomson 60 Case Hardened, chrome plated linear race
- ½" ID, SS6U-8-WW Thomson Super Smart Ball Bearings

Specifications:

- Dynamic load capacity: 265lb

Table 14: Thompson linear motion parts and specifications

The maximum calculated dynamic load of 250lb from Figure 47 is less than the 265lb specification for Thomson's smart ball bearings [*Linear Ball Bushing Bearings and Components* 2003]. This maximum force however occurs when the leg is fully abducted to which the Thomson ½" bearings have a safety factor of about unity. During normal walking the human leg remains very close to the vertical where the bearing forces are much lower. The bearing design have a safety factor of greater than unity at any other abduction angle assuming that the applied force is still 75lb. Friction exists in the cam mechanism so that the force that is transmitted to the bearing will actually be less than the calculated value.

3.3.5 Hip abduction spring

When the exoskeleton wearer stands on one leg, a moment is created by the backpack load since it is off center from the biological hip joint. This moment is undesirable and can cause discomfort. A 250 kN/m abduction spring was implemented to the hip joint to help counter the backpack moment.

To analyze the abduction moment about the hip a free body diagram of the hip harness was considered which is illustrated below in Figure 49. The backpack load and the reaction force from the exoskeleton leg cause a moment about the biological hip center.

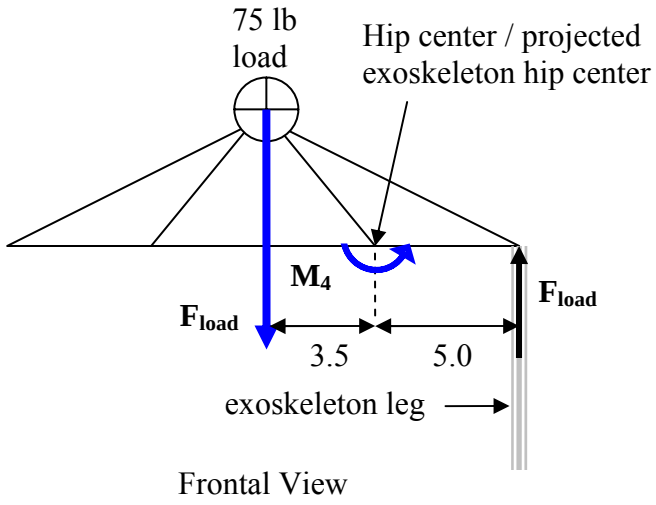

Figure 49 Free body diagram of the harness
The backpack load causes a 75 lb force vertically downward in the center of the harness. The reaction force on the exoskeleton leg is also F_{load}. The moment M_4 is the net moment that the biological hip joint feels.

The M_4 moment experienced by the human is about 13 Nm. A hip abduction spring was implemented in the hip joint to counter this moment. The abduction spring is a compression spring that is located where the 'K-linear' arrow is located in Figure 50. The spring is located 15mm below the joint's rotational axis.

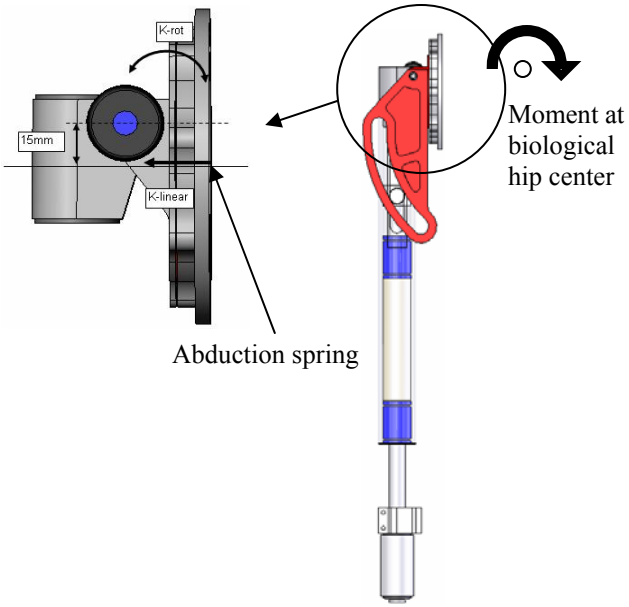

Figure 50: Abduction spring
The backpack load and the reaction force from the exoskeleton leg cause an overturning moment at the biological hip center. This moment caused discomfort for the participant. An abduction spring was implemented to provide a counter moment. The spring implemented is a 250 kN/m compression spring that is 15mm below the exoskeleton joint located where the 'K-linear' arrow is.

To provide a counter moment of 13Nm over a 10 degree range, a linear spring with a stiffness of 325 kN/m was needed. From qualitative feedback from the user, it was preferred to implement a slightly lighter spring. A compression spring with a spring constant of 250 kN/m was selected and placed inside the hip joint. The linear spring engages at an angle of 5˚ of leg abduction, such that when the participant stands straight the spring is compressed half way. The spring is uni-directional and creates a counter moment when the abduction angle is less than 5˚ and no moment otherwise. The abduction spring worked as designed and the test participants preferred having the abduction spring present rather than not having it installed.

3.3.6 Hip extension spring

3.3.6.1 Energy Storage

Motivated by the energy management analysis, a uni-directional hip spring was implemented at the hip joint. The LHC-187R-4-M compression spring from Lee Spring was selected since it has a spring constant of 99 lb/in with 2" travel and a 4" free length.

Chapter 2 specified a spring constant of 110 lb/in. The plunger can be adjusted to a variety of engagement angles. A clear plastic finger guard was also installed for safety.

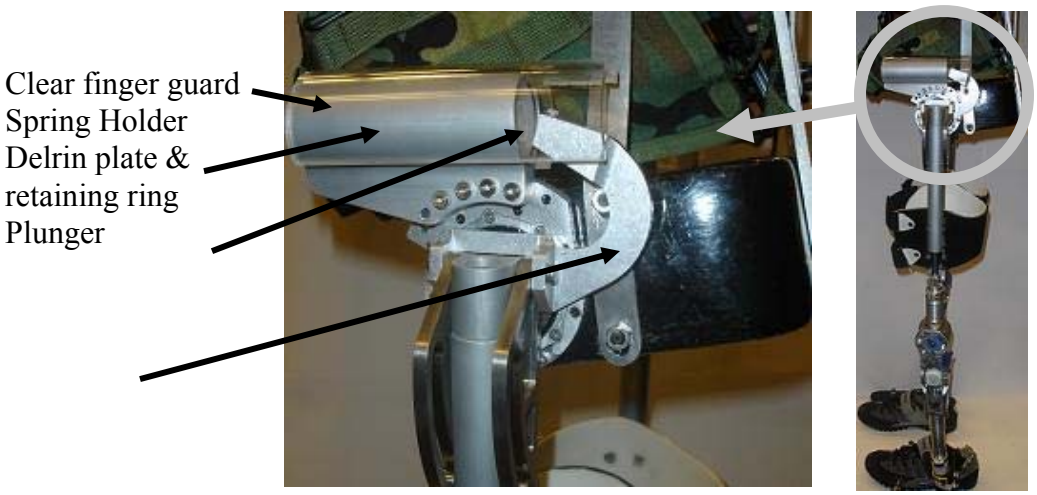

Figure 51: Hip extension spring
The hip extension spring stored energy during hip extension and released it during the thrusting phase. The hip spring was implemented with a 110 in/lb spring with a 1.5" diameter and 4" length. A plunger was grounded to the Titanium cam. During hip extension, the plunger would compress the spring. A thin Delrin plate covered the spring and allowed a low friction surface to contact the plunger. A clear finger guard was placed on top of the spring holder for safety.

3.3.6.2 Anti moment

The exoskeleton wearer cannot stand upright since the backpack load is offset behind the human and creates an overturning moment that could cause the human to fall backwards as shown in Figure 52. To counter this, the human would lean forward so that the center of gravity of their upper body is over their feet. However, because of the hip extension spring, the human can stand upright. The hip springs create a counter moment which offsets the overturning backpack moment. The test participants agreed that the hip springs made standing and walking more comfortable.

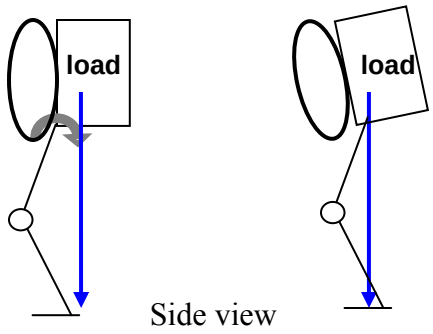

Figure 52: Backpack overturning moment
The hip extension springs assist and countering the overturning moment caused by the backpack load. Left: overturning moment caused by the backpack, Right: upper body center of gravity over the feet.

3.4 Thigh

A thigh cuff was used to help the exoskeleton track the kinematic motion of the human leg. The cuff was padded and Velcro was used to tighten the fit. A spring steel plate was installed between the exoskeleton leg and the thigh cuff. The steel plate was compliant in the coronal plane to adjust to the leg contours of different participants, but it was rigid in the sagital plane to allow for good tracking during walking. A spacer was inserted to angle the thigh cuff inward for better fit.

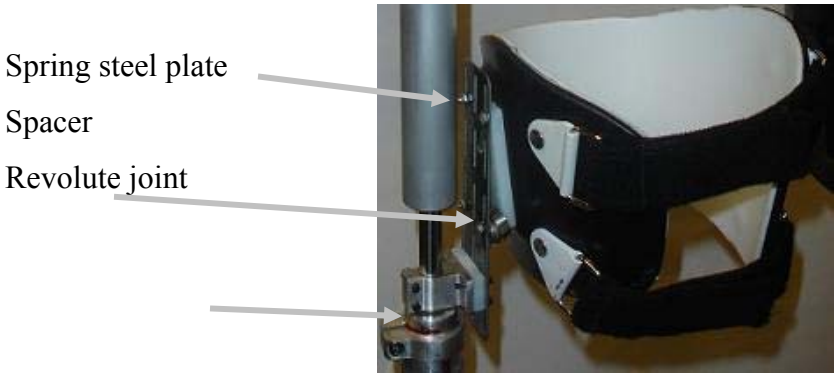

Figure 53: Frontal view of thigh cuff
The thigh cuff constrains the human thigh to be next to the exoskeleton thigh. A plastic shell holds the human thigh and is tightened with Velcro. A spacer helps align the thigh cuff to the follow the contour of the human leg. A steel spring plate interconnects the thigh cuff to the exoskeleton. The plate is compliant in the frontal plane allowing the thigh cuff to fit the human comfortably and is stiff in the sagital plane allowing the exoskeleton leg to closely track the human leg.

3.5 Knee

The variable-damping knee, made by Össur in Iceland, was chosen for the knee joint since it is a variable damper. This magnetorheological prosthetic knee is an electronic

knee that can adjust its damping level for different gait phases such as stance and swing [Herr 2003]. The knee's rotary potentiometer and force sensors provide the onboard computer with sufficient information to detect the phase of gait and adjust the dampening accordingly. The proprietary software program allowed for general parameters to be adjusted by means of a portable data assistant. Since the software could not be changed, a new state-machine algorithm could not be written. The variable-damping knee can output a maximum peak dampening torque of about 60 Nm which is below the 35 Nm that is needed from the passive element optimization analysis. The variable-damping knee has a small battery pack on board and during normal operation it consumes 2 Watts of power. The variable-damping knee was invented by Professor Hugh Herr and his peers during his tenure at the MIT A.I. Laboratory [Herr et al. (2003); Deffenbaugh et al. (2001)].

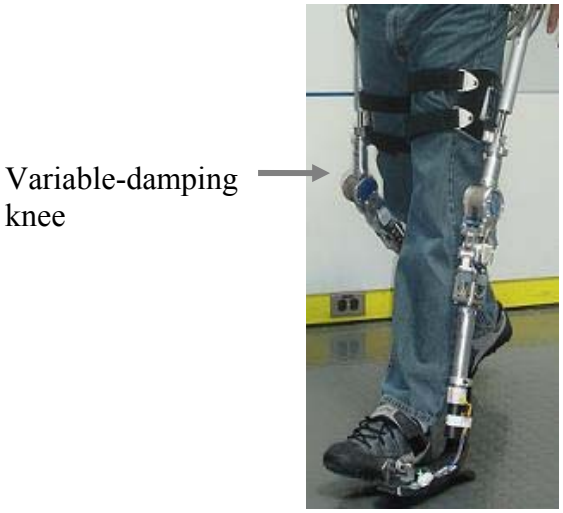

Figure 54: Variable-damping knee
The variable-damping knee that can change its damping constant in real time. The knee consists of thin plates that shear iron particles suspended in magneto-rheological fluid. As the magnetic field is increased, the irons particles form chains and the damping is increased. The variable-damping knee was invented at the MIT Leg Laboratory [Herr et al. (2003); Deffenbaugh et al. (2001)] and is now a commercial product manufactured by Össur in Reykjavik, Iceland. When the exoskeleton leg was on the ground, the variable-damping knee damping was increased to keep the knee straight. A minimal amount of damping is needed during the pre-swing phase as described in Table 8 and Figure 23.

3.6 Ankle

A carbon fiber foot-ankle made my Össur was selected. The carbon fiber bi-directional spring and stores and releases energy efficiently in both flexion and extension. The joint between the exoskeleton and the human foot was chosen to be a revolute joint

since it allowed for human heel to come up off the ground during the thrusting phase in power plantar flexion. A cycling shoe is used for the human interface since it has a firm sole and its threaded mounting plate underneath. The revolute joint was assembled using 7075-T6 aluminum machined parts and spring steel plates. Oil impregnated bearings and a clevis pin were used in the joint itself. The length to diameter ratio of the joint is 2.25in to 0.25in or 9.0. The carbon fiber foot-ankle was chosen before the ankle spring analysis was complete. The bi-directional ankle spring did not work as hoped, and this will be expounded upon in Chapter 6. Chapter 7 will describe a uni-directional ankle spring.

Figure 55: Carbon-fiber foot-ankle
The Carbon-fiber foot-ankle, made my Össur, was implemented for the exoskeleton ankle joint. Carbon fiber which is very efficient at storing and releasing energy. The foot-ankle shown is a bi-directional springed ankle. It was found that for the exoskeleton, a spring in ankle dorsi-flexion spring is undesirable since it caused the variable-damping knee to brake. A uni-lateral springed ankle is discussed in the Chapter 7.

3.7 Summary

A rigid parallel orthotic exoskeleton structure was the fundamental architecture to transfer the backpack load forces to the ground. The exoskeleton interfaced to the human by means of shoulder straps, a hip harness, thigh cuffs, and a shoe attachment. Natural walking kinematics was preserved by co-locating the exoskeleton hip, knee, and ankle joints to their biological counterparts as best as possible. A cam mechanism was implemented at the hip joint to project the exoskeleton hip center near the biological hip center. The cam mechanism also corrected for discrepancies between the exoskeleton and biological legs during abduction. The passive spring elements were implemented at the hip and ankle and a variable damper was implemented at the knee.

Chapter 4 Experimental Methods

4.1 Introduction

The research objective is to build an orthotic device to assist a human in carrying a 75 lb load during walking. The utility of the exoskeleton can be quantified by comparing the metabolic cost for loaded walking with and without the exoskeleton. This chapter outlines the experimental methods and metrics for quantifying the metabolic cost. The experiments attempted to answer the hypotheses of this thesis. The two hypotheses from Chapter 1 are restated here for convenience.

- Hypothesis 1: I hypothesize that a quasi-passive leg exoskeleton implementing elastic storage elements at the hip and ankle and a dissipative variable damper at the knee will improve metabolic walking economy for carrying a 75lb load compared with unassisted loaded walking.
- Hypothesis 2: I hypothesize that a quasi-passive leg exoskeleton implementing elastic storage elements at the hip and a dissipative variable damper at the knee will improve metabolic walking economy for carrying a 75lb load compared with a leg exoskeleton without any elastic energy storage or variable-damping capability.

Table 15 Hypotheses Restated

Testing hypothesis 2 was broken into two parts (1) testing the metabolic advantage of the knee damper and (2) testing the metabolic advantage of the energy storage elements i.e. the springs.

4.2 Study Participant

The energy management analysis was based on data from Natick Army Labs who's experimental participants had a mass and leg length described in Table 16 [Harman (2000)]. One participant volunteered for the MIT study and he had similar physical characteristics to the participants in the Natick study. Informed consent was obtained from the participant involved in adherence to the procedures outlined by the Committee

on the Use of Humans as Experimental Participants (COUHES) at the Massachusetts Institute of Technology (MIT). The characteristics of the test participant are also listed in Table 16.

[n]	Participants	Age [yr]	Sex [M/F]	Payload [kg]	Mass [kg]	Leg Length [m]	Walking Speed [m/s]
1	Participant 1	25	M	34 load + 15.5exo	91	0.94	0.82 ± 0.11
16	Natick / Harman	30 ± 9	16M 0F	47	77 ± 9	0.96 ± .04	1.33 ± 0.18
several	Bogert			0	70	0.9	1.2

Table 16 Experimental Participants for studies done by MIT and Natick Army Labs

4.3 Quantifiable Metric

Metabolic cost can be quantified by measuring the volume of oxygen (VO_2) that the human consumes while performing a physical task. Measuring metabolic cost is appropriate since there is a proportional relationship between the mechanical work done by the human and metabolic cost [Donelan (2002)].

To quantify the metabolic advantage of the exoskeleton, VO_2 was measured for three cases: (1) Resting metabolic rate, (2) walking with a 75lb backpack, and (3) walking using the exoskeleton assist with a 75lb load. The resting metabolic rate would be treated as a DC offset that is subtracted out of the other two VO_2 measurements. The metabolic advantage of the exoskeleton is determined by the following equation.

$$\%Metabolic\ Advantage = \frac{(backpack\,VO_2 - rest\,VO_2) - (exoskeleton\,VO_2 - rest\,VO_2)}{(backpack\,VO_2 - rest\,VO_2)} \quad (4.1)$$

4.4 Experimental Procedure

On the day of the experiment, the Cosmed K_4B_2 VO_2 equipment was calibrated following the procedures outlined in the Cosmed user manual [K4B2 User manual, X Edition (2004)].

The participant adhered to the following guidelines:

1. No smoking for 2 - 3 hrs
2. No intense or prolonged exercise for 24 hours
3. No caffeine for 3 hours

4. No heavy meals for 3 hours
5. Stay hydrated
6. No talking when wearing the VO_2 mask
7. Maintain a consistent walking speed and walking cadence

Table 17 Participant guidelines

The order of events of the experiment was as follows:

1. *Tune exoskeleton to participant:* The participant wore the exoskeleton and it was adjusted and tuned to achieve an optimal fit.
2. *Acclimating to the exoskeleton:* The participant walked wearing the exoskeleton for a few minutes to acclimatize to the hardware and to find a self-selected walking speed and cadence.
3. *VO_2 system worn:* The Cosmed VO_2 mask was fastened tightly to the participants face to prevent any air leakage. The Cosmed portable unit was strapped to the participant's chest.
4. *Calibrating walking speed:* A motorized golf caddy was used to control walking speed for the participant. The speed of golf caddy was calibrated to a nominal target speed using a section of the track and a stop watch.
5. *Resting metabolic rate:* The participant sat and 8 minutes of resting metabolic rate were measured and recorded.
6. *Exoskeleton test:* Wearing the exoskeleton, the participant walked around an indoor track for 10 minutes. The participant would match their walking speed to that of the motorized golf caddy.
7. *Resting metabolic rate:* The participant sat for 8 minutes and the resting metabolic rate was measured again.
8. *Resting:* The participant took a small break and drank some water.
9. *Acclimating to the backpack:* The participant spent a few minutes to acclimatize to walking with the backpack. With the help of the golf caddy, the participant maintained the same walking speed as in the exoskeleton test.
10. *Backpack test:* Wearing the backpack, the participant walked along the indoor track for 10 minutes.

11. *Resting metabolic rate:* The participant sat for 8 minutes and the resting metabolic rate was measured.
12. *Subsequent Tests:* Subsequent exoskeleton tests were done following the pattern.

Table 18 Experimental Procedure

Chapter 5 Experimental Results

5.1 Quantitative Results

Metabolic tests were performed on several exoskeleton configurations. The results from these experiments are compiled in Table 19. The actual measured VO_2 data from these tests can be viewed in the appendix of this thesis. Both walking and resting data were taken for each configuration. The resting metabolic rate shown in the table is the average of the resting rates measured both before and after the walking test. Resting metabolic rate acts like a DC offset and must be subtracted out when comparing metabolic results. Thus, the metabolic values shown in the difference column have been adjusted for the resting rate and can be compared to each other. Note that 'pin' joints refer to a simple revolute joint with no springs, and the 'carbon composite foot-ankle' refers to a bi-directional ankle spring.

Date	Tests	VO2			Velocity	Location
2005		rest [mL/min]	walk [mL/min]	diff [mL/min]	Vel. [m/s]	MIT
22-Apr	Exoskeleton, 75lb, hip springs, variable-damping knee, carbon composite foot-ankle	320	1084	**764**	0.71	Johnson Track
26-Jun	Exoskeleton, 75lb, no hip springs, pin knee, pin ankle	336	1189	**853**	0.84	Johnson Track
26-Jun	Exoskeleton, 75lb, hip springs, pin knee, carbon composite foot-ankle	418	1046	**628**	0.82	Johnson Track
26-Jun	Exoskeleton, 0lb, no hip springs, pin knee, pin ankle	397	817	**420**	0.82	Johnson Track
27-Jun	Backpack, 75lb	340	807	**467**	0.86	Johnson Track
27-Jun	Backpack, 0lb	337	658	**321**	0.86	Johnson Track

Table 19 Experimental metabolic results
Metabolic tests were performed on several exoskeleton configurations as well as the backpack configuration. The difference column adjusts the walking metabolic rates by subtracting out its corresponding resting rate.

The tests in Table 19 can be regrouped such that more meaningful results can be extrapolated from the data. The tables on the following pages show these more specific

results. Reasons for these results will be discussed in Chapter 6. For the tables on the following pages 'V.D.' means variable-damper and 'C.C.' means carbon composite.

It was found that all of the exoskeleton configurations tested provided a negative metabolic advantage compared to unassisted loaded walking. The exoskeleton configuration incorporating elastic storage elements at the hip and ankle and a variable-damper at the knee yielded a metabolic advantage of -64% compared to unassisted loaded walking. When the variable-damping knee was substituted with a pin joint, then the metabolic cost improved to -34% compared to unassisted loaded walking. If the springs were then removed from this exoskeleton, then the metabolic cost worsened dramatically to -83% compared to unassisted loaded walking. These results are summarized in Table 20.

Comparison 1	Dif. VO2	Speed	Advantage**
Exoskeleton, 75lb, hip springs, V.D. knee, C.C. foot-ankle	764	0.71	**-64%**
Exoskeleton, 75lb, hip springs, pin knee, C.C. foot-ankle	628	0.82	**-34%**
Exoskeleton, 75lb, *no* hip springs pin knee, pin ankle	853	0.84	**-83%**
Backpack, 75lb	467	0.86	**0%**
**Relative metabolic benefit compared to Backpack, 75lb			

Table 20 Comparing exoskeleton configurations
All of the exoskeleton configurations provided a negative metabolic advantage relative to the unassisted backpack case. Some however, were better than others.

The current implementation of the variable-damping knee performed worse than a simple pin joint at the knee for the exoskeleton configuration incorporating hip and ankle elastic storage elements. When the variable-damping knee was replaced with a simple pin joint knee, the metabolic rate decreased by 18% for the aforementioned exoskeleton. This result is summarized in Table 21.

Comparison 2	Dif. VO2	Speed
Exoskeleton, 75lb, hip springs, V.D. knee, C.C. foot-ankle	764	0.71
Exoskeleton, 75lb, hip springs, pin knee, C.C. foot-ankle	628	0.82

Table 21 Comparing knee joints
At the knee joint, implementing a pin joint relative to the variable damper reduces the metabolic cost by 18%.

It was found that elastic energy storage elements implemented at the hip and ankle of a pin joint exoskeleton decreased the metabolic rate of carrying 75lb by 26% compared to an equivalent exoskeleton without elastic energy storage elements. This result is summarized in Table 22.

Comparison 3	Dif. VO2	Speed
Exoskeleton, 75lb, *no* hip springs, pin knee , pin ankle	853	0.84
Exoskeleton, 75lb, hip springs, pin knee, C.C. foot-ankle	628	0.82

Table 22 Comparing springs and no springs
At the hip and ankle joints, implementing springs relative to simple pin joints reduces the metabolic cost by 26%.

It was found that an empty, unloaded exoskeleton increases the metabolic rate of walking by 31% compared to unassisted, unloaded walking. This result is summarized in Table 23.

Comparison 4	Dif. VO2	Speed
Exoskeleton, 0lb, *no* hip springs, pin knee, pin ankle	420	0.82
Backpack, 0lb	321	0.86

Table 23 Unloaded exoskeleton baseline
The unloaded exoskeleton increases the metabolic cost of unloaded walking by 31%.

It was found that the incremental metabolic cost of adding 75lb to the exoskeleton configuration was 42% greater than the incremental metabolic cost of adding 75lb to the unassisted walking configuration. This result is summarized in Table 24.

Comparison 5	Dif. VO2	Speed
Exoskeleton, 75lb, hip springs, pin knee, C.C. foot-ankle	628	0.82
Exoskeleton, 0lb, *no* hip springs, pin knee, pin ankle	420	0.82
Incremental Cost	*208*	
Backpack, 75lb	467	0.86
Backpack, 0lb	321	0.86
Incremental Cost	*146*	

Table 24 Incremental Cost
The increased incremental cost of adding 75lb to the exoskeleton configuration relative to the backpack configuration is 42%.

5.2 Qualitative Results

The test participant explained that carrying the 75lb load felt more comfortable when wearing the exoskeleton compared with the backpack alone. The exoskeleton efficiently transferred the load forces to the ground. Conversely, without the exoskeleton, the entire payload force was transmitted through the human's shoulders, hips, and legs. This resulted in an experience of discomfort at the shoulder strap and waist belt interfaces. The exoskeleton implemented a hip extension spring which countered the backward overturning moment of the load. For the backpack configuration, the participant needed

to compensate for the overturning moment by leaning forward to move the center of gravity of their upper body over their feet. The participant preferred to walk and stand in an upright posture and mentioned that the exoskeleton enabled this capability while the backpack configuration did not.

Chapter 6 Discussion

6.1 Introduction

Why did the metabolic cost of walking while carrying a 75lb load increase for wearing the exoskeleton as compared to wearing only the backpack? What were the advantages of incorporating the spring and damper elements into the exoskeleton? This chapter suggests several possible reasons why the exoskeleton increased the metabolic cost of unassisted load carrying. In addition, the chapter describes the effects of elastic energy storage and variable-damping on exoskeleton load carrying.

6.2 Discussion of Experimental Results

6.2.1 Comparison 1

Comparison 1 showed that the three exoskeleton configurations for carrying a 75lb load resulted in a higher metabolic cost compared to the nominal loaded backpack configuration. Factors that contributed to the higher metabolic cost include the additional distal mass of the exoskeleton along the leg, constrained leg motion, and misalignment of the exoskeleton to the human leg. Some of the exoskeleton configurations were higher than others and the subsequent comparisons attempt to explain why.

6.2.2 Comparison 2

Comparison 2 showed that a pin joint at the knee provided a lower metabolic cost than the variable damping knee although Chapter 2 supported the use of a damper at the knee. Implementing the variable damping knee on the exoskeleton may not have worked because it may have added too large of a distal mass which is metabolically costly. The variable damping knee is an energy dissipative device having a finite minimal damping level. Thus, the variable damping knee would always dissipate energy throughout the walking cycle even at zero input current. The variable damper had some programming quirks which caused it to brake at the wrong time and not brake when it should have. This irregular behavior of the variable damper may have also added to the increased

metabolic disadvantage. The variable damper is discussed further in detail in section 6.3.1.

6.2.3 Comparison 3

Comparison 3 showed that implementing springs at the hip and ankle joints reduced the metabolic cost relative to having plain revolute pins at these joint locations. The fact that the hip and ankle springs provided a metabolic advantage is consistent with the analysis in Chapter 2. Although the theoretical metabolic advantage of 56% (see Table 9) is greater than the actual advantage of 26%, the analytical results did not take into account the effect of the added distal mass nor any altered gait patterns that may have resulted as a consequence of wearing the exoskeleton.

6.2.4 Comparison 4

Comparison 4 showed that an unloaded exoskeleton increased the metabolic cost of unloaded walking by 31%. Griffen et al. found that for a 10% body mass increase at the body's center of mass results in a 15% increase in metabolic cost [Griffen et al. (2003)]. The exoskeleton weighs 34 lb and our test participant weighs 200 lb. Assuming that Griffen's result can be extrapolated linearly then a 34 lb mass at the body's center of gravity would yield a 25% increase in metabolic cost for our participant. The exoskeleton increased the metabolic cost by 31%, which is reasonable because the exoskeleton mass is distributed along the human leg, and it has been shown that distal mass is more metabolically costly than centralized mass [Royer et al. (2005)]. Any advantage provided by the exoskeleton structure and passive energy elements when loaded must first overcome this initial setback. Reducing the weight of the exoskeleton should have significant metabolic advantages.

A more detailed experiment to determine the kinematic efficiency of the exoskeleton is proposed in section 7.4.

6.2.5 Comparison 5

Comparison 5 showed that the incremental metabolic cost associated with adding a 75lb load to both the exoskeleton and backpack configurations was greater for the

exoskeleton configuration by 42%. This means that even after discounting the initial metabolic setback of an empty exoskeleton, the incremental metabolic cost of adding weight to the passive exoskeleton was still worse than the backpack case. This suggests that the disadvantage caused by the exoskeleton is more involved than simply the additional mass of the exoskeleton.

It has been shown that humans naturally optimize their gait to walk in the most metabolically efficient manner possible [Anderson & Pandy (2001)]. It is reasonable to expect that any deviation from this natural human trajectory would result in an increase in metabolism. If the exoskeleton constrained or altered normal human walking trajectories then this may explain the observed increase in metabolic rate. Slight differences between the exoskeleton and the human could be responsible for the altered gait pattern. For example, the exoskeleton knee joint is a simple pin joint with a fixed center of rotation while the human knee does not have a fixed center of rotation [Sutherland et al. (1994)]. In addition, the exoskeleton ankle joint is a single degree of freedom carbon composite elastic spring while the human ankle consists of seven bones that provide ankle inversion/eversion and dorsi/plantar flexion degrees of freedom [Inman et al. (1981)]. Still further, the exoskeleton hip harness is a rigid frame where the human body's vertebra is a flexible member. These differences between the exoskeleton and the human may have caused an altered gait pattern and an increase in metabolic rate.

6.3 Design

From analyzing the data, the video, and feedback from the professional orthotist, the exoskeleton design engineers, and the participants, three areas of the exoskeleton design were targeted as areas that could be improved. They are the controllability of the variable-damping knee, the bi-directional constraint of the Carbon-fiber foot-ankle feet, and the flexion in the hip harness.

6.3.1 Controllability of the Variable-Damping Knee

The variable-damping knee made by Össur of Reykjavik, Iceland is a commercial prosthetic knee for amputees. The knee has an onboard microprocessor programmed with a state machine controller to adjust the dampening of the knee for normal amputee

walking [Herr (2003)]. The state machine controller was coded with Össur's proprietary software and could not be modified. Össur provided a portable data assistant that could plug into the knee and allow for some general parameters to be tuned, but the overall controller algorithm could not be altered.

The exoskeleton is using the variable-damping knee not as a prosthetic device but rather as a primary joint of an orthosis. The current state machine controller is not ideally suited for use in the exoskeleton. The current state controller did not always impede early stance knee flexion, causing the exoskeleton leg to buckle under the 75lb load. The exoskeleton leg was designed to act as a column and support load when extended straight such that the human would pivot over the leg in an inverted pendulum motion. However, if the exoskeleton knee buckles, the forces are then transferred to the human leg causing discomfort and straining of the leg muscles.

The participant was able to adjust their gait to prevent the knee from buckling. Prior to early stance, during the swing phase, the participant would actively extend their leg in front of their body to ensure that the knee was fully extended at heel strike. The participant could then pivot over the exoskeleton leg as designed. The participant had to add energy to the knee to achieve this objective. It can be seen from Figure 16 that the knee absorbs energy during the swing phase for normal walking. Thus it was very metabolically costly to counter normal knee functionality changing the kinematics from negative power to positive power. The participant commented after the experiment that they felt their thigh muscles ache from having to adjust their gait.

The participant could either choose to not adjust his gait having the variable-damping knee buckle during early stance causing a spike in force in his leg or he could choose to adjust his gait during the swing phase and make his thigh muscles work harder. The participant preferred altering his gait for comfort reasons. Both of these options were metabolically detrimental. A solution to this problem is outlined in Chapter 7.

6.3.2 The carbon composite foot-ankle bi-directional constraint

The bi-directional carbon composite foot-ankle system shown in Figure 55 was a contributing factor to why the variable-damping knee braked in the early stance phase. The carbon composite foot-ankle would store energy for both ankle extension and

flexion. During early stance, the forefoot would rotate forward as seen in 'A' and 'B' in Figure 56, which would cause a moment about the ankle joint. This moment caused the exoskeleton shank to rock forward causing the variable-damping knee to flex. A spring for the ankle dorsiflexion is still needed during periods 'C', 'D', and 'E' as outlined in Chapter 2. A solution to the moment problem is outlined in Chapter 7.

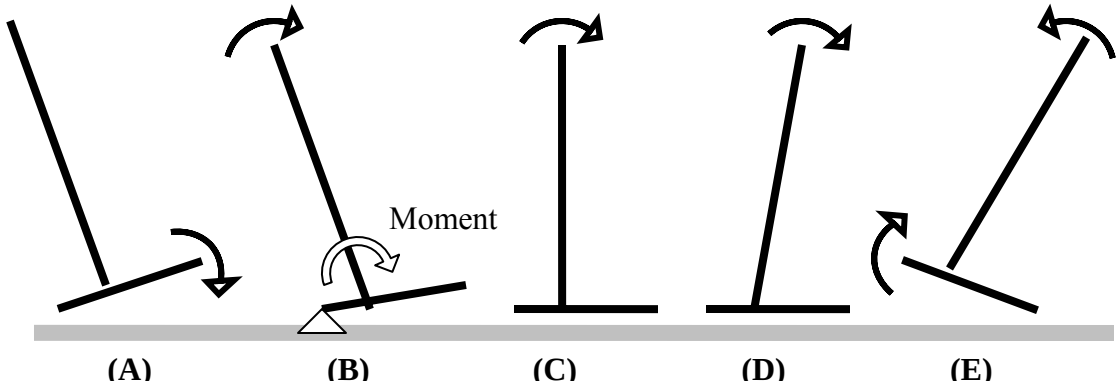

Figure 56 Bi-directional ankle action
(A) Heel strike is followed by controlled dorsi-flexion. (B) Controlled dorsi-flexion causes a moment about the ankle, rocking the shin forward. The moment caused by the shin causes the variable-damping knee to brake. Energy is stored in the ankle spring. (C) The shin rocks forward releasing the previous stored energy. (D) The shin rocks forward and stores energy in the ankle spring again. (E) The energy in the spring is released and assists in power plantar flexion.

6.3.3 Flexion in hip harness

The hip harness in Figure 31 was reinforced with stiffeners to add rigidity, but it still flexed slightly. The compliance in the harness was not ideal for transferring the backpack load to the ground. The harness was assembled using an aluminum back plate, carbon fiber 'L' brackets, and four aluminum stiffeners. Chapter 7 outlines a new harness to be designed that is stiffer, lighter, and a single piece.

6.4 Summary

In summary, springs are necessary components in exoskeleton design. It was found that elastic storage elements at the exoskeleton's hip and ankle joints reduced metabolism by 26% compared to an equivalent exoskeleton without elastic storage elements. Although not found in this study, the variable-damping knees, if implemented correctly, may also offer a metabolic advantage. The additional distal mass and kinematic constraints of the exoskeleton contribute to the overall unfavorable metabolic cost

compared with unassisted load carrying. The various quasi-passive exoskeleton configurations were unable to pay for themselves metabolically when loaded with 75 lb.

Chapter 7 Future Work

7.1 Introduction

Several areas of improvement are targeted for future work of the exoskeleton project. Greater care and attention to detail in interfacing the exoskeleton to the human is a priority. A new state machine control algorithm needs to be programmed for the variable-damping knees. The bi-directional elastic carbon composite foot-ankle needs to be replaced by an ankle employing uni-directional elastic energy storage. A stiffer and lighter hip harness is needed. A biomechanics data set measured directly from the exoskeleton itself would benefit further analysis. Adding power at the hips of the passive exoskeleton may yield metabolic savings. More metabolic testing is needed to verify if these changes help reduce the metabolic cost of walking.

7.2 Redesign

7.2.1 Alignment

From the metabolic results and feedback from the test participant, it can be concluded that aligning the exoskeleton to the human such that the exoskeleton does not impede normal human motion is a very important problem to be solved. Much care was taken to achieve an exoskeleton that did not impede the human, but it appears that more can be done. Further work should be focused on how to interface the rigid exoskeleton to the human such that it enables fluid, un-impeded motion.

7.2.2 Variable-Damping Knee

As mentioned in the previous chapter, the variable-damping knee was designed as a prosthetic device for normal amputee walking. The current state machine controller does not always impede knee flexion during early stance, which is not ideal for use in the exoskeleton. To circumvent this hindrance, it will be necessary to implement new electronics and a custom microcontroller so that a new algorithm could be written to meet the needs of the exoskeleton. The current variable-damping knee mechanical hardware

would remain unchanged. The new state machine controller would lock the knee straight at heel strike and keep it locked throughout the early stance phase. A primitive state machine for level ground walking may be implemented as follows.

- State 1: When the exoskeleton heel contacts the ground at heel strike, the variable damper sets to the maximum value. The variable damper effectively would lock the exoskeleton leg straight.
- State 2: From 54% to 62% gait cycle the knee brakes during the pre-swing phase. During this period, the variable damper is set to simulate a constant dampening constant which was found in Table 8 and shown in Figure 23. The resistive torque that the damper would deliver would be proportional to the knee angular velocity.
- State 3: Otherwise the damper would be turned off or set at the minimal value of damping.

7.2.3 Uni-directional Ankle Spring

The current bi-directional ankle spring created a moment about the lower leg shank which caused the variable-damping knee to buckle. A uni-directional spring ankle is proposed that allows free ankle controlled plantarflexion and stores energy during controlled dorsiflexion. The free extension from 'A' to 'B' in Figure 57 eliminates the moment about the ankle that caused the knee to buckle. During ankle dorsiflexion from 'C' to 'D', the spring stores energy and then releases that energy during the thrusting phase in period 'E'. The spring constant and engagement angle were outlined in Chapter 2. A conceptual sketch of the new ankle is described in the figure below. The red line represents a compression spring.

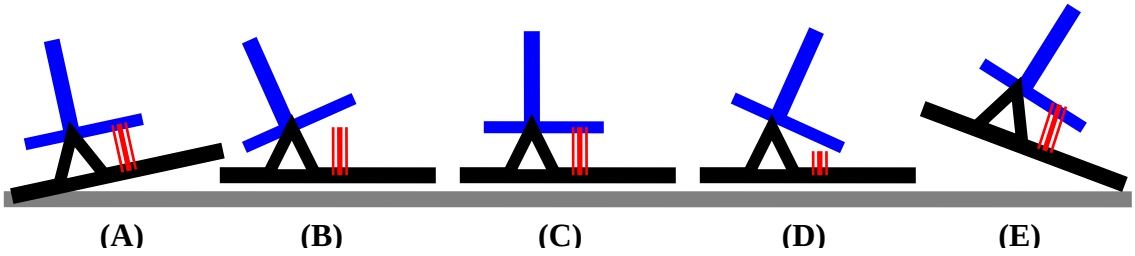

Figure 57 Uni-directional ankle action
(A) Heel strike is followed by controlled dorsiflexion. (B) Controlled dorsiflexion about the ankle. A moment is not created about the shin. (C) The red uni-directional ankle spring engages. (D) As the shin rocks forward, energy is stored in the ankle spring. (E) The energy in the spring is released and assists in power plantar flexion.

College Park of Fraser, Michigan makes a carbon fiber ankle joint called the Tribute Foot [*Tribute Information Sheet* (2005)] whose functionality closely aligns with needs of the exoskeleton ankle. The Tribute Foot's posterior bumper can be removed and an anterior spring could be selected such that its spring constant matches the value found in Chapter 2. The Tribute foot is shown in Figure 58.

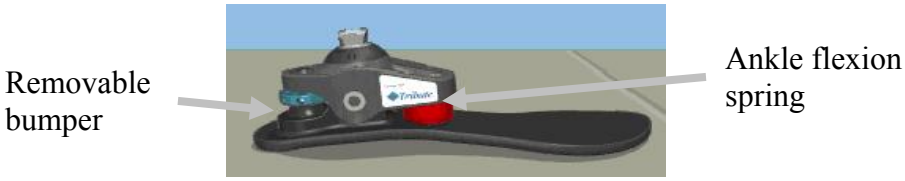

Figure 58 College Park Tribute
The Tribute ankle is made by College Park of Fraser, Michigan and is a candidate for a unidirectional spring ankle which was described in Figure 57.

7.2.4 Hip Harness

A new hip harness is proposed that is lightweight, stiff, and a single piece. Carbon fiber is the favored material since it can be molded to achieve almost any shape and has a high strength to weight ratio. Stiffeners can also be embedded in the harness for added stiffness.

7.3 Exoskeleton Data Set

Chapter 2 used biomechanics data based on a human carrying a loaded backpack [Harman (2000)]. To provide more accurate results for optimizing the exoskeleton, two new data sets will be acquired. The first data set will be the human wearing the exoskeleton with a 75lb payload but with the passive elements disabled. The second data set will be with the passive elements enabled. Both data sets can be obtained once the

modified variable-damping knee, new ankle spring, and new harness are implemented in the exoskeleton.

7.4 Measuring the Exoskeleton's Kinematic Efficiency

The kinematic efficiency of the exoskeleton is a metric of how well the exoskeleton is able to carry a payload. It attempts to show how much of a metabolic advantage/disadvantage is due to the added mass and to the constrained kinematics caused by the exoskeleton. This test is a close variation to the 'Comparison 5' test in section 5.1. Metabolic testing of four configurations would need to be performed, they are:

1. Exoskeleton loaded: the quasi-passive exoskeleton described in this thesis carrying a payload.
2. Exoskeleton unloaded: the quasi-passive exoskeleton described in this thesis without a payload.
3. Backpack loaded: backpack with a payload with additional mass strapped to thigh, shin, and foot equivalent to the exoskeleton mass.
4. Backpack unloaded: backpack with no payload but with additional mass strapped to thigh, shin, and foot equivalent to the exoskeleton mass.

The incremental cost of adding mass to the exoskeleton would be:

Exoskeleton loaded - Exoskeleton unloaded

The incremental cost of adding mass to the equivalent backpack would be:

Backpack loaded - Backpack unloaded

The kinematic efficiency of the exoskeleton would be

$$\%Kinematic\ Efficiency = \frac{\text{Exoskeleton loaded - Exoskeleton unloaded}}{\text{Backpack loaded - Backpack unloaded}} \qquad (7.1)$$

These tests could be performed over a range of loads and an efficiency curve could be produced which would tell the exoskeleton's kinematic efficiency as a function of load.

7.5 Adding Power

Once the passive exoskeleton is complete, additional metabolic reductions may be possible if power is added to the system. One strategic location to add power is at the

hips since the added motor mass would be closer to the body's center of gravity compared to a motor at the knee or ankle. Adding power at the hips could assist in retracting and protracting the legs throughout the gait cycle, specifically during the 'H1' and 'H3' regions shown in Figure 15. The power input would also assist in walking uphill, where the actuators would provide the power needed for increasing the potential energy of the system.

Chapter 8 Conclusions

Anti-gravity experiments [Jiping et al. (1991); Farley & McMahon (1992); Griffen et al, (2003); Gottschall & Kram (2003)] suggest that it may be possible to build an exoskeleton that reduces the metabolic cost for walking while carrying a 75lb load. The theoretical results from Chapter 2 suggest that implementing springs at the hip and ankle joints and a damper at the knee joint may decrease the metabolic cost for loaded walking. To attain a metabolic reduction, the benefits of the passive elements must outweigh the disadvantages of the additional distal mass needed to implement the passive element [Royer et al. (2005)]. Initial experimental results across three exoskeleton configurations were unable to demonstrate a decrease in metabolic cost for loaded walking. Thus, the first hypothesis of Table 1 was not supported by these pilot data. The quasi-passive leg exoskeleton implementing springs at the hip and ankle and a dissipative variable damper at the knee was not able to improve metabolic walking economy for carrying a 75lb load compared with unassisted loaded walking.

The experimental results showed that implementing springs in the exoskeleton was advantageous while the current implementation of the variable damping knee was not. Thus, the second hypothesis of Table 1 was supported by the pilot data. The quasi-passive leg exoskeleton implementing springs at the hip and ankle improved metabolic walking economy for carrying a 75lb load compared to a leg exoskeleton without any elastic storage or variable damping capability.

The proposed future work offers suggestions of what could be done to improve the design of the passive exoskeleton. The qualitative and quantitative evidence presented in this thesis suggest that the fundamental problematic area of exoskeleton design is the interfacing issue such that the exoskeleton does not impede normal human motion. If this problem was solved and power was added to this hypothetical exoskeleton, then a metabolic advantage could possibly be achieved.

Exoskeletons for human augmentation have application for military and service personnel, as well as for patients with muscular impairments. Soldiers, fireman,

construction workers, freight handlers, and the physically disabled are all potential future benefactors of exoskeletons.

Bibliography

Anderson, F.C. & Pandy, M.G. (2001), 'Dynamic Optimization of Human Walking', J. of Biomechanical Engineering ,Vol. 123, Issue 5, pp. 381-390.

Au, S.K. (2005), 'An Artificial Ankle-Foot System with Spring, Variable-Dampening, and Series-Elastic Actuator Components', Internal Report at the MIT Biomechatronics Research Group.

van den Bogert, A.J. (2003), 'Exotendons for assistance of human locotion'. *Biomedical Engineering Online*, 2:17.

Deffenbaugh, B., Herr, H., Pratt, G., & Wittig, M., inventors. (2001), 'Electronically Controlled Prosthetic Knee', US Patent 6,764,520.

De Looze, M.P., Toussaint, H. M., & Commissaris, D.A. (1994), 'Relationships Between Energy Expenditure and Positive and Negative Mechanical Work in Repetitive Lifting and Lowering', *Journal Applied Physiology* pp. 77:420-426.

Dick, J. & Crapuchettes, B., (2000), ' Servo-Assisted Lower-Body Exoskeleton With a True Running Gait', DARPA Workshop on Exoskeletons for Human Performance Augmentation (EHPA), Washington, DC.

Dick, J. & Edwards, E., inventors. (1991), 'Human Bipedal Locomotion Device', US Patent 5,016,869.

Donelan J.M., Kram, R., & Kuo, A.D. (2002), 'Mechanical work for step-to-step transitions is a major determinant of the metabolic cost of human walking', *Journal of Experimental Biology* pp. 205; 3717–372.

Farley, C.T. & Ferris, D.P. (1998), 'Biomechanics of Walking and Running: from Center of Mass Movement to Muscle Action', *Exercise and Sport Sciences Reviews* pp. 26:253-285.

Farley, C. & McMahon, T. (1992), 'Energetics of walking and running: insights from simulated reduced-gravity experiments', *The American Physiological Society* pp. 2709-2712.

Gottschall, J.S. & Kram, R. (2003), 'Energy cost and muscular activity required propulsion during walking', *Journal Applied Physiology* pp. 94: 1766–1772, 2003.

Griffin, T.M., Tolani, N.A., & Kram, R. (1999), 'Walking in simulated reduced gravity: mechanical energy fluctuations and exchange', *Journal Applied Physiology* pp. 383-390.

Harman, E., Han, K., Frykman, P., Pandorf, C. (2000), 'The Effects of Backpack Weight on the Biomechanics of Load Carriage', *USARIEM Technical Report* pp. T100-17, Natick, Massachusetts.

Herr, H. & Wilkenfeld, A. (2003), 'User-Adaptive Control of a Magnetorheological Prosthetic Knee', *Industrial Robot: An International Journal* pp. 30: 42-55.

Huang, G.T. (2004), 'Demo: Wearable Robots', *Technology Review*, pp. July/August 2004.

Inman, V.T., Ralston, H.J., & Todd., F. (1981), 'Human Locomotion', in: *Human Walking*, Rose, J. & Gamble, J. G., eds., Williams and Wilkins, Baltimore.

Jansen, J., Richardson, B., Pin, F., Lind, R., & Birdwell, J. (2000), 'Exoskeleton for soldier enhancement systems feasibility study', Technical Report TM-2000/256, Oak Ridge National Laboratory.

Jiping, H., Kram, R., & McMahon, T. (1991), 'Mechanics of running under simulated low Gravity', *Journal Applied Physiology* pp. 71(3): 863-870.

K4B2 User manual, X Edition (2004), COSMED Srl, Rome, Part N. C01508-02-91, pp 14.

Kawamoto, H. & Sankai, Y. (2002), 'Power assist system HAL 3 for gait disorder person', Computers Helping People with Special Needs 8th International Conference, ICCHP 2002. Proceedings (Lecture Notes in Computer Science Vol. 2398) 196-203.

Kazerooni, H. (1996), 'The human power amplifier technology at the University of California, Berkeley', *Robotics Autonomous Systems* pp. 19:179-187.

Kazerooni, H., Racine, J.L., Huang, L., & Steger, R. (2005), 'On the Control of the Berkeley Lower Extremity Exoskeleton (BLEEX)', IEEE International Conference of Robotics and Automation pp. 4364-4371.

Linear Ball Bushing Bearings and Components (2003), Danaher Motion, pp. 16, 135.

Oberg, E., Jones, F.D. & Horton, J.H. (2000), *Machinery's Handbook, 26th ed.* New York: Industrial Press, pp. 239.

Paluska, J.D. (2004), 'Ankle Springs Memo', Internal Memo at the MIT Biomechatronics Research Group.

Rab, G.T. (1994), 'Muscle', in: *Human Walking*, Rose, J. & Gamble, J. G., eds., Williams and Wilkins, Baltimore, pp. 103–121.

Royer, T.D. & Martin, P.E. (2005), 'Manipulations of Leg Mass and Moment of Inertia: Walking', *Medicine & Science in Sports & Exercise* pp. 37(4):649-656.

Skinner, S. (1994), 'Development of Gait,' in: *Human Walking*, Rose, J. & Gamble, J. G., eds., Williams and Wilkins, Baltimore, pp. 123–138.

Sutherland, D.H., Kaufman, K.R., Moitoza, J.R. (1994), 'Kinematics of Normal Human Walking,' in: *Human Walking*, Rose, J. & Gamble, J. G., eds., Williams and Wilkins, Baltimore, pp. 38.

Tilley, A.R. (1993), 'The measure of man and woman,' in: *Human Factors Design*, Henry Dreyfuss Associates, New York, pp. 22–23.

Tribute Information Sheet (2005), College Park, Fraser, Michigan.

Vukobratović, M., Borovac, B., Surla, D., Stokić, D. (1990), *Biped Locomotion: Dynamics, Stability, Control, and Application*, Springer-Verlag, Berlin, pp. 321-330.

Yagn, N., inventor. (1890), ‘Apparatus for facilitating walking, running, and jumping,’ US Patents 438,830 & 420,179.

Appendix

A.1 Natick Army Lab Data

A.2 Metabolic Data

A.1 Natick Army Lab Data [Harman et al. (2000)]

(Hip Angle not Available)

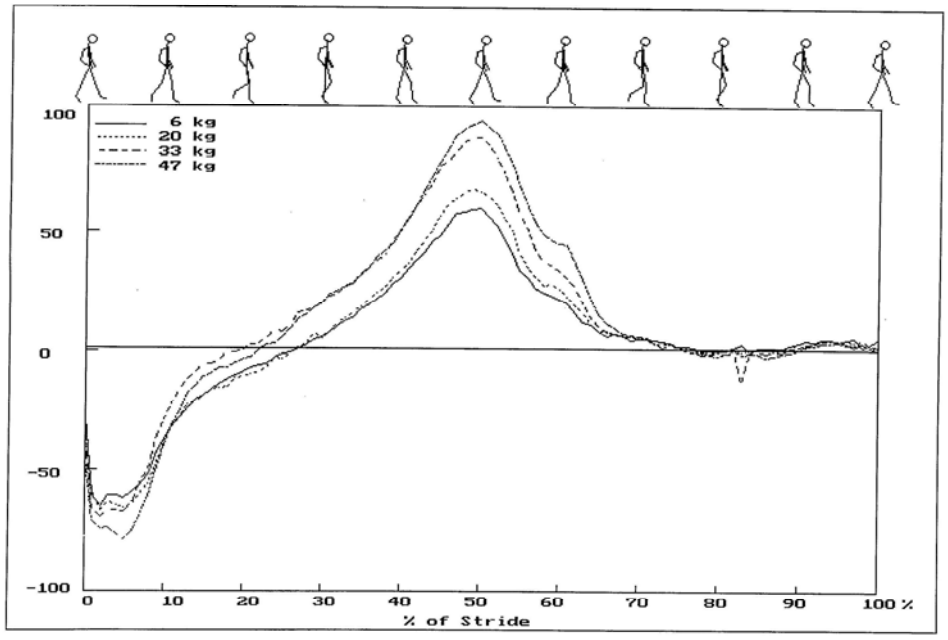

Figure 12. Load effects for hip torque (N•m).

39

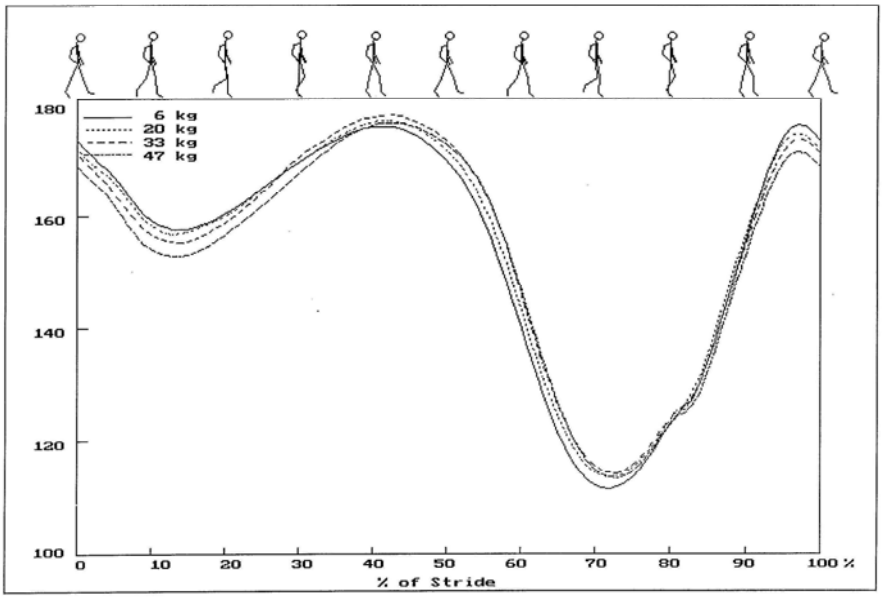

Figure 5. Load effects for knee angle (degrees).

27

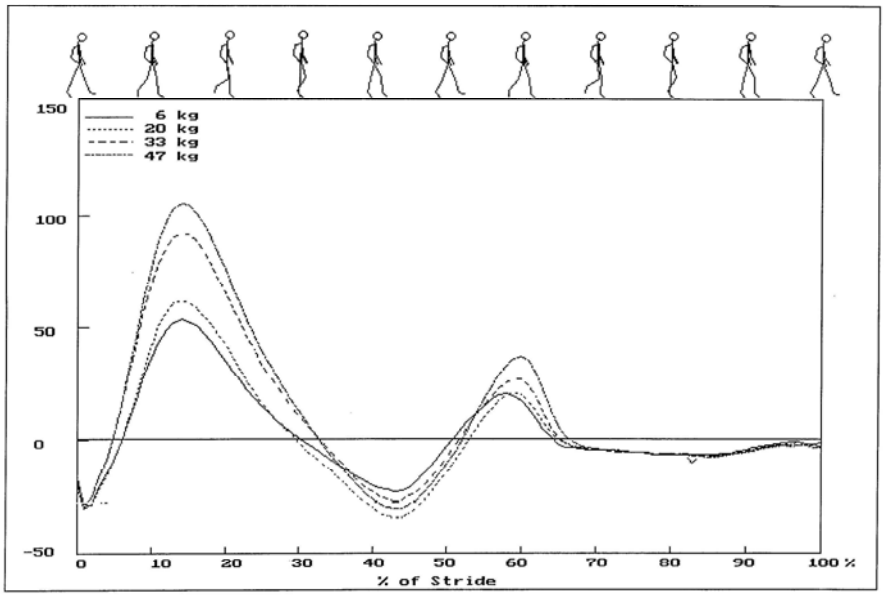

Figure 11. Load effects for knee torque (N•m).

38

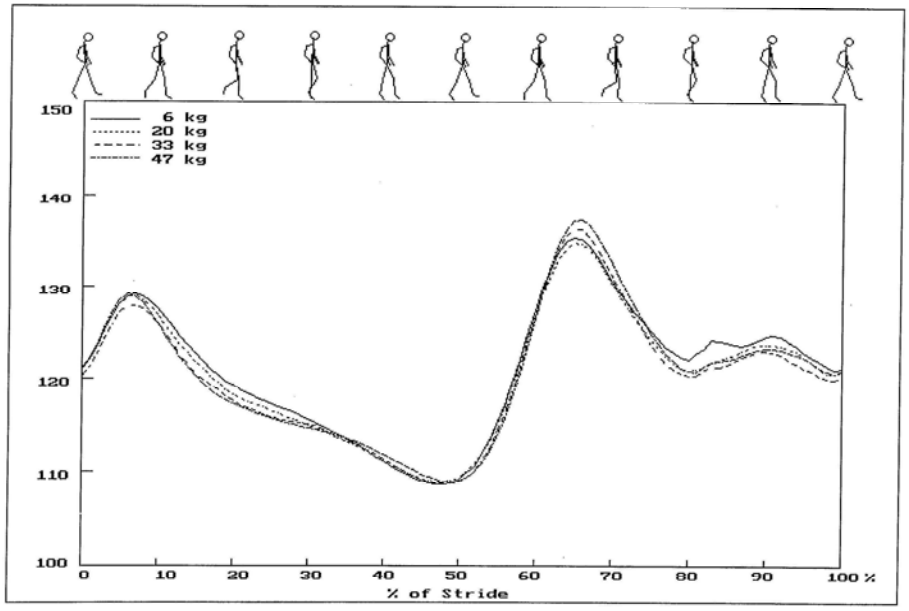

Figure 4. Load effects for ankle angle (degrees).

26

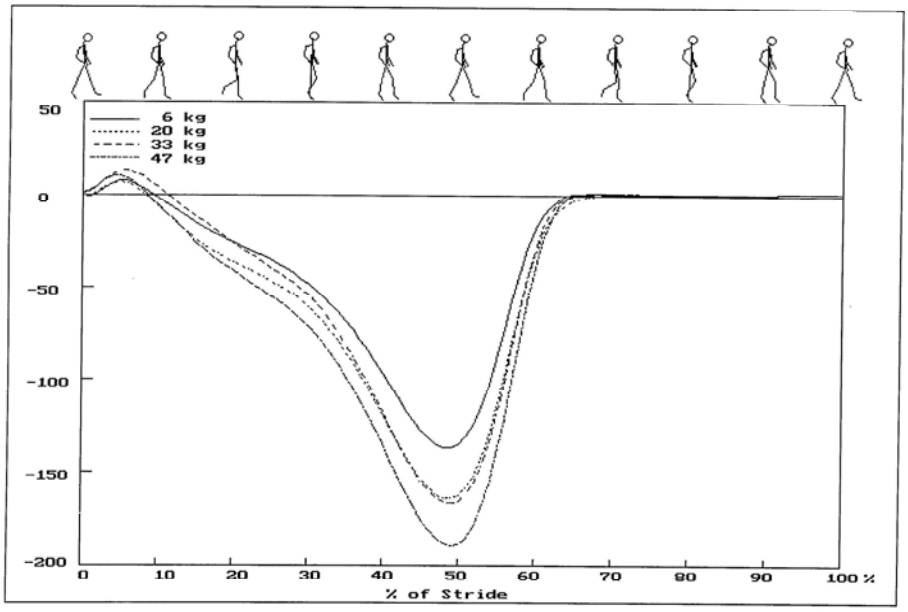

Figure 10. Load effects for ankle torque (N•m).

37

A.2 Metabolic Data

VO_2 was calculated by averaging the values between the dotted vertical lines.

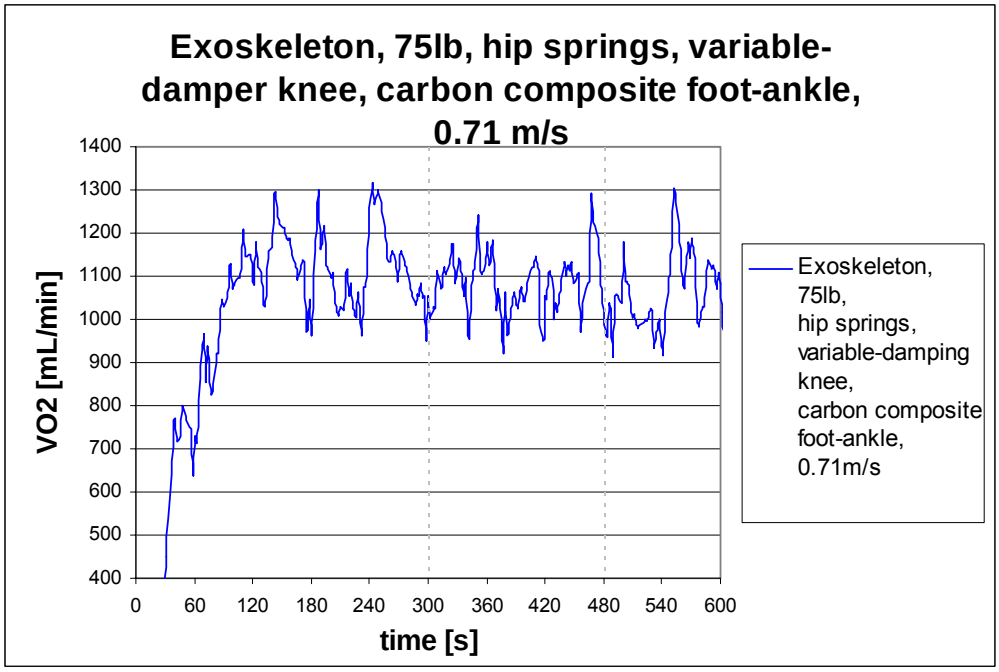

Figure 59 Average walking metabolic rate: 1084 mL/min

Exoskeleton, 75lb, hip springs, variable-damping knee, carbon composite foot-ankle, 0.71m/s.

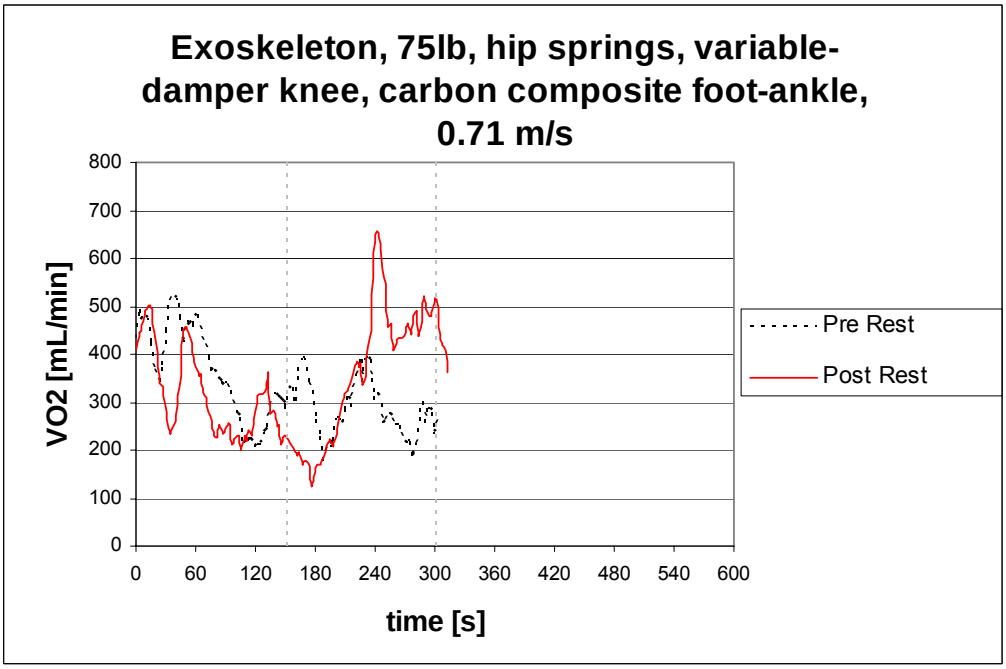

Figure 60 Average resting metabolic rate: 320 mL/min

Exoskeleton, 75lb, hip springs, variable-damping knee, carbon composite foot-ankle, 0.71m/s

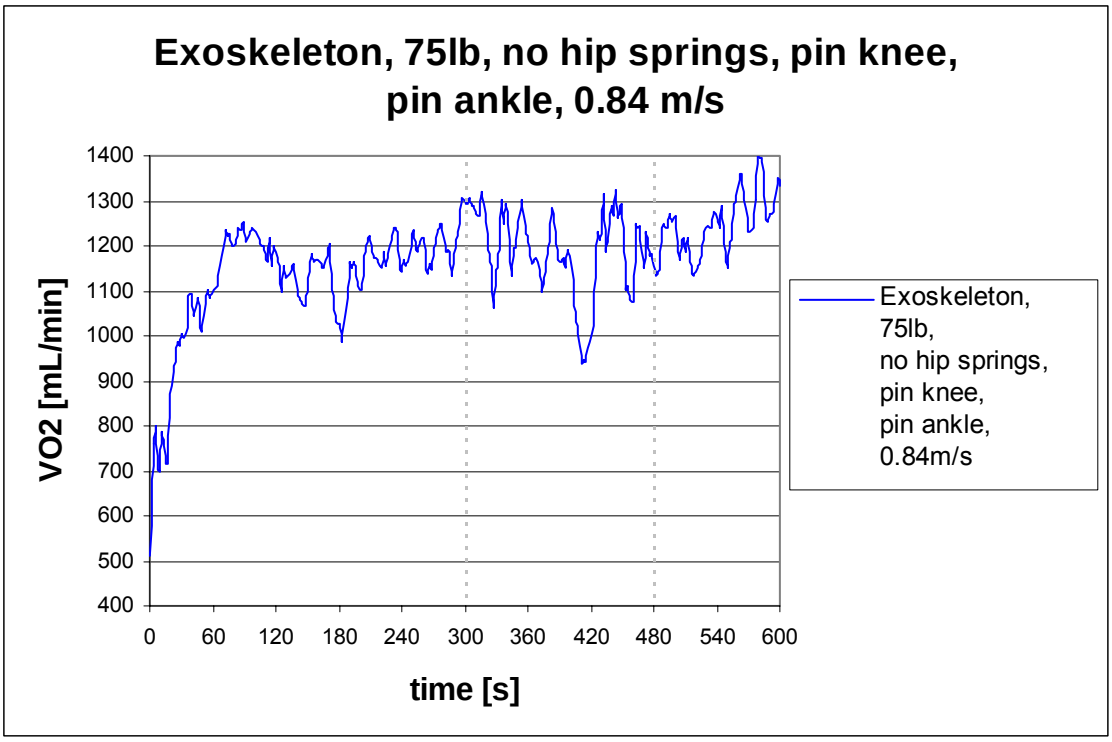

Figure 61 Average walking metabolic rate: 1089 mL/min
Exoskeleton, 75lb, no hip springs, pin knee, pin ankle, 0.84 m/s

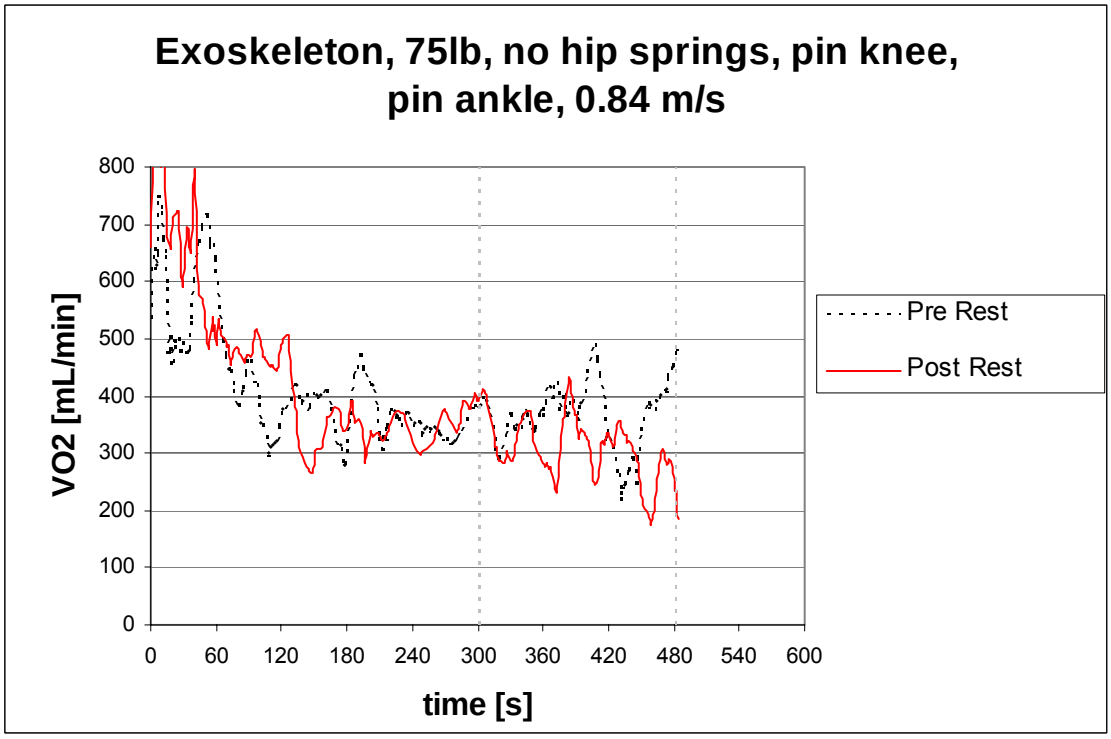

Figure 62 Average resting metabolic rate: 336 mL/min
Exoskeleton, 75lb, no hip springs, pin knee, pin ankle, 0.84 m/s

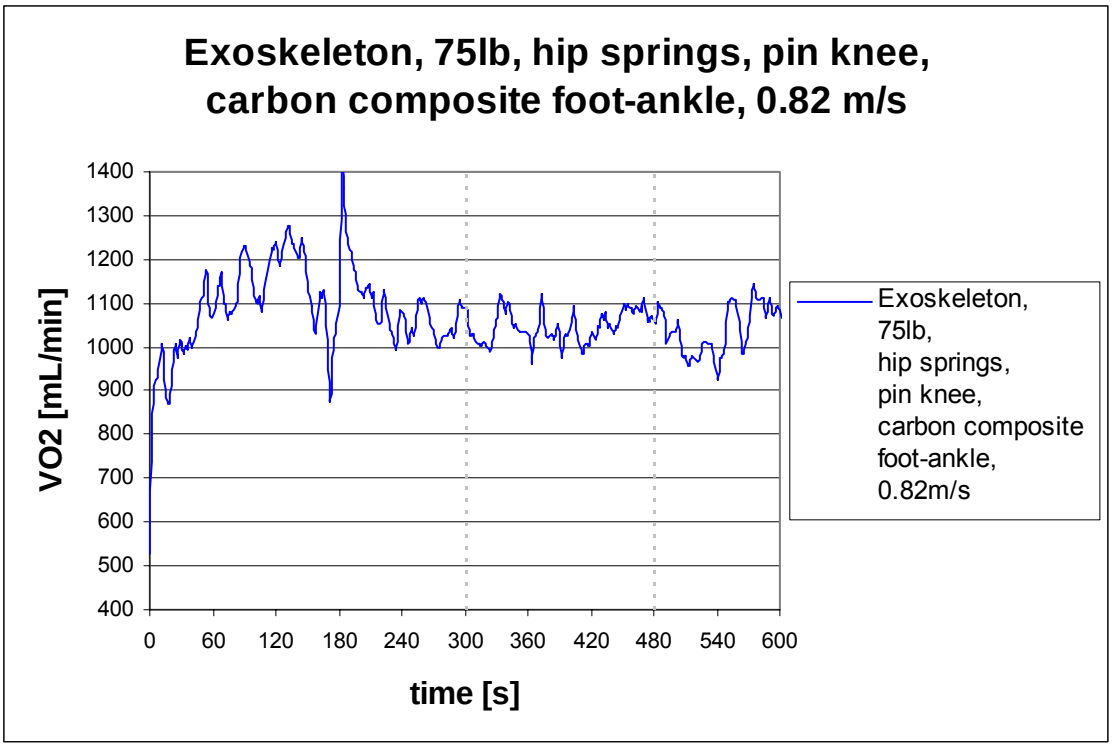

Figure 63 Average walking metabolic rate: 1046 mL/min
Exoskeleton, 75lb, hip springs, pin knee, carbon composite foot-ankle, 0.82 m/s

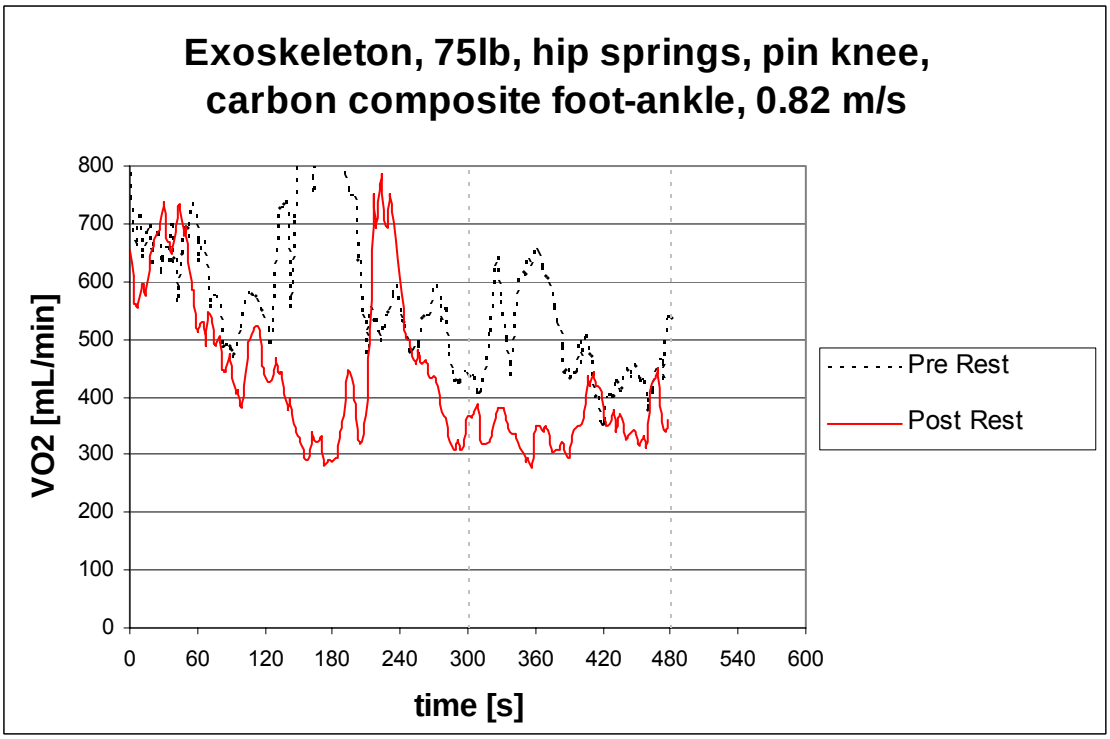

Figure 64 Average resting metabolic rate: 418 mL/min
Exoskeleton, 75lb, hip springs, pin knee, carbon composite foot-ankle, 0.82 m/s

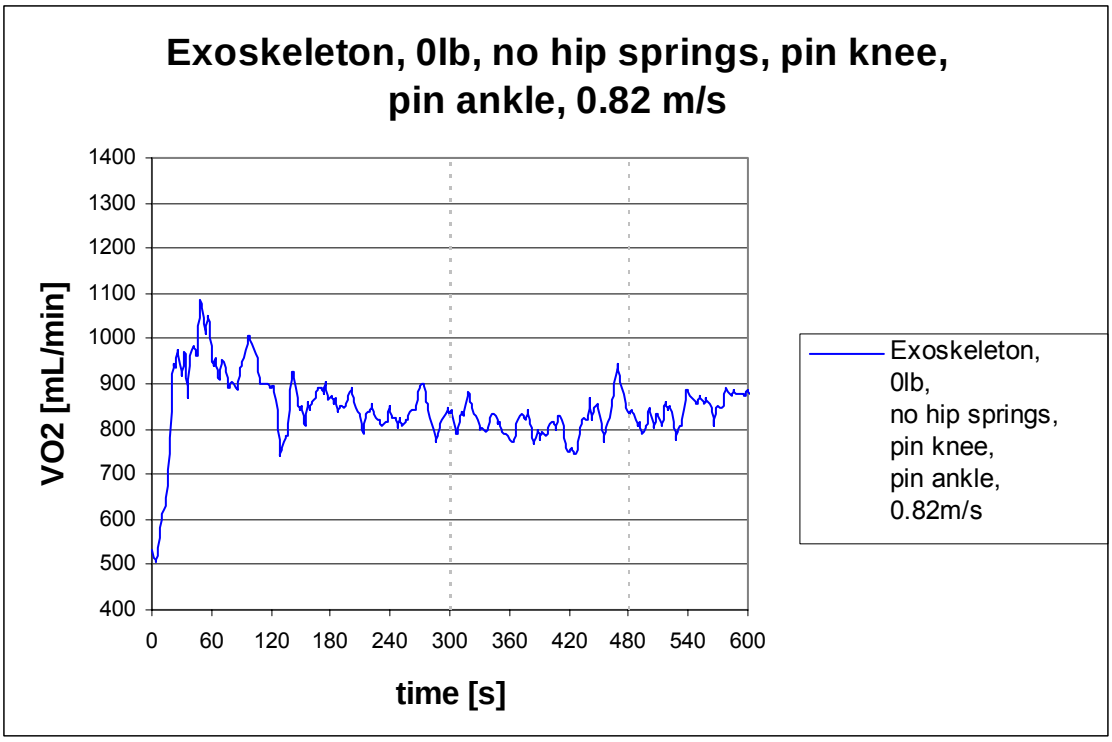

Figure 65 Average walking metabolic rate: 817 mL/min
Exoskeleton, 0lb, no hip springs, pin knee, pin ankle, 0.82 m/s

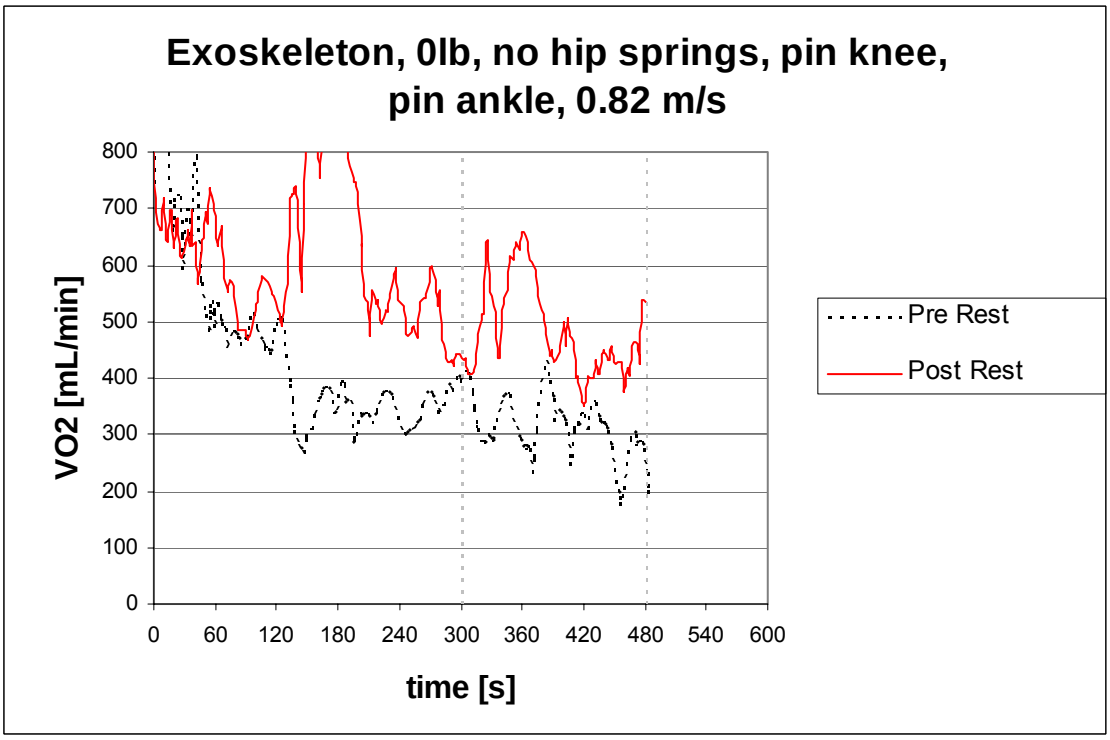

Figure 66 Average resting metabolic rate: 397 mL/min
Exoskeleton, 0lb, no hip springs, pin knee, pin ankle, 0.82 m/s

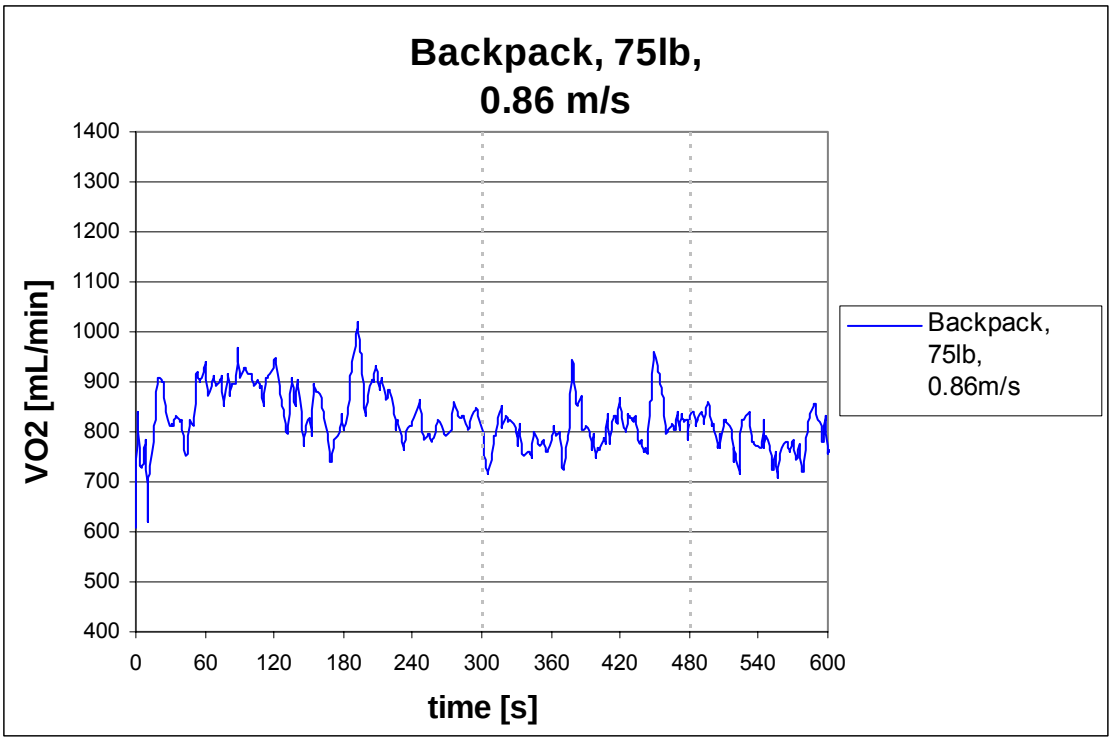

Figure 67 Average walking metabolic rate: 807 mL/min
Backpack, 75lb, 0.86 m/s

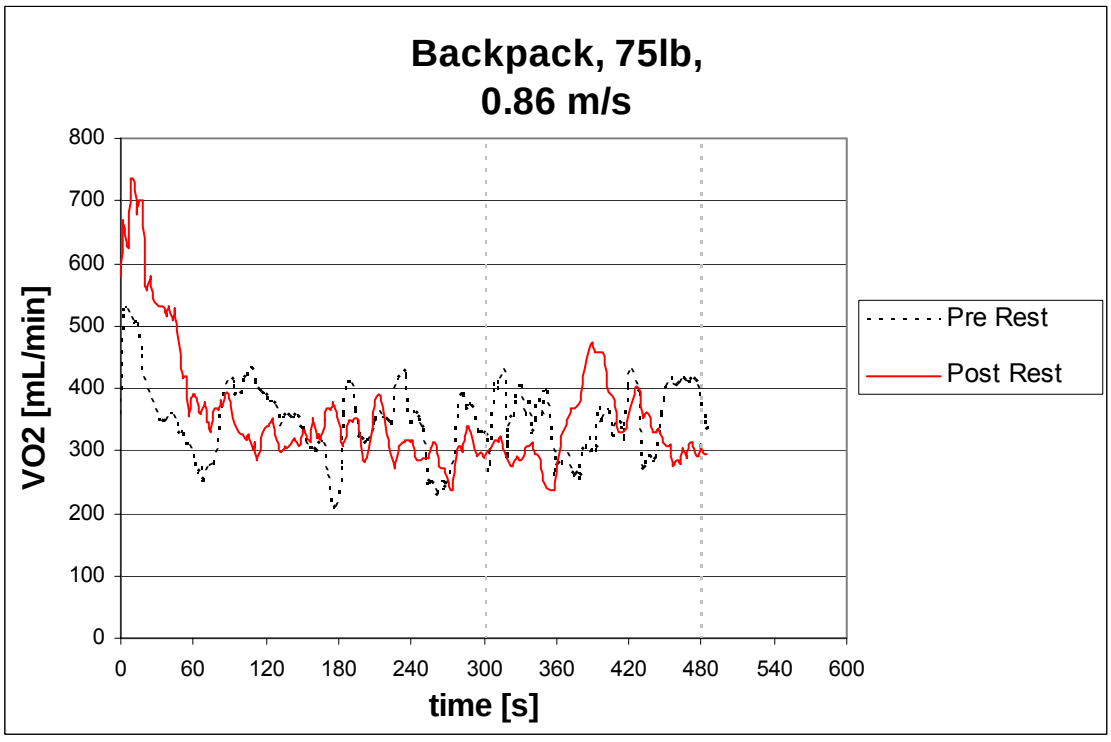

Figure 68 Average resting metabolic rate: 340 mL/min
Backpack, 75lb, 0.86 m/s

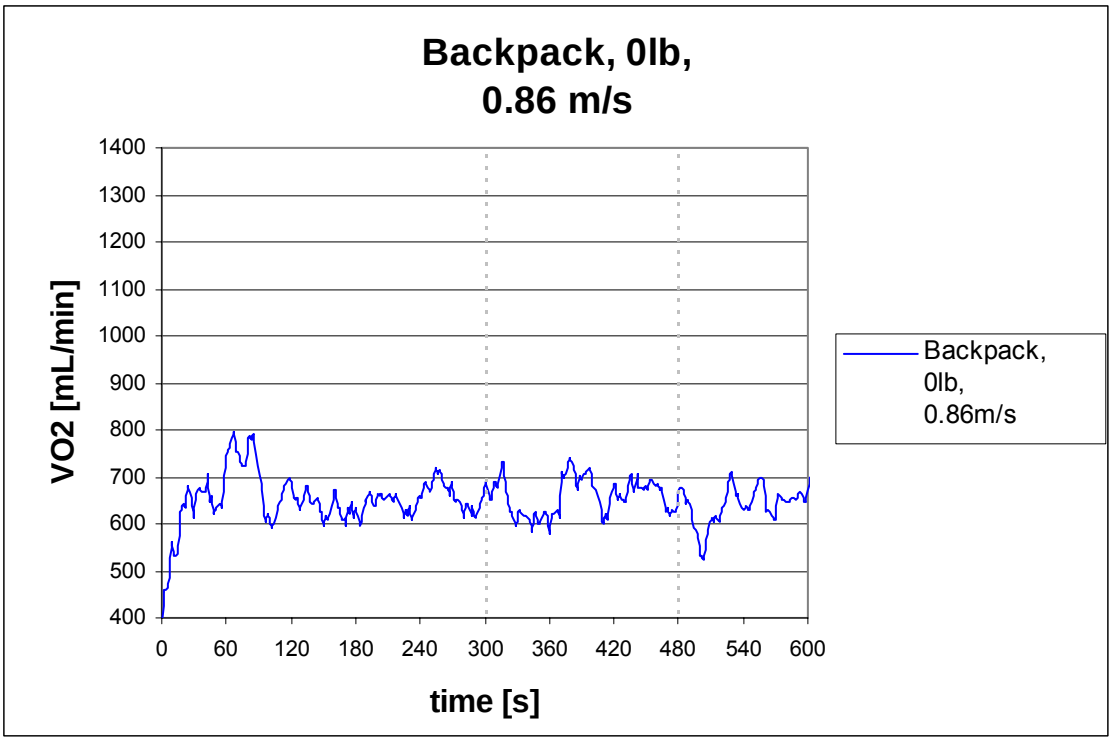

Figure 69 Average walking metabolic rate: 658 mL/min
Backpack, 0lb, 0.86 m/s

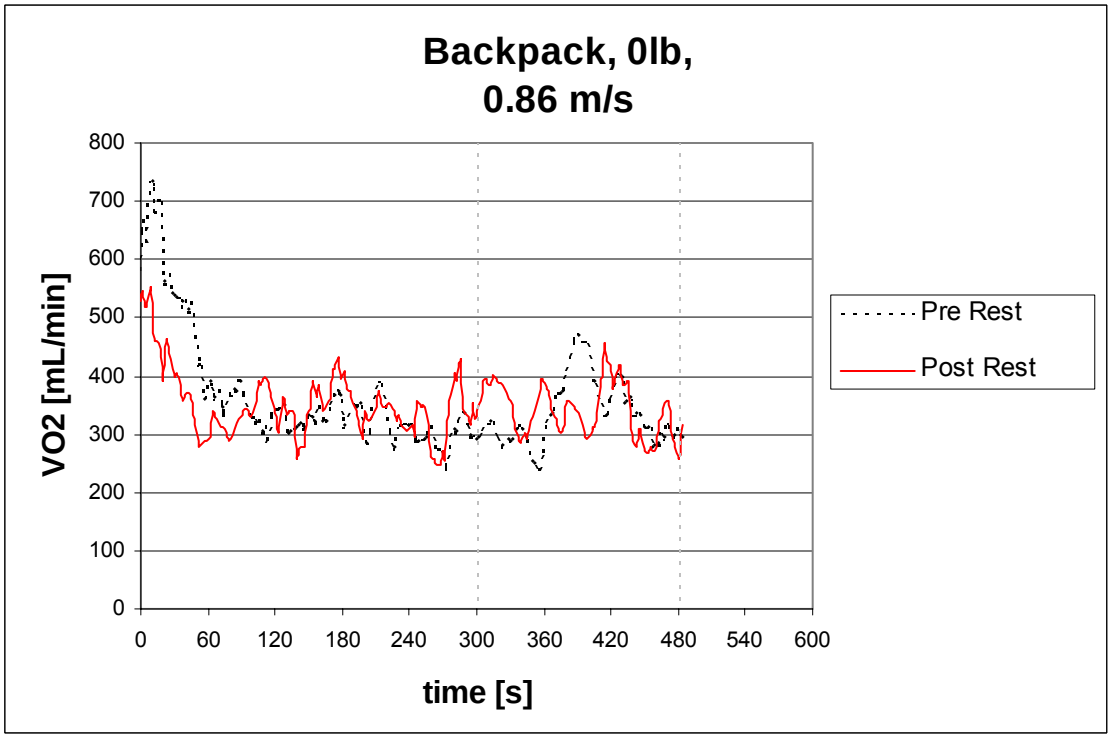

Figure 70 Average resting metabolic rate: 337 mL/min
Backpack, 0lb, 0.86 m/s

To God be the glory.

FIN